Crystal structure of the ligand-free G-protein-coupled receptor opsin

— **Source link** ⎋

Jung Hee Park, Patrick Scheerer, Klaus Peter Hofmann, Klaus Peter Hofmann ...+3 more authors

Institutions: Charité, Humboldt University of Berlin, Chonbuk National University

Topics: Rhodopsin, Opsin and Ligand (biochemistry)

Related papers:

- Crystal Structure of Rhodopsin: A G Protein-Coupled Receptor

- Crystal structure of opsin in its G-protein-interacting conformation

- High-Resolution Crystal Structure of an Engineered Human β2-Adrenergic G Protein–Coupled Receptor

- The 2.6 Angstrom Crystal Structure of a Human A2A Adenosine Receptor Bound to an Antagonist.

- Structure of a beta1-adrenergic G-protein-coupled receptor.

Crystal structure of ligand-free G-protein-coupled receptor opsin

Dissertation

zur Erlangung des akademischen Grades

doctor rerum naturalium

(Dr. rer.nat.)

im Fach Biophysik

eingereicht an der

Mathematisch-Naturwissenschaftlischen Fakulität I

der Humboldt-Universität zu Berlin

von

Dipl.-Chem. Jung Hee Park
geboren am 25.02.1973 in Seoul, S. Korea

Präsident der Humboldt-Universität zu Berlin

Prof. Dr. Christoph Markschies

Dekan der Mathematisch-Naturwissenschaftlichen Fakulität I

Prof. Dr. Lutz-Helmut Schön

Gutachter: 1. Prof. Dr. Klaus Peter Hofmann

2. Prof. Dr. Andreas Herrmann

3. Prof. Dr. Martin Engelhard

Tag der mündlichen Prüfung:10. February. 2010

ABSTRACT IN GERMAN

Bei der biologischen Signaltransduktion dienen reversible Interaktionen zwischen zahlreichen Komponenten der zellulären Signalketten der Assemblierung und Dissoziation von räumlich und zeitlich begrenzten molekularen Komplexen. Protein-Protein Interaktionen sind dabei wichtige Mittel zur Integration mehrerer Signale in koordinierte zelluläre Antworten. Die visuelle Kaskade ist eines der am intensivsten untersuchten Gebiete im Bereich der Signaltransduktionsforschung. Obwohl die dreidimensionale Strukturen des entsprechenden G-Protein gekoppelten Rezeptors (GPCRs) Rhodopsin, des heterotrimeren G-Proteins Transducin und des Signalabschaltproteins Arrestin enorm zur Klärung des molekularen Mechanismus der visuellen Signaltransduktion beigetragen haben, sind die Strukturen vieler hieran beteiligten Proteine und Proteinkonformationen unbekannt. Die vorliegende Arbeit beschäftigt sich mit dem ligandfreien GPCR, Opsin, das beim Photobleichprozess entsteht und an der Lichtadaption des visuellen Systems beteiligt ist.

Rhodopsin ist als Sehpigment der Photorezeptorzellen einer der am aktivsten untersuchten GPCRs. Es besteht aus dem Apoprotein Opsin und dem inversen Agonisten 11-*cis*-Retinal. Der inaktivierende Ligand ist in der sieben Transmembran- Helix (TM)-Struktur des Rezeptors kovalent gebunden und muss durch Licht *cis/trans*-isomerisiert werden, um den Rezeptor zu aktivieren. Der aktivierte Rezeptor katalysiert den Nukleotidaustausch im G-Protein und zerfällt innerhalb von Minuten in Opsin und all-*trans*-Retinal. Das visuelle Pigment wird dann durch erneute Beladung des Opsins mit 11-*cis*-Retinal wieder hergestellt. In der vorliegenden Arbeit wird die erfolgreiche Kristallisation des nativen Opsins aus der Stäbchenzelle der Rinderretina und die Bestimmung der Proteinstruktur bei 2.9 Å Auflösung dargestellt. Im Vergleich zur bekannten Struktur des inaktiven Rhodopsins zeigt Opsin deutliche Strukturänderungen in den konservierten E(D)RY und NPxxY$(x)_{5,6}$F Regionen und in TM5-TM7. Auf der intrazellulären Seite ist TM6 ca. 6-7 Å nach außen gekippt, während die TM5 Helix verlängert und näher zu TM6 verschoben ist. Durch die strukturellen Änderungen, von denen einige einem aktiven GPCR Zustand zugeschrieben werden können, wird die leere Retinalbindungstasche reorganisiert, um zwei Öffnungen für Aus- und Eintritt von Retinal bereitzustellen. Die Struktur von Opsin liefert neue Erkenntnisse zur Bindung von hydrophoben Liganden an GPCRs, zur GPCR-Aktivierung und zur Signalübertragung auf das G-Protein.

Schlagwörter: Signaltransduktion, GPCRs, Opsin, konservierten E(D)RY und NPxxY$(x)_{5,6}$F Regionen, GPCR-Aktivierung

ABSTRACT IN ENGLISH

In biological signal transduction, reversible interactions between numerous components of cellular signaling pathways allow formation and dissociation of spatially and temporally confined molecular complexes. Protein-protein interactions are important means of integrating multiple signals into coordinated cellular responses. The visual cascade is one of the most intensely studied topics in the field of signal transduction research. Although three-dimensional structures of the corresponding G-protein-coupled receptor (GPCR) rhodopsin, the heterotrimeric G protein transducin, and the signal shut-off protein arrestin contribute enormously to the elucidation of the molecular mechanism of visual signal transduction, there are still many proteins of the visual system and key protein conformations, which remain to be structurally determined. This thesis focuses on the ligand-free GPCR opsin which participates in the photobleaching process and is involved in light adaptation of the visual system.

Rhodopsin as the visual pigment in photoreceptor cells is one of the most actively studied GPCRs. It consists of the apoprotein opsin and the inverse agonist, 11-*cis*-retinal. The inactivating ligand is bound in the seven-transmembrane helix (TM) bundle and *cis*/*trans*-isomerized by light to activate the receptor. The active receptor state is capable of catalyzing nucleotide exchange in the G protein and decays within minutes into opsin and all-*trans*-retinal. The visual pigment is then restored by reloading opsin with new 11-*cis*-retinal. In the present work, the successful crystallization of native opsin from bovine retinal rod cells and determination of the protein structure to 2.9 Å resolution is presented. Compared with the known structure of inactive rhodopsin, opsin displays prominent structural changes in the conserved E(D)RY and NPxxY$(x)_{5,6}$F regions and TM5-TM7. At the cytoplasmic side, TM6 is tilted outwards by 6-7 Å, whereas the helix structure of TM5 is more elongated and close to TM6. These structural changes, of which some are attributed to an active GPCR state, reorganize the empty retinal binding pocket to disclose two openings for exit and entry of retinal. The opsin structure thus sheds new light on binding of hydrophobic ligands to GPCRs, GPCR activation and signal transfer to the G protein.

Keyword: Signal transduction, GPCRs, Opsin, conserved E(D)RY and NPxxY$(x)_{5,6}$F regions, GPCR activation

CONTENTS

LIST OF FIGURES

LIST OF TABLES

ABBREVIATIONS

Å	Ångström
β_1-AR	β_1-adrenergic receptor
β_2-AR	β_2-adrenergic receptor
B-factor	Temperature factor, Debye-Waller factor
BSA	Bovine serum albumin
BTP	1,3-bis(tris[hydroxymethyl]methylamino)propane
C	Carbon atom
cGMP	Guanosine 3',5'-cyclic monophosphate
C1 – C3	Cytoplasmic loops 1 – 3
CMC	Critical micelle concentration
CNS	Crystallography & NMR System
DEER	Double electron-electron resonance
DTT	Dithiothreitol
EDTA	Ethylenediaminetetraacetic acid
EG	Ethylene glycol
E1 – E3	Extracellular loops 1 – 3
EPR	Electron paramagnetic resonance spectroscopy
$F_{(h,k,l)}$	Structure factor (or amplitude)
FTIR	Fourier transform infrared spectroscopy
G_t	Transducin, the G protein corresponding to rhodopsin
$G_t\alpha\beta\gamma$	α-, β- and γ-subunit of transducin
$G_t\beta\gamma$	$\beta\gamma$-dimer of transducin
$G_t\alpha CT$	synthetic peptide derived from C-terminus of transducin α-subunit
GPCR	G-protein-coupled receptor
$h\nu$	Photon
K	Kelvin
kDa	Kilodalton
LDAO	Lauryldimethylamine N-oxide
MES	2-(N-Morpholino)ethanesulfonic acid sodium salt

Meta I	Metarhodopsin I
Meta II	Metarhodopsin II, active form of rhodopsin
Mw	Molecular weight
NMR	Nuclear magnetic resonance spectroscopy
β-OG	β-D-octylglucopyranoside
Opsin*	Active conformation of opsin; opsin at low pH
PAGE	Polyacrylamide gel electrophoresis
PDB	Protein Data Bank
PDE	cGMP-specific phosphodiesterase
R*	Active conformation of rhodopsin
RFZ	Rotation function Z-score
RK	Rhodopsin kinase
rms	Root mean square
ROS	Rod outer segment
S	Entropy
SDS-PAGE	Sodium dodecylsulfate polyacrylamide gel electrophoresis
σ	Sigma, control level of electron density map
TFZ	Translation function Z-score
TM	Transmembrane helix
UV	Ultraviolet
Amino acids	Amino acid residues are given in three letter code
Residue numbering	In the Ballesteros-Weinstein nomenclature of GPCRs [1] the most highly conserved residue in each TM helix is assigned the number 50 (Asn1.50, Asp2.50, Arg3.50, Trp4.50, Pro5.50, Pro6.50 and Pro7.50 on TM1 − TM7, respectively). All other residues on a TM helix are numbered relative to this position.

PUBLICATIONS

Parts of the dissertation have been published in:

Park, J. H.*, Scheerer, P.*, Hofmann, K. P., Choe, H.-W. & Ernst, O. P. Crystal structure of the ligand-free G-protein-coupled receptor opsin. Nature, 454, 183-187 (2008).

Scheerer, P.*, Park, J. H.*, Hildebrand, P. W., Kim, Y. J., Krauß, N., Choe, H.-W., Hofmann, K. P. & Ernst, O. P. Crystal structure of opsin in its G-protein-interacting conformation. Nature, 455, 497-502 (2008).

Hildebrand, P. W., Scheerer, P., Park, J. H., Choe, H.-W., Piechnick, R., Ernst, O. P., Hofmann, K. P. & Heck, M. A ligand channel through the G protein-coupled receptor opsin. PLoS ONE, 4, e4382 (2009).

Scheerer, P., Heck, M., Goede, A., Park, J. H., Choe, H.-W., Ernst, O. P., Hofmann, K. P. & Hildebrand, P. W. Receptor-G protein coupling: Modeling signal transfer through the rhodopsin-transducin interface. Proc. Natl. Acad. Sci. U.S.A., 106, 10660-10665 (2009).

Hofmann, K. P., Scheerer, P., Hildebrand, P. W., Choe, H.-W., Park, J. H., Heck, M. & Ernst, O. P. A G protein-coupled receptor at work: the rhodopsin model. Trends Biochem. Sci., in press.

* These authors contributed equally to this work

1   INTRODUCTION

1.1   G-protein-coupled receptors (GPCRs)

G-protein-coupled receptors (GPCRs) are cell surface receptors and constitute the most prominent family of validated pharmacological targets in biomedicine [2,3]. GPCRs form a large and diverse multigene superfamily of integral membrane proteins involved in many important physiological functions [3,4]. The functions are highly variable as they play a crucial role in all major peripheral organ systems and the brain of mammals.

In humans, ~800 GPCRs are known which have been generally classified in six major families (see Table 1.1; [5]). Although there is a lack of sequence similarity between the six classes of the GPCR superfamily, the primary structure of GPCRs is characterized by a common structural motif of seven transmembrane-spanning segments. According to GPCR crystal structures, these segments form transmembrane helices (TM) that are connected by three intracellular and three extracellular loops [2,6]. Due to their topology, GPCRs are also called 7TM or heptahelical receptors. Class A or rhodopsin-like GPCRs comprise 672 members including 388 olfactory GPCRs, accounting thus for over 80% of all GPCRs [7,8]. Class A GPCRs often contain two conserved cystein residues, which link the extracellular end of TM3 and the extracellular domain by a disulfide bridge, as well as two conserved motifs, i.e. the E(D)RY motif in TM3 and the $NPxxY(x)_{5,6}F$ motif in TM7, that might have a prerequisite role in the physiological function [8].

Table 1.1. GPCR classes according to the GPCRDB database (http://www.gpcr.org/7tm/) [9].

GPCRDB family	Description
Class A	Rhodopsin-like GPCRs
Class B	Secretin-like GPCRs
Class C	Metabotropic glutamate/ pheromone receptors
Class D	Fungal pheromone receptors
Class E	Cyclic adenosine monophosphate (cAMP) receptors
Class F	Frizzled/ smoothened receptors
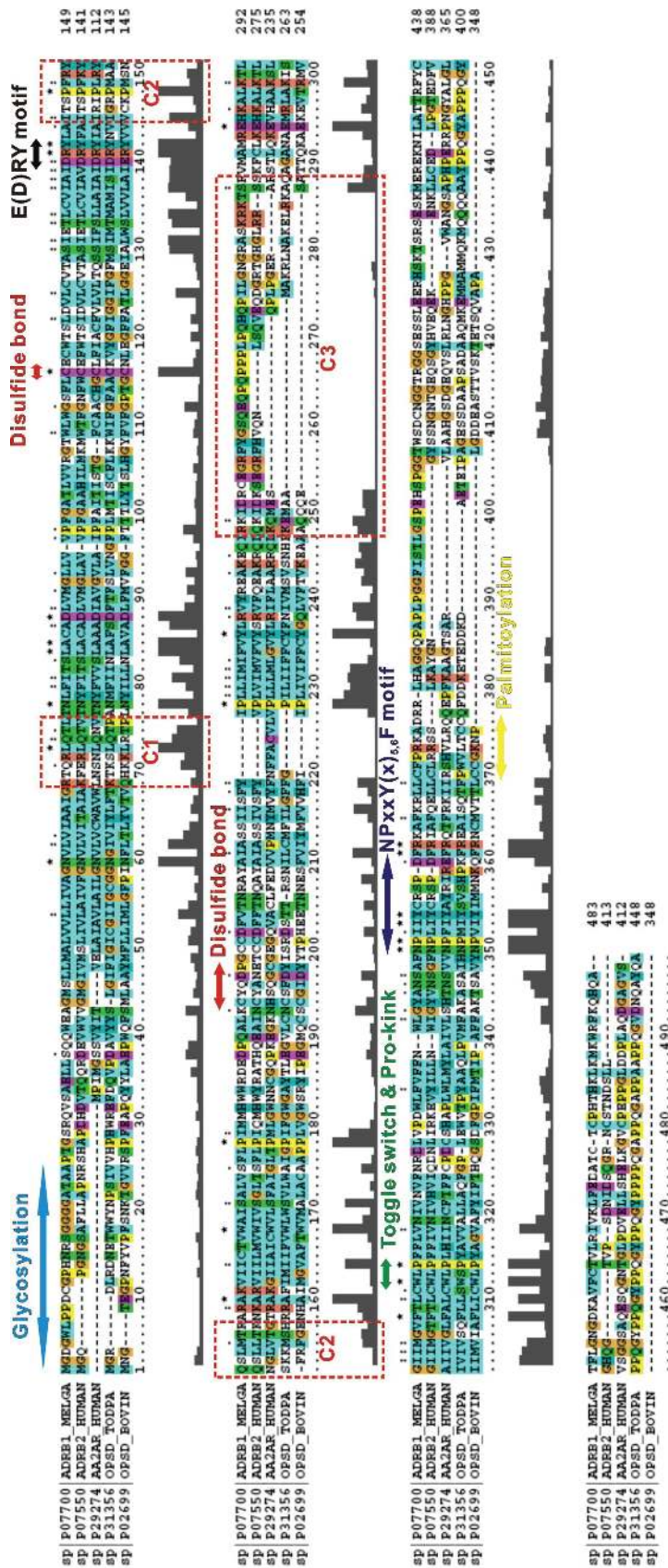
Figure 1.1. Sequence aligment of selected class A GPCRs

Sequence alignment of class A GPCRs with known crystal structure: OPSD_TODPA, Squidrhodopsin; AA2AR_Human Alpha2A Adenosine Receptor; ADRB1_MELGA, Turkey Beta1 Adenergic receptor; ADRB2_HUMAN Beta2 Adrenergic receptor. Indicated are: site of Asn glycosylation (cyan arrow), disulfide bond formation (red arrow) Cys palmitoylation (yellow arrow); conserved E(D)RY (black arrow) and NPxxY(x)$_{5,6}$F (blue arrow) motifs, and conserved residues of the rotamer toggle switch/ proline kink (green arrow; see below). The sequence identity of each residue is indicated by grey bars. Cytoplasmic loop regions (C1-C3) are presented as red dot box.

Only for class A, crystal structures of four GPCRs are known (see 1.3) providing detailed molecular information on these receptors. A sequence alignment of GPCRs with known tertiary structure (Figure 1.1) reveals the E(D)RY and NPxxY(x)$_{5,6}$F motifs, as well as a conserved CWxP motif in TM6 involved in GPCR activation ("toggle switch residues", see discussion). Common to class A GPCRs are also glycosylation sites at the N-terminus, palmitoylation sites after TM7 and phosphorylation sites in the C-terminus. An overview based on available structural and sequence data is provided in Figure 1.1 and Table 1.2.

GPCRs have extremely diverse ligands that comprise biogenic amines, peptides, large proteins, nucleotides, lipids, and eicosanoids [10,11]. Binding of these specific ligands to the extracellular or transmembrane regions causes structural changes of the receptor to enable signal transfer via the cytoplasmic domain to heterotrimeric guanine nucleotide-binding regulatory proteins (G proteins, Gαβγ). GPCR signaling to the G protein is further regulated by receptor kinases which phosphorylate the active GPCR to allow arrestins to bind phosphorylated GPCRs, thus blocking the cytoplasmic receptor domain for interaction with the G protein.

Abnormalities of signaling by GPCRs have been associated with several diseases, such as hypertension [12,13], precocious puberty [14,15], hyperthyroidism [16], nephrogenic diabetes insipidus [14,17], cancer [18] and blindness [19,20]. The sequencing of the human genome [21,22,23] has revealed several hundred members of GPCRs including orphan GPCRs with yet unknown ligands, indicating the future therapeutic potential of targeting the GPCR superfamily [8].

Rhodopsin is the eponym and prototype of the GPCR class A. It was discovered more than 130 years ago as visual pigment in the vertebrate eye and is one of the most actively studied GPCRs [24,25,26]. Rhodopsin consists of the apoprotein opsin and its chromophore 11-*cis*-retinal. 11-*cis*-retinal is covalently bound by a Schiff base to Lys-296 on TM7 and acts as an inverse agonist to stabilize rhodopsin in its inactive ground state. This dissertation focuses on the bovine ligand-free GPCR opsin. A phylogenetic tree of bovine class A GPCRs is presented in Figure 1.2 showing the sequence relation between different class A GPCRs.

Table 1.2. Sites of modifications in GPCRs with known crystal structure

GPCR Accessions: PDB UniProtKB (Swiss-Prot)	Glycosylated residues (Refs.)	Palmitoylation sites (Refs.)	Phosphorylation sites (Refs.)	Disulfide bond (Refs.)
Bovine rhodopsin/ opsin 1F88, 1GZM, 1U19, 2PED, 2HPY, 2I37, 3CAP, 3DQB P02699 (OPSD_BOVIN)	Asn-2 and Asn-15 [27]	Cys-322 and Cys-323 [28,29]	Ser-334, Ser-338, Ser-343, Thr-335, Thr-336, Thr-340, Thr-342 phosphorylated by GRK1 (RK)* [29,30]	Cys-110/ Cys-187 [31]
Squid rhodopsin 2Z73, 2ZIY P31356 (OPSD_TODPA)	Asn-8	Cys-336 and Cys-337 [32]	unknown	Cys-108/ Cys-186 [32]
Human A_{2A}-adenosine receptor 3EML P29274 (AA2AR_HUMAN)	unknown	unknown	unknown	Cys-77/ Cys-166
Turkey β_1-adrenergic receptor 2VT4 P07700 (ADRB1_MELGA)	Asn-14 *(Probable position)*	Cys-358 *(by similarity with β_2-AR)*	unknown	Cys-114/ Cys192 [33]
Human β_2-adrenergic receptor 2RH1, 2R4R, 3D4S P07550 (ADRB2_HUMAN)	Asn-6 and Asn-15 *(Probable positions)*	Cys-341 [34,35]	Ser-345 and Ser-346 Phosphorylated by PKA* and β_2-ARK* [34]	Cys-106/ Cys-184 [36]

*G-protein-coupled receptor kinase (GRK). RK, rhodopsin kinase; β_2-ARK, β_2-adrenergic receptor kinase; PKA, cyclic AMP-dependent protein kinase.
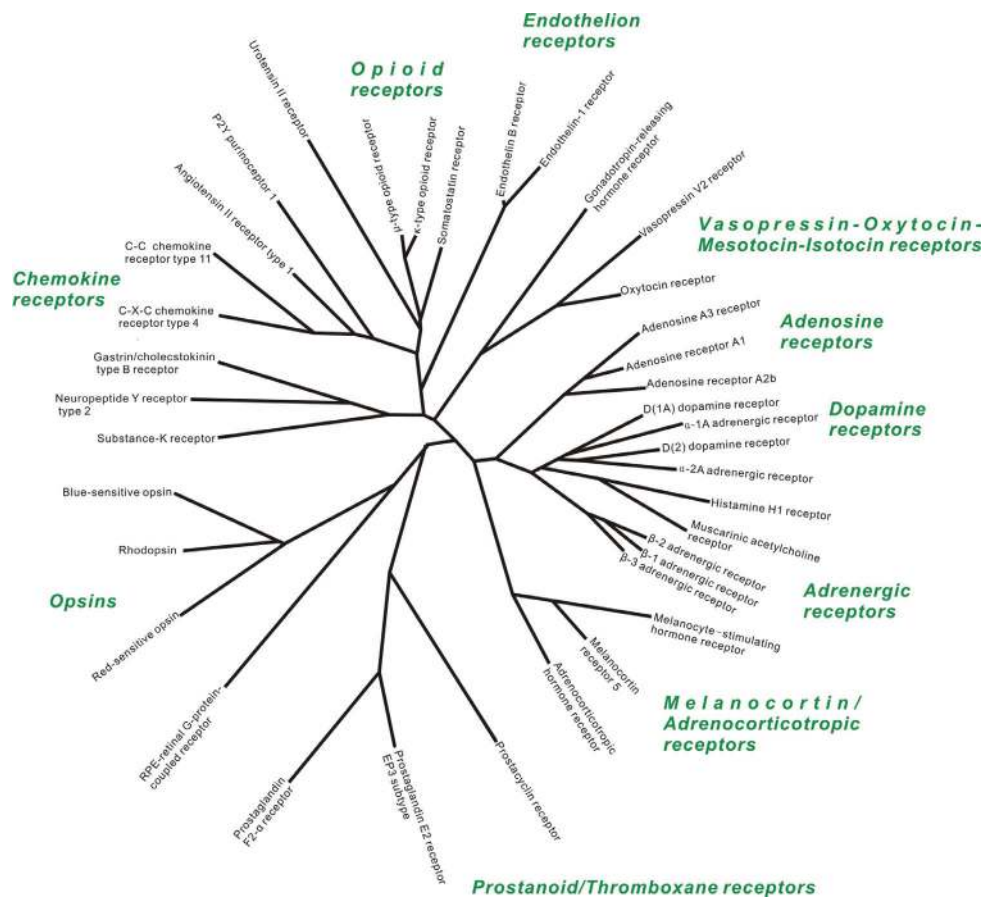
Figure 1.2. Phylogenetic tree of bovine class A GPCRs

Phylogenetic relationship between class A GPCRs, based on sequence alignment of bovine GPCRs that have been reported in the Uniprot database (http://www.uniprot.org/). The tree was built using the standard online tool from Phylogeny.fr (http://www.phylogeny.fr/) [37]. The opsins comprise blue- and red-sensitive opsin, and rhodopsin. The RPE-retinal G-protein-coupled receptor is a related retinal protein.

1.2   Visual signal transduction

In the vertebrate eye, the lens focuses an image on the retina. The retina is composed of tightly stacked cell layers among which the photoreceptor cell layer converts light into an electrical signal. The signal is relayed from the rod and cone photoreceptor cells via horizontal cells, bipolar cells, and amacrine cells to the ganglion cells, which convey the signal to the brain [38,39]. A human retina contains approximately 1×10^8 rod cells and 5×10^6 cone cells. The rod cells are specialized for the detection of dim light (scotopic vision), whereas the cone

cells function in bright light (photopic vision) and mediate color vision. In the human retina, there are three types of cones, each with different spectral response [40].

The visual pigment and GPCR rhodopsin is concentrated in the disk membrane of the rod outer segment of rod photoreceptor cells. Transmission of the light signal into the cell is initiated by *cis*/*trans* isomerization of rhodopsin's 11-*cis*-retinal chromophore after absorption of visual light. The isomerization of the chromophoric ligand triggers a conformational change of rhodopsin leading to an active state (R*) called Metarhodopsin II (Meta II). For signal transduction, R* interacts with the cytoplasmic heterotrimeric G protein transducin ($G_t\alpha\beta\gamma$) to catalyze transducin activation via GDP→GTP nucleotide exchange in the $G_t\alpha$-subunit. The activated form of transducin ($G_t\alpha\bullet$GTP) stimulates the hydrolytic activity of phosphodiesterase (PDE) by relieving its inhibitory γ-subunits. The activated catalytic subunit of PDE ($PDE\alpha\beta^*$) then hydrolyzes guanosine 3',5'-cyclic monophosphate (cGMP) to 5'-GMP. The decrease of cGMP concentration leads to the closure of cyclic nucleotide-gated cation channels, which stops the influx of cations and thus hyperpolarizes the plasma membrane of the photoreceptor outer segment [41].

The G-protein activation phase and thus signaling is terminated by phosphorylation of R* by rhodopsin kinase (RK) and subsequent binding of visual arrestin to phosphorylated R*, thus blocking receptor/G protein interaction. Concurrently, the retinal Schiff base is hydrolyzed and the photolyzed all-*trans*-retinal is released from its binding site. Regeneration of the light-sensitive rhodopsin ground state requires the supply of new 11-*cis*-retinal from the pigment epithelial through the so-called retinoid cycle [42,43,44,45,46]. Abnormalities in the regeneration pathway have been associated with different forms of blindness such as Oguchi and Stargardt disease [42]. During the regeneration phase, one experiences the phenomenon of bleaching desensitization. The key to understand the complex functional implications of these phenomena is the receptor state in which the retinal binding site is empty and the apoprotein opsin waits for reconstitution with 11-*cis*-retinal.

1.3   Structure of rhodopsin

The first crystallographic model of the bovine rhodopsin ground state was provided by Palczewski and colleagues [31]. Further detailed insight into the structure and location of internal water molecules were given by subsequent high-resolution models (up to 2.2 Å) obtained from tetragonal ($P4_1$) and trigonal ($P3_1$) crystal forms [47,48]. Together with theoretical studies of the chromophore geometry a clear picture of the retinal binding site emerged [47].

The crystal structures confirmed the predicted 7TM topology of rhodopsin with seven transmembrane-spanning helical segments connected by cytoplasmic (C1 – C3) and extracellular (E1 – E3) loops, respectively (Figures 1.3 and 1.4). In addition a cytoplasmic helix (H8) following TM7 was revealed which runs along the membrane surface. The model in Figure 1.4 also includes two oligosaccharides attached to Asn-2 and Asn-15 and two palmitoylate chains linked to Cys-322 and Cys-323. TM6 is strongly distorted by Pro-267 which is one of the most conserved residues among GPCRs. A disulfide bond between Cys-110 on TM3 and Cys-187 in E2 tethers a compact extracellular domain, the so-called "retinal plug" to the 7TM domain. The "retinal plug" includes two antiparallel β-sheets in the N-terminus (strands β1/β2) and in loop E2 (strands β3/β4), respectively [49]. E2 folds back into the protein to contribute Ser-186 to Ile-189 of strand β4 to the retinal binding site. The retinal chromophore in its binding pocket is surrounded by hydrophobic residues (Cys-187, Ile-189, Met-207, Phe-212, Phe-261, Trp-265 and Ala-292) and the counterion (Glu-113; [50]) of the protonated Schiff base. Two water molecules interact with Thr-94/Glu-113 and Glu-181/Ser-186, respectively [47]. Rhodopsin and other GPCRs contain two conserved motifs. The E(D)RY motif (in TM3) is part of a hydrogen bonded network – the so-called "ionic lock" [51,52,53,54] – which tethers Arg-135 (on TM3) to Glu-247 (on TM6). A second motif, the $NPxxY(x)_{5,6}F$ motif links Tyr-306 (on TM7) and Phe-313 (on H8).

Besides the crystal structure of bovine rhodopsin, the structures of squid rhodopsin [32] and other GPCRs are known including β_1-adrenergic receptor (β_1-AR; [33]), β_2-adrenergic receptor (β_2-AR; [36,55]) and A_{2A} adenosine receptor [56]. Common to all structures is a bound ligand which lacks the capability to activate the GPCRs.
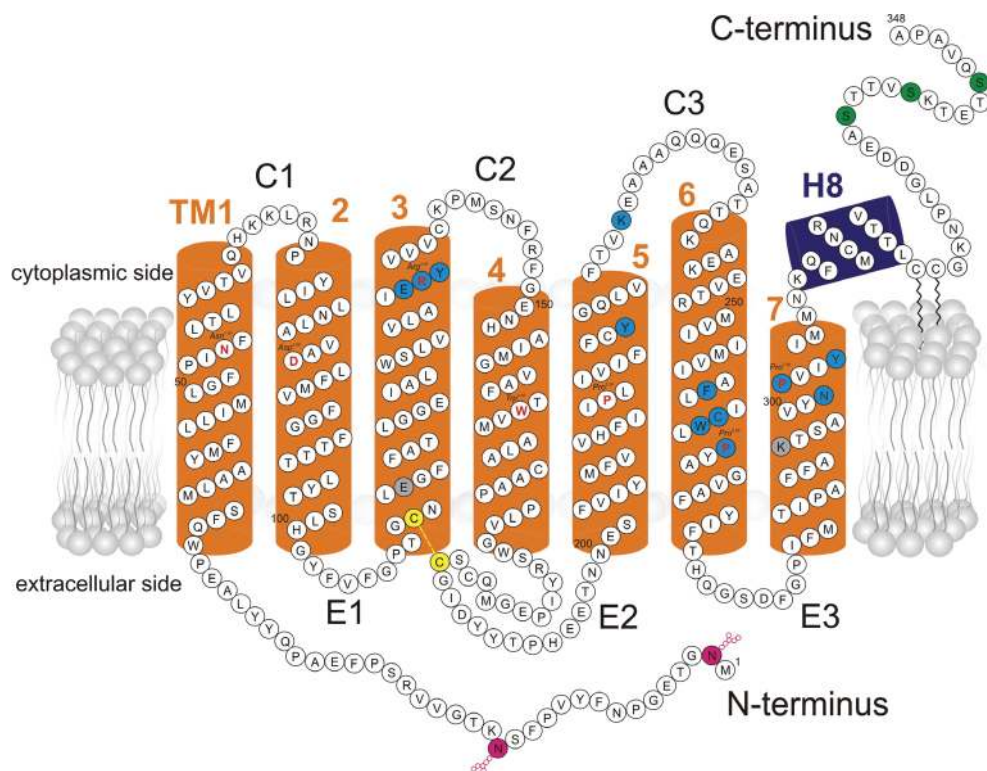
Figure 1.3. Secondary structure of rhodopsin and conserved elements

The secondary structure of rhodopsin shows seven transmembrane helices that are connected by cytoplasmic and extracellular loops, the cytoplasmic helix H8 running parallel to the surface of the membrane, and the two terminal regions. The N-terminus is glycosylated at Asn-2 and Asn-15, H8 is terminated by palmitoylated Cys-322 and Cys-323. A conserved disulfide bridge (shown in yellow) between Cys-110 (on TM3) and Cys-187 (E2) tethers loop E2 to the extracellular part of TM3. The motifs E(D)RY in TM3 and NPxxY(x)$_{5,6}$F in TM7/H8 are conserved in GPCRs [57]. In the course of receptor deactivation, the preferred phosphorylation sites for rhodopsin kinase, Ser-334, Ser-338 and Ser-343 (shown in green), get phosphorylated to allow binding of arrestin. Lys-296 (grey) on TM7 represents the residue where 11-cis-retinal is attached via a protonated Schiff base. In the three-dimensional structure, Glu-113 (grey) on TM3 is close to the protonated Schiff base and serves as counterion. The most conserved amino acids are highlighted in red and are numbered using the Ballesteros-Weinstein nomenclature of GPCRs [1] where the most highly conserved residue in each TM helix is assigned the number 50 (Asn1.50, Asp2.50, Arg3.50, Trp4.50, Pro5.50, Pro6.50 and Pro7.50 on TM1 – TM7, respectively). All other residues on a TM helix are numbered relative to this position.
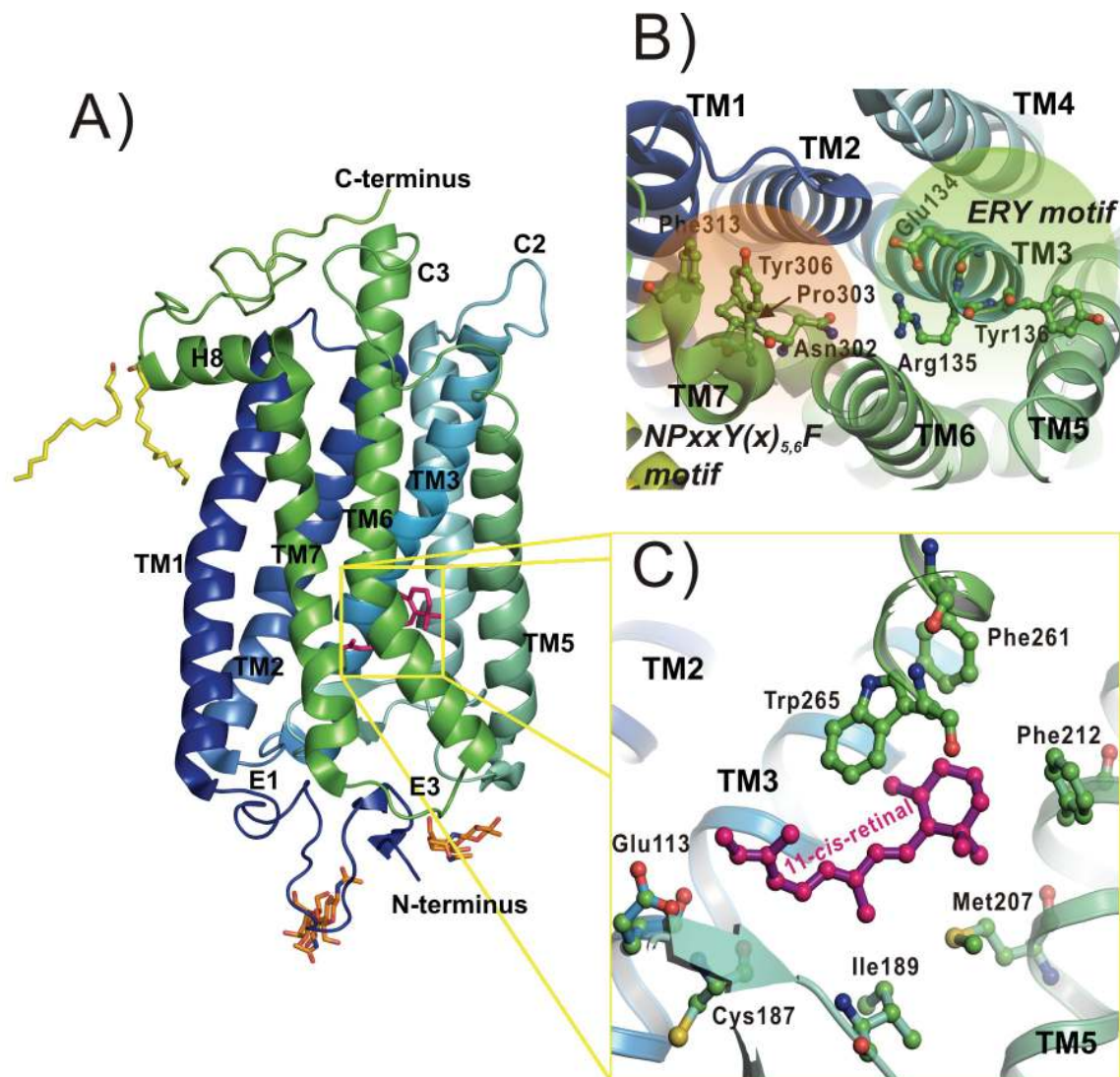
Figure 1.4. Crystal structure of bovine rhodopsin

*Structure of bovine rhodopsin at 2.2 Å (PDB accession: 1U19, [47]). **A)** Overall monomer structure of bovine rhodopsin. Seven transmembrane helices (TMs), three cytoplasmic loops (C1 – C3) and three extracellular loops (E1 – E3) are labeled. Stick models show 11-cis-retinal (magenta), two oligosaccharides (orange) attached to Asn-2 and Asn-15 and two palmitoylate (yellow) chains attached to Cys-322 and Cys-323 at the end of cytoplasmic helix 8 (H8). **B)** Cytoplasmic view: highly conserved motifs, E(D)RY and $NPxxY(x)_{5,6}F$, in GPCRs. The motifs are highlighted by green and orange circles, respectively. **C)** Close-up view: residues in the retinal binding site and 11-cis-retinal are shown as ball and stick model, respectively.*

1.4   Photoactivation of rhodopsin

GPCRs are typically activated by binding of small ligands which have diverse chemical structures (see e.g. Ref. [11]). The ligand of the β_2-AR, for example, is a biogenic amine hormone. In rhodopsin, however, light as physical stimulus converts the bound retinal ligand into a chemically different ligand with new properties that is capable to activate the receptor. The photon energy is used to isomerize the highly effective inverse agonist 11-*cis*-retinal (inactivating ligand) present in rhodopsin into the agonist all-*trans*-retinal (activating ligand). Due to retinal isomerization, the stabilizing salt bridge between the protonated 11-*cis*-retinal Schiff base and its counterion (Glu-113 on TM3) present in the inactive rhodopsin ground state is broken [25,31,58]. As a consequence conformational rearrangements of the opsin moiety occur which lead in the rhodopsin activation process to a succession of at least five different photoproducts, including the two early intermediates, Batho- and Lumirhodopsin (Batho, Lumi), and the late Metarhodopsin intermediates, Meta I, Meta II and Meta III, that are generated by thermal conversion [59,60,61] (Figure 1.5). Each intermediate is well characterized by its UV/Vis absorption maximum and typical infrared difference spectrum [62,63].

Triggered by uptake of photon energy and the geometrical change of retinal, rhodopsin converts within milliseconds via Batho and Lumi to the active Meta II state which is in a pH-, temperature- and detergent-dependent equilibrium with its inactive precursor Meta I (Figure 1.5) [64,65]. Formation of Meta II is accompanied by deprotonation of the retinal Schiff base [64]. Meta III forms via two different pathways, either by thermal isomerization from Meta I or by light-induced isomerization of the retinal Schiff base bond in the Meta II state. Meta II and Meta III decay slowly into opsin and all-*trans*-retinal by hydrolysis of the Schiff base allowing photolyzed all-*trans*-retinal to be released from the retinal binding site. By uptake of 11-*cis*-retinal into opsin and Schiff base formation the rhodopsin ground state is regenerated [42].

To understand the photoactivation process and concomitant conformational changes, it was attempted to obtain crystallographic models of the intermediates. This was possible for Batho, Lumi and a photoactivated rhodopsin with properties of Meta II [66,67,68]. Batho forms on a picosecond timescale and contains retinal in the all-*trans*-15-*anti* configuration with a quite

distorted polyene chain. No significant conformational change of the opsin moiety in Batho relative to rhodopsin was found in the crystal structure at 2.6 Å resolution [66]. The 2.8 Å crystal structure of Lumi which forms by thermal conversion from Batho on a microsecond timescale, suggests that the chromophore reaches in Lumi a nearly completely relaxed all-*trans* configuration [67]. While the location of the protonated Schiff base did not change, substantial alterations of nearby residues in the retinal binding pocket (Thr-118, Gly-120, and Gly-121) occurred. A different orientation of retinal's β-ionone ring towards TM3 and TM4 was observed in Lumi [67] which is in agreement with a movement of the β-ionone ring as suggested by photoaffinity labeling experiments using 11-*cis*-3-diazo-4-oxo-retinal [69].

A crystal structure of Meta I is not known, but electron crystallography revealed that Meta I formation does not involve large rigid-body movements of helices [70]. To obtain a structure of active Meta II, crystals of rhodopsin were illuminated under conditions where Schiff base deprotonation, the signature of Meta II, occurred. The structure of this photoactivated rhodopsin at 4.2 Å resolution does not show large rigid-body movements of the helices but small changes at the cytoplasmic surface [68].

EPR measurements on spin-labeled rhodopsin mutants showed that upon formation of Meta II a 6 Å rigid body tilt of the cytoplasmic half of TM6 relative to TM3 out of the helix bundle occurs [71,72,73]. TM6 movement and concomitant breakage of the "ionic lock" is thought to be initiated by displacement of the β-ionone ring during transition of Meta I to Meta II. Besides changes in the E(D)RY motif, changes in the $NPxxY(x)_{5,6}F$ motif are necessary to adopt the active receptor conformation as indicated by previous biochemical, mutational and spectroscopic analyses [25,53,71,74,75,76,77,78,79]. Since Meta II consists of the subspecies Meta II_a and Meta II_b [80,81] with Meta II_b containing a tilted TM6 [72], the crystal structure of photoactivated rhodopsin described above may represent Meta II_a, the precursor of the active Meta II_b species [72,80].
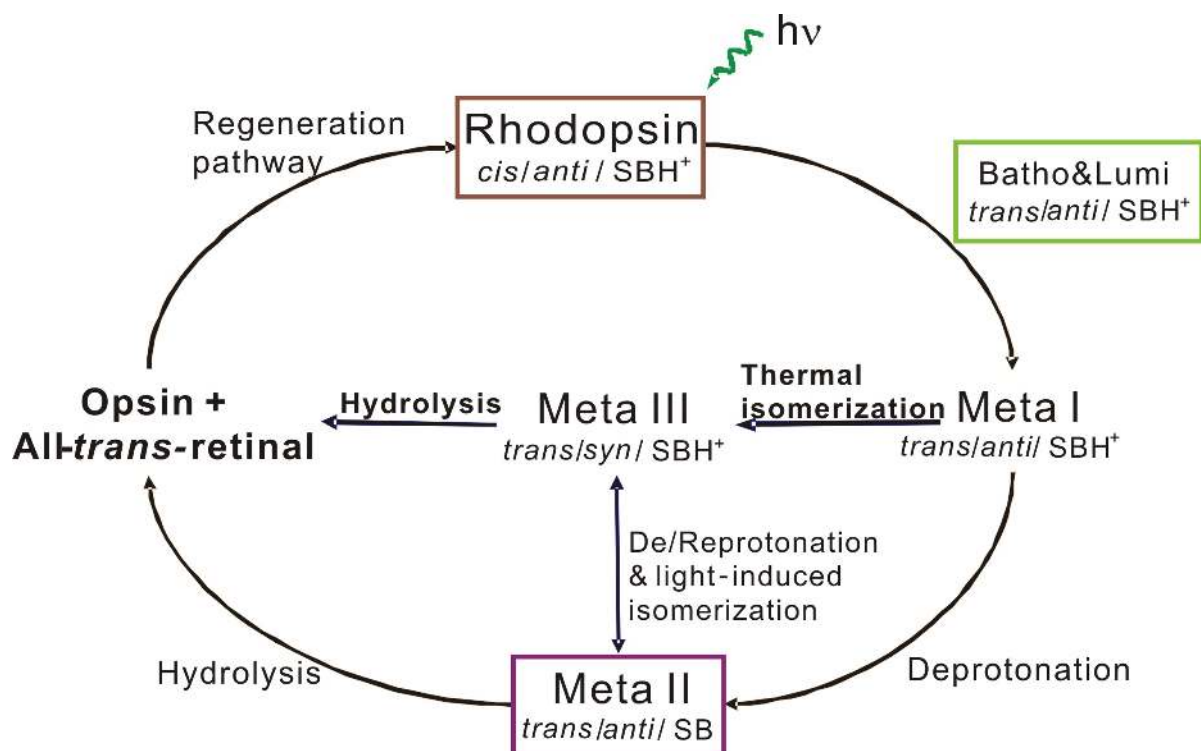
Figure 1.5. Photoproducts of rhodopsin

The photoactivation process of rhodopsin is initiated by photon (hν) absorption. Light-induced isomerization of 11-cis-retinal leads to a series of thermo-labile intermediates, constituting the so-called "photobleaching process". The intermediates are characterized by their absorption maxima, the cis/trans configuration of the C_{11}-C_{12} bond and anti/syn configuration of the C-N Schiff base (SB) bond [63,82,83]. Opsin is formed from Meta II and Meta III by hydrolysis of the SB bond and all-trans-retinal release. The absorption maxima and time scales of product formation are indicated. Meta I and Meta II are in equilibrium. Meta II consists of the MIIa and MIIb subspecies with MIIb as active photointermediate [72]. Photointermediates with known crystal structures are boxed.

1.5   Opsin, the ligand-free state of rhodopsin

Ligand-free opsin is the decay product of light-activated rhodopsin and is capable to take up new 11-*cis*-retinal to regenerate rhodopsin. In the visual process opsin is produced by dissociation of the phosphorylated Meta II•arrestin complex, hydrolysis of the retinal Schiff base bond and dephosphorylation of the receptor. The hypothesis of rhodopsin regeneration after bleaching by light has been suggested early by Hecht [46]. However, the release step of all-*trans*-retinal from its binding pocket and the uptake step of new 11-*cis*- retinal are not clearly understood yet.

Opsin has a low activity towards the G protein [84,85,86,87], but the activity is enhanced by several orders of magnitude when all-*trans*-retinal is present to form a non-covalent complex with opsin [88,89,90]. By infrared spectroscopy *in vitro* on disk membranes it was shown that opsin exists in a pH-dependent equilibrium of two conformations with a pK_a of 4.1 at 30 °C [91] (Figure 1.6). The infrared difference spectrum between opsin and rhodopsin at low pH is similar to the difference spectrum between Meta II and rhodopsin at neutral pH, suggesting that the low pH form of opsin represents an active opsin conformation (opsin*) similar to Meta II. Analogous to the equilibrium between opsin* and the inactive opsin conformation, Meta II is favoured at the expense of its precursor Meta I by low pH. The high pH opsin conformation may thus be similar to inactive Meta I.
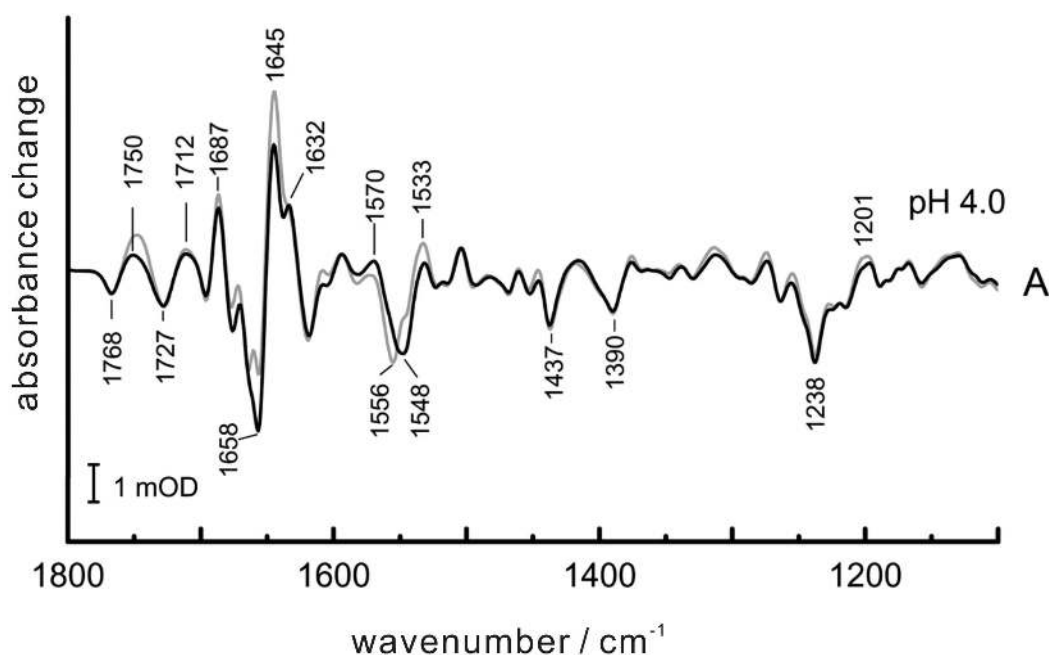
Figure 1.6. Infrared spectrum of the active conformation of opsin, opsin*

Infrared difference spectra photoproduct minus dark state is shown. Black line: difference spectrum Meta II minus rhodopsin obtained by light-activation of rhodopsin at pH 4. Grey line: difference spectrum opsin/ all-trans-retinal minus rhodopsin at pH 4. The opsin/all-trans-retinal mixture was obtained as decay product of Meta II. Data taken from Ref. [91].

Transducin activation by opsin is pH-dependent and most efficient at pH 5 - 6 [92]. It was shown by mutagenesis studies that the salt bridge between Lys-296 and Glu-113 stabilizes the inactive state opsin conformation. Removal of either charge by replacing Lys or Glu, respectively, resulted in constitutive activity of the mutants which could be further increased by lowering pH [92,93]. From proton uptake measurements on the E134Q mutant Glu134 was suggested as the possible proton acceptor group [94].

1.6   Aim of this thesis

So far crystallographic models of the rhodopsin ground state, inactive early photointermediates (Batho and Lumi) and photoactivated rhodopsin are known [31,47,66,67,68]. However the models provide only limited information on the mechanism of rhodopsin activation and signal transfer to the G protein because no model of an active conformation R* (Meta II) is available. Crystallization of Meta II is hampered by the fact that Meta II decay due to retinal release is occurring during the time needed for the crystallization process. Therefore a new strategy to obtain a crystallographic model of an R* conformation has to be devised. Based on the fact that opsin exists at low pH in an R*-like conformation, the aim was i) to crystallize opsin to possibly get structural insight into the R* conformation and ii) to provide – if possible – a new GPCR structure template for homology modeling to serve for drug discovery and design.

Although research in the last decades has contributed much to understanding GPCR activation, many questions on the activation mechanism and signal transfer to the G protein at the molecular level remain elusive. The opsin structure solved in this work is close to the conformation of Meta II and will provide information on the following questions:

1.   What conformational changes are necessary to adopt the R* conformation?
2.   How can active opsin (opsin*) activate transducin (Gt)?
3.   How is activation of opsin by all-*trans*-retinal related or the ligand-free state?
4.   How can retinal be released or taken up, respectively?
5.   What changes occur in the ligand binding pocket upon retinal binding?

2   MATERIALS AND METHODS

2.1   Materials

2.1.1 Chemicals and consumables

β-D-dodecylmaltoside and β-D-octylglucopyranoside were from Biomol (Hamburg). Chemicals and buffers in highest quality were purchased from Sigma-Aldrich and Fluka. Bovine serum albumin (BSA) was purchased from Sigma-Aldrich and Roth (Karlsruhe). Sucrose was from Fluka or Merck (Darmstadt). Crystallization screen kits and all crystallization tools were purchased from Hampton Research (Laguna Niguel, CA, USA). Bovine eyes were obtained from a local slaughter house in Germany.

2.1.2 Soft- and hardware

High-quality X-ray diffraction data suitable for structure determination were collected at beamlines BL14.1 and BL14.2 of the Protein Structure Factory at BESSY (Elektronenspeicherring BESSY II, Helmholtz-Zentrum Berlin für Materialien und Energie GmbH, Germany) equipped with MAR-165CCD detectors. Data were processed using the HKL 2000 package [95], the crystallographic refinement was done using the CCP4 program PHASER [96] and the Crystallography & NMR System (CNS) program [97]. Electron density maps were interpreted and structural models were fitted into the maps using the graphics program COOT [98], the structure was validated with the programs PROCHECK [99] and WHAT_CHECK [100]. All crystal structure superpositions of C_α traces were performed using CCP4 program LSQKAB [101]. All molecular graphics representations were created using PyMol [102]. In order to investigate general features of GPCRs, multiple sequence alignment and phylogenetic tree representations were made using programs ClustW and PhyML (http://www.phylogeny.fr/) [37].

2.1.3 Equipment

Equipment/ apparatus	Supplier and model
Centrifuges	Beckman Coulter ^{TM}, Avanti ^{TM} centrifuge J-25 and J-30I
	Beckman L-70 Ultracentrifuge
	Beckman Optima ^{TM} TLX Ultracentrifuge, 120,000 rpm (rotor: TLA 100.4)
	Eppendorf centrifuge, 5417C
Rotors	8 x 50 ml angle rotor (Beckman JA20)
Incubators	Innova ^{TM} 4230, New Brunswick Scientific
	Mytron, WBK 200
Sonificator	Bandelin electronic, UW 70 type
UV/Vis spectro-photometer	Varian CARY Bio 50
Microscope	Leica, Mz12$_5$
Glass/glass Potter homogenizer	Wheaton (40 ml)
Photometer	Eppendorf biophotometer

2.2   Materials and chemicals

2.2.1 Materials

Crystallization tools (Hampton Research, Laguna Niguel, CA, USA):
Cryoloops (outer diameters 0.5, 0.7 or 1.0 mm), micro-tool set, capillary wax, cryo-protectant screen kit, Linbro plates, micro bridges, 22 mm siliconized circle cover slides, high vacuum grease

2.2.2 Buffers

Milli-Q-purified water was used for buffer preparation. Most solutions were degassed and filtered through a 0.22 μm sterile filter.

Buffers for preparation of rod outer segment (ROS) from bovine retina:

Sucrose buffer	45% sucrose in buffer P
Buffer O	20 mM BTP, 120 mM KCl, 0.2 mM MgCl$_2$, 5 mM DTT, pH 6.9
Buffer P	41 mM K$_2$HPO$_4$, 26 mM KH$_2$PO$_4$, 1 mM Mg-Acetate, 0.1 mM EDTA, 1 mM DTT, 0.1 mM PMSF, 0.1 μM aprotenin, 5 μM leupeptin, 10 mM glucose, pH 7.0

Buffers for preparation of opsin membranes:

Buffer A (Hydroxylamine buffer)	10 mM Na-Phosphate (Na$_2$HPO$_4$ x 2H$_2$O) pH 7.0, 10 mM Hydroxylamine/HCl
Buffer B (Urea buffer)	10 mM Na-Phosphate (Na$_2$HPO$_4$ x 2H$_2$O) pH 6.5, 5 M Urea
Buffer C (BSA buffer)	10 mM Na-Phosphate (Na$_2$HPO$_4$ x 2H$_2$O) pH 6.5, 2% BSA (fatty-acid free)
Buffer D (Phosphate buffer)	10 mM Na-Phosphate (Na$_2$HPO$_4$ x 2H$_2$O) pH 6.5,
Buffer E (BTP buffer)	20 mM Bis-Tris-Propane pH 7.5, 130 mM NaCl
Buffer F (10% Sucrose buffer)	20 mM Bis-Tris-Propane pH 7.5, 130 mM NaCl, 10% sucrose
Buffer G	20 mM Bis-Tris-Propane pH 7.5, 130 mM NaCl, 1% β-D-dodecylmaltoside

Solubilization buffers of opsin:

Washing buffer:	20 mM Bis-Tris-Propane pH 7.5
Solubilization buffer:	20 mM Bis-Tris-Propane pH 7.5
	1- 1.5% β-D-octylglucopyranoside

SDS-PAGE:

During all purification steps SDS-PAGE was performed to check protein purity.

Table 2.1. Buffers for SDS-PAGE

Separating gel buffer:	1.5 M Tris-HCl / SDS, pH 8.8
Stacking gel buffer:	0.5 M Tris-HCl / SDS, pH 6.8
1 x SDS sample solution:	50 mM Tris, 2% (w/v) SDS, 2.5% (v/v) β-mercaptoethanol, 0.01% (w/v) bromo-phenol blue, 10% (v/v) glycerol
10 x Electrophoresis buffer:	30 g Tris, 144 g Glycerin, 10 g SDS (for 1 liter)
Coomassie staining solution:	0.2% (w/v) coomassie blue R-250, 5% (v/v) acetic acid, 25% (v/v) ethanol
Destaining solution:	5% (v/v) acetic acid, 25% (v/v) ethanol

Table 2.2. SDS-PAGE pipetting scheme

	12% Separating gel	15% Separating gel	Stacking gel
Acrylamide/bis (30%)	2.8 ml	3.5 ml	0.26 ml
H$_2$O dest.	2.345 ml	1.645 ml	1.22 ml
1.5 M Tris-HCl/SDS, pH 8.8	1.82 ml		0.52 ml
20% Ammonium persulphate	175 µl		5 µl
TEMED (N,N,N',N'-Tetra-methylethylenediamine	28 µl		1.4 µl

Buffers for crystallization of proteins:

Sample buffer:	20 mM Bis-Tris-Propane pH 7.5,
	1% β-D-octylglucopyranoside
Precipitants:	2.8 – 3.2 M $(NH_4)_2SO_4$
	in 0.1 M MES or Na-Acetate pH 6.0

2.3   Methods

2.3.1 Isolation of rod outer segment (ROS) from retina

Under dim red light, rod outer segments were prepared from frozen bovine retinas using a sucrose gradient procedure as described [103]. 80-100 retinas were mixed with 45% sucrose in buffer P (41 mM K_2HPO_4, 26 mM KH_2PO_4, 1 mM Mg-Acetate, 0.1 mM EDTA, 1 mM DTT, 0.1 mM PMSF, 0.1 μM aprotenin, 5 μM leupeptin, 10 mM glucose, pH 7.0). The suspension was strongly shaken for 2 min and centrifuged for 5 min at 5,000 rpm. The supernatant was filtrated using cotton gauze, diluted with buffer P (1:1 ratio) and centrifuged for 10 min at 10,000 rpm. The membrane pellet obtained after centrifugation was resuspended in 26% sucrose in buffer P. The membrane suspension was applied onto a discontinuous gradient (d: 1.11, 1.13 and 1.15 g/ml) to get only a layer of rod outer segments. Hypotonically stripped disc membranes were obtained by a Ficoll floating procedure similar to the procedure described in Ref. [104] except that 2% (w/v) Ficoll instead of 5% was used. This procedure yielded osmotically intact disc vesicles with a size > 400 nm. Contamination by vesicle aggregates was removed by a 2 μm filter (Roth, Karlsruhe, Germany). Membranes were either kept on ice and used within four days without any loss of activity or stored at -80 °C until use. Rod outer segments (ROS) were resuspended in buffer O (20 mM BTP, 120 mM KCl, 0.2 mM $MgCl_2$, 5 mM DTT, pH 6.9) containing a protease inhibitor tablet (Roche). The final rhodopsin concentration was determined from ROS solubilized with buffer F containing 5 mM $MgCl_2$ and 1.15% LDAO detergent. An extinction coefficient (ε_{500}) of 40.000 $M^{-1}cm^{-1}$ was used for calculation of the rhodopsin concentration from its absorption maximum.

2.3.2 Opsin preparation

Aliquots of bovine rod outer segments (ROS, ca. 20 mg of rhodopsin) were thawed and re-suspended in 30 ml ice-cold buffer A (10 mM Na-Phosphate (Na_2HPO_4 x $2H_2O$) pH 7.0, 10 mM Hydroxylamine/HCl) under dim red light. All centrifugations were performed at 4 °C and subsequent steps were undertaken on ice. ROS were disrupted by sonification (Bandelin electronic, UW 70 type) for 10 seconds. After that, buffer A was added up to 100 ml to the ROS and the suspension was subsequently illuminated by white light for 10 minutes and centrifuged at 20,000 rpm for 20 minutes. In the light, the ROS pellet was resuspended with 35 ml of buffer B (10 mM Na-Phosphate (Na_2HPO_4 x $2H_2O$) pH 6.5, 5 M Urea) and was gently homogenized using a glass/glass Potter homogenizer. Buffer B was added up to 50 ml to the homogenized sample and the sample was centrifuged at 20,000 rpm for 20 minutes. The pellet was washed four times by resuspension with buffer C (10 mM Na-Phosphate (Na_2HPO_4 x $2H_2O$) pH 6.5, 2% BSA (fat-acid free)) and centrifugation to remove retinal oxime which was produced by the action of hydroxylamine on all-*trans*-retinal. The opsin membrane was then washed four times with buffer D (10 mM Na-Phosphate (Na_2HPO_4 x $2H_2O$) pH 6.5). It was washed one more time with buffer E (20 mM Bis-Tris-Propane pH 7.5, 130 mM NaCl). Opsin membrane concentration was determined from its absorption spectrum using $\varepsilon_{280} = 81,200$ $M^{-1}cm^{-1}$ [84]. Opsin membranes were resuspended in buffer F (20 mM Bis-Tris-Propane pH 7.5, 130 mM NaCl, 1 mM $MgCl_2$, 10% Sucrose) and stored at –80 °C until use.

2.3.3 Crystallization of opsin

Single protein crystals are needed to determine the three-dimensional structure of proteins by X-ray analysis. There are three kinds of methods to crystallize proteins; hanging-drop vapour diffusion method, sitting-drop vapour diffusion method and micro-dialysis liquid diffusion method (Figures. 2.1 and 2.2). One of them, the hanging drop method was usually used to find the crystallization point of native opsin using crystallization screen kits from Hampton Research.

Hanging drop and sitting drop method by vapour diffusion

Hanging drop: 2-5 µl of a protein solution (>1% w/v) are mixed on a circle of siliconized glass with the same volume of precipitating agents. This glass is then tightly sealed with grease upside down on a well which contains 1 ml of an appropriate precipitating agent. The drop is hanging on the glass; therefore, this method is called "hanging drop". Vapour equilibrium will be reached with time. The precipitant concentration in the reservoir and the protein drop will then be almost the same [105]. The hanging drop method is usually used to screen the crystallization of proteins.
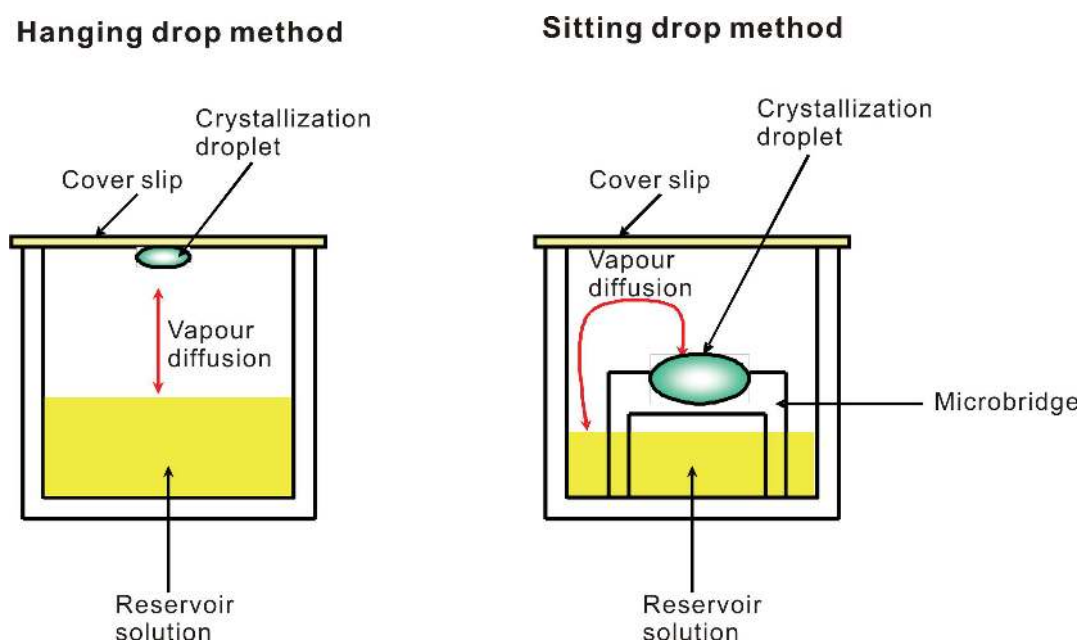
Figure 2.1. Protein crystallization: vapour diffusion method
Vapor diffusion is the standard method used for protein crystallization, because of the small volumes used, easy set-up and possibility to check crystallization. Typically, a hanging or sitting drop contains a solution of protein plus precipitant at a concentration insufficient to precipitate the protein. The drop is equilibrated against a larger reservoir of solution containing precipitant or another dehydrating agent. After sealing, the solution equilibrates to achieve supersaturating concentrations of protein and thereby induces crystallization in the drop [105,106].

Sitting drop: This method is in general used to get large single protein crystals. 20-30 µl of concentrated protein solution are usually mixed with reservoir solution and the well is sealed tightly with a glass cover slip and grease. Then vapour diffusion occurs and the concentration of precipitating agent on the concave of the bridge and the reservoir will be equilibrated with time [106].

Microdialysis by liquid diffusion

Another method to crystallize proteins is microdialysis (Figure 2.2). Zeppezauer et al. first described microdiffusion cells [107]. The microdiffusion cells, which may contain down to 10 microliters of protein, are made from 30 mm or 50 mm long capillary tubes of Pyrex glass or Plexiglas. The end of the tubes should have a smooth surface to avoid damage to the dialysis membrane. To build the microdiffusion cell, a dialysis membrane is attached to the end of the capillary with a piece of soft, transparent PVC tube. The tube has two feet to hold the membrane off the bottom. The cell is filled with protein solution and put into a scintillation bottle containing 5 ml reservoir solution. The precipitating agent is diffusing with time through the semi-permeable membrane into the protein compartment to induce crystallization.
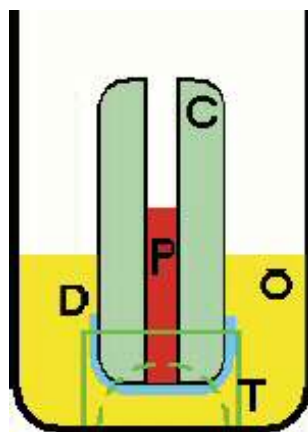
C: Capillary, P: Protein, O: Outer solution,

D: Dialysis membrane, T: Tubing with feet

Figure 2.2. Protein crystallization: liquid diffusion method
This method is also called microdialysis method. Liquid diffusion occurs between the protein solution in the capillary and the surrounding solution, leading eventually to protein crystallization [107].

The frozen opsin membranes were thawed, resuspended and centrifuged to remove the storage buffer. The membrane pellet was resuspended with solubilization buffer (20 mM Bis-Tris-Propane pH 7.5, 1 - 1.5% β-D-octylglucopyranoside) and incubated at 4 °C for 2 hours. The suspension was then centrifuged at 60,000 rpm for 10 minutes to separate solubilized opsin from the unsolubilized membrane fraction. The concentration of solubilized opsin was determined from the absorption spectrum using $\varepsilon_{280} = 81,200$ $M^{-1}cm^{-1}$. Crystallization of opsin was attempted by the sparse-matrix method [108] by using the crystal screens from Hampton Re-

search. With these screens, precipitating points of opsin for different precipitating reagents were obtained. Based on these precipitating points, a systematic crystallization of opsin was performed by the hanging drop method. Conditions yielding precipitation were chosen for further optimization of the crystallization conditions. Each hanging drop was prepared on a siliconized coverslip by mixing equal volumes (2 µl each) of solubilized opsin (5 mg/ml) and reservoir solution.

2.3.4 Structure determination by X-ray crystallography

The protein structure determination of opsin was performed as summarized in Figure 2.3 using the molecular replacement method.

Crystallizatin of opsin

⇩

Data collection

⇩

Calculation of electron density

⇩

Interpretation of electron density map
on graphics terminal

⇩

Model building of opsin molecule

⇩

Refinement

⇩

Validation and deposit
in Protein Data Bank
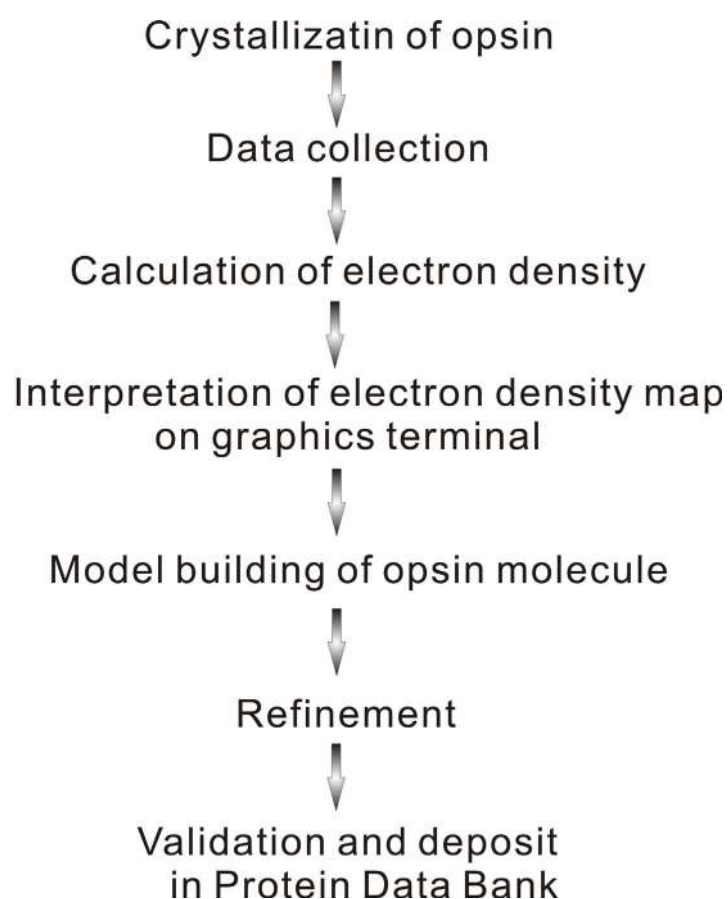
Figure 2.3. Steps in opsin crystal structure determination

Data collection

After growing crystals which were suitable for X-ray structure analysis, single crystals were mounted into cryoloops, treated with cryo-protectant consisting of 90% (v/v) reservoir solution and 10% (w/v) trehalose, and flash-frozen in liquid nitrogen. Diffraction data from native crystals were collected at low temperature (T = 100 K) in order to prevent rapid damaging of the crystal by the intense synchrotron X-ray beam. The space group and unit cell constants of the crystals were then determined from collected diffraction data.

Calculation of electron density map and model building

Initial attempts were performed by molecular replacement as implemented in the program PHASER [96]. Several sets of coordinates of different rhodopsin structures were selected from the Protein Data Bank (PDB) as search models (PDB accessions 1U19 [47], 1GZM [48] and 1HZX [109]). Using PHASER, it was first tried to determine the orientation of the search molecule by calculating the rotation function, then the translation function was calculated to find the correct position and finally a rigid body refinement was performed to obtain optimal agreement between the trial solution and the diffraction data (Figure 2.4).
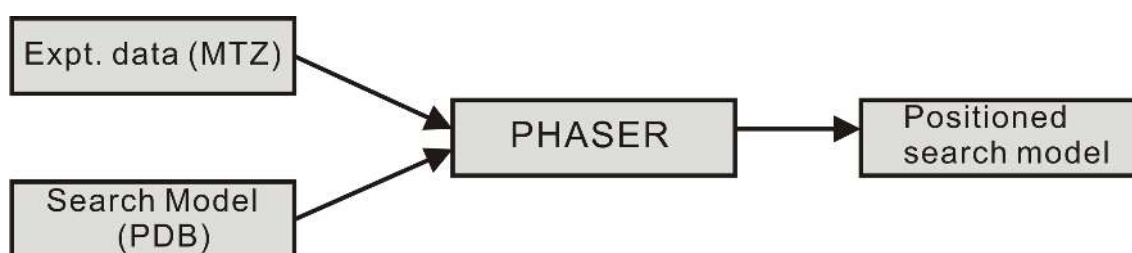
Figure 2.4. Molecular Replacement Scheme
The program PHASER uses experimental data and a known model obtained from the Protein Data Bank (PDB) to provide solutions to solve the phase problem. The solutions are produced depending on rotation function Z-score (RFZ) and translation function Z-score (TFZ), e.g. the molecular replacement method can be completely performed at more than 8 of the translation function Z-score.

The program Crystallography & NMR System (CNS) was subsequently used to calculate initial Molecular Replacement phases and to improve them by electron density modification

methods [97]. Following density modification, model building of opsin was carried out with the program COOT [98].

Refinement

After the initial model of opsin was built, it was subjected to several refinement steps using the software package CCP4 [96]. Each refinement step included electron density calculation and interpretation, which were necessary to correct or extend the actual structural model. A special feature of the program CNS is the method of "simulated annealing", which makes use of algorithms originally applied in molecular dynamics simulations and consists of a "heating" step to a nominally extremely high temperature (e.g. T = 2500 K) followed by a slow cooling sequence and final energy minimization. The advantage of this method over comparable methods implemented in other programs is its remarkably large radius of convergence, which means that "simulated annealing" allows for unusually big shifts of coordinates leading to an improvement of the fit of the model to the measured data. The program uses a classical mechanical force field, which is further extended by adding a so-called "crystallographic" energy term, which applies a "penalty" proportional to the sum of differences between observed and calculated structure factor amplitudes. The force field parameters are based on the structures of similar macromolecules or small molecules [110]. After the final refinement, the geometry of the structural model was checked by comparing bond lengths, bond angles, torsion angles and nonbonding distances with the ideal parameters, which are part of the force field used during the refinement. Regions of the structural model, which show significant deviations from the ideal geometry, were inspected using the program COOT together with the corresponding electron density maps in order to find out possible errors of the model and to correct them if possible.

Validation and model deposition

By using the programs WHAT_CHECK and PROCHECK program, the model was checked with regard to e.g. close contacts, bond distances and angles, covalent bond lengths, torsion angles and chirality between residues or ligands, distance of solvents and missing atoms [99,100]. Refinement was performed again until possible errors were minimized. The coordi-

nates obtained from final refinement were deposited in the Protein Data Bank (PDB) with accessions 3CAP.

3   RESULTS

3.1   Preparation of opsin

Experiments for protein structure determination by X-ray crystallography and NMR spectroscopy require large amounts of protein (> 10 mg). For this purpose, opsin membranes were prepared from rod outer segment (ROS) disc membranes of bovine retina by using a sucrose gradient floatation method [88,103]. In the course of membrane preparation, rhodopsin in the ROS was bleached in the presence of hydroxylamine to hydrolyze the retinal Schiff base bond and to form retinal oxime ($\lambda_{max} = 362$ nm). Retinal oxime was removed subsequently by washes of the ROS membranes with fatty acid free bovine serum albumin solution. The prepared membranes containing retinal-free opsin were solubilized with 1 - 1.5% β-D-octylglucopyranoside in solubilization buffer at 4 °C for 2 hours. After solubilization, pellet and supernatant were separated by centrifugation at 60,000 rpm for 10 min at 4 °C. The concentration of solubilized opsin was determined from the absorption spectrum using $\varepsilon_{280} = 81,200$ M^{-1}cm^{-1} (Figure 3.1A).

A)   **B)**
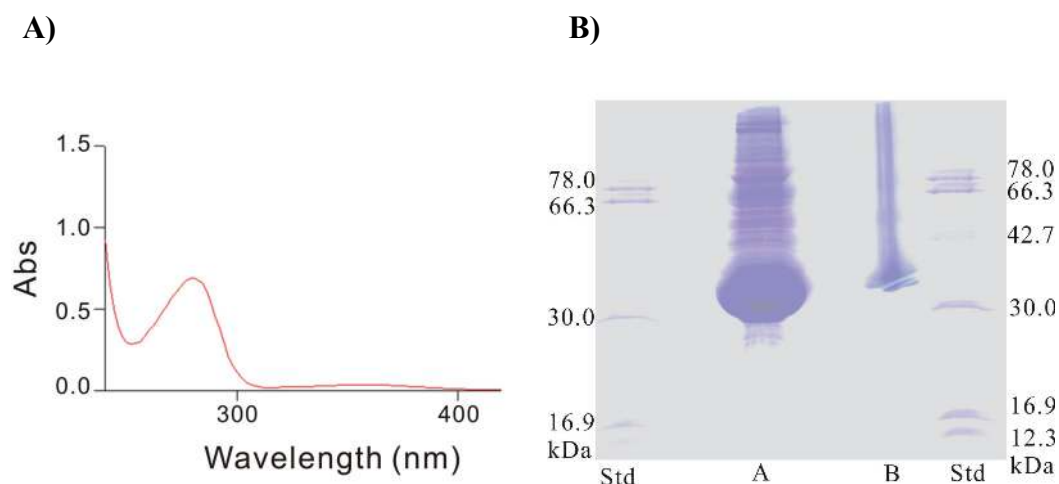
Figure 3.1. Characterization of opsin preparation
A) *UV/visible spectrum of solubilized opsin extracted from ROS membranes containing opsin.* **B)** *SDS polyacrylamide electrophoresis (SDS PAGE) of opsin (12% SDS-polyacrylamide gel and staining with coomassie blue). Lanes 1 and 4, molecular mass standards (Std); lane 2 (A): 10 μl ROS/opsin membranes (ca. 7-10 mg opsin per ml) solubilized with SDS PAGE sample buffer; lane 3 (B): 10 μl β-D-octylglucopyranoside solubilized and extracted opsin fraction (3 mg ml-1) mainly containing opsin with an apparent molecular weight around 35 kDa.*

To confirm the extraction of opsin and determination of purity, the supernatants were analyzed by 12% SDS-polyacrylamide gel electrophoresis (SDS-PAGE; Figure 3.1B). Attempts to further purify opsin by various chromatographic methods did not yield crystallizable protein.

3.2   Crystallization of opsin

Initial crystallization conditions of opsin were screened by the sparse-matrix method [108] using the corresponding crystallization screen kits of Hampton Research. After systematic screening, the crystallization conditions of opsin were narrowed down to two conditions by using the hanging drop method. 0.1 M MES buffer or 0.1 M Na-Acetate buffer (pH 5.6 - 6.0) and ammonium sulphate as precipitating agent yielded reproducibly crystals. Opsin could only be crystallized by using inorganic precipitants because the aggregation behaviour of opsin was stronger in organic precipitants like 2-methyl-2,4-pentanediole, ethylene glycol or polyethylene glycol.

A)   **B)**
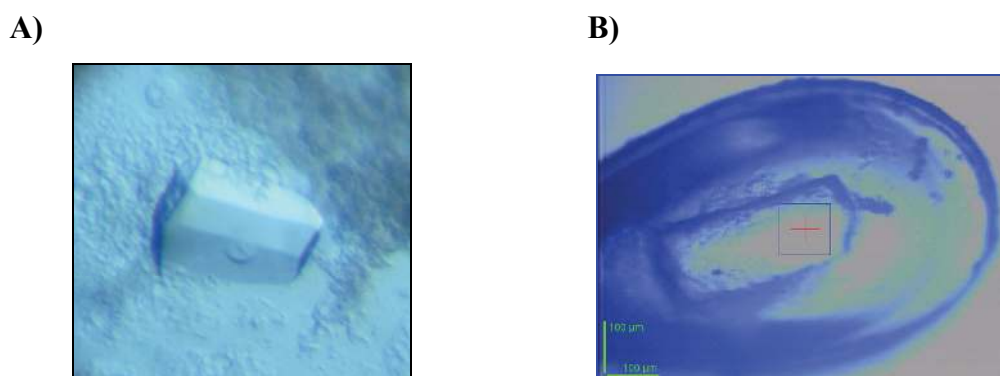
Figure 3.2. Crystals of opsin obtained with the hanging drop method
*Opsin was crystallized with 2.9 - 3.2 M $(NH_4)_2SO_4$ in 0.1 M MES or Na(OAc) pH 5.6. **A)** large single opsin crystal in hanging drop. **B)** Single opsin crystal containing 10% trehalose as cryoprotectant mounted in a cryoloop.*

The crystals obtained using inorganic precipitants were very unstable at room temperature and often grew together. Large opsin crystals could be grown by the hanging drop vapour diffusion method at 277 K using 24-well Linbro plates with 2.8 - 3.2 M ammonium sulphate as precipitant. The crystals appeared within 3 days and grew further for 5 days (Figure 3.2). Fully grown crystals had dimensions of 0.1 x 0.1 x 0.2 mm^2. Crystals grown within 7 days

were cryoprotected in 10% trehalose and frozen in liquid nitrogen for data collection using synchrotron X-ray sources.

3.3   Structural analysis of opsin

3.3.1 Data collection

Diffraction data sets of opsin crystals were collected at the synchrotrons BESSY (Elektronen-speicherring BESSY II, Helmholtz-Zentrum Berlin für Materialien und Energie GmbH, Germany) and ESRF (European Synchrotron Radiation Facility, Grenoble, France). The best data set (diffraction up to 2.9 Å) was collected at 100 K using synchrotron beamline BL 14.2 of the protein structure factory and Freie Universität Berlin at BESSY (Berlin, Germany). The crystal belonged to rhombohedral space group H3, with unit cell dimensions a = 242.92 Å, b = 242.92 Å, c = 110.42 Å, $\alpha = \beta = 90°$, $\gamma = 120°$. The asymmetric unit contains two molecules, corresponding to a crystal volume per protein mass $V_M = 8.03$ $Å^3 Da^{-1}$ [111], equivalent to a solvent content of 84.69% by volume. The diffraction image and crystal data collection statistics are shown in Figure 3.3 and Table 3.1. All images were indexed, integrated and scaled using HKL2000 [95].
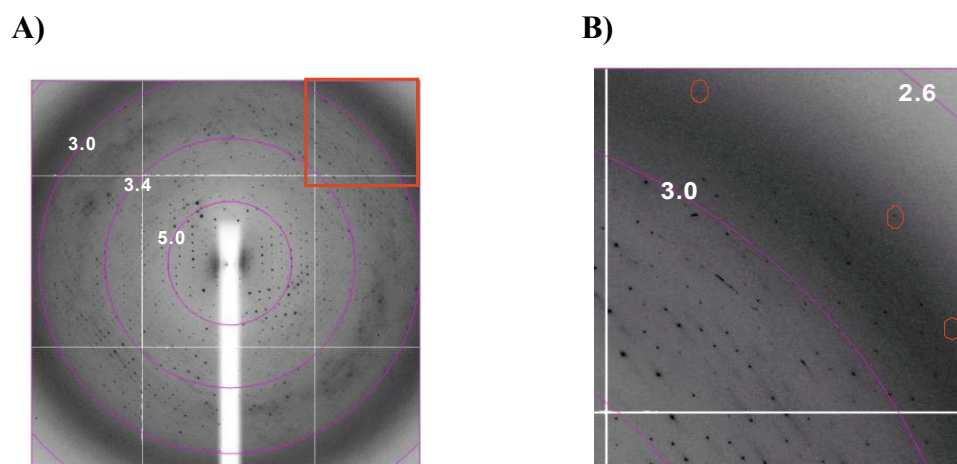
Figure 3.3. Diffraction pattern of a single opsin crystal

A) *X-ray diffraction image of opsin, collected at T = 100 K at the synchrotron beamline ID29 at ESRF in Grenoble. The outmost purple circle corresponds to 2.9 Å and the rotation range was 0.5°, exposure time 6 s.* **B)** *Close-up view of the red box shown in the image on the left.*

Table 3.1. Crystal data and data collection statistics of opsin

Data set	BESSY – Beamline BL 14.2 (native crystal)
Wavelength [Å]	0.9184
Temperature	100 K
Space group	H3
Unit cell parameters:	a = 242.92 Å
	b = 242.92 Å
	c = 110.42 Å
	$\alpha = \beta = 90°$, $\gamma = 120°$
Content of asymmetric unit	2 molecules
Matthews coefficient	$V_M = 8.03$ Å^{3}Da^{-1}
Resolution limits [Å]	121.27 - 2.9 (3.0 - 2.9)[1]
No. of observations	120,046
No. of unique reflections	53,227
Completeness [%]	99.7 (99.9)
R_{merge}[2]	0.056 (0.439)
$\langle I/\sigma(I)\rangle$	15.1 (2.0)
Mean redundancy	2.3 (2.2)

[1] Values in parentheses belong to the highest resolution shell.

[2] $Rmerge = \sum_{hkl} \sum_{j} \mid I_{hkl}(j) - \langle I_{hkl}\rangle \mid / \sum_{hkl}\sum_{j} I_{hkl}(j)$, where $\langle I_{hkl}\rangle$ is the mean intensity and $I_{hkl}(j)$ are individual intensity measurements of the reflection (*hkl*)

3.3.2 Model building and refinement of opsin structure

The molecular replacement method was used to solve the three-dimensional structure of opsin. As described in 2.3.4, several structural models of rhodopsin deposited in the PDB (PDB

accessions 1U19 [47], 1GZM [48] and 1HZX [109]) were used without cytoplasmic and extracellular regions and without the cytoplasmic half of TM6 (see Figure 3.6 below) for initial search trials. The initial electron density map of native opsin, which was calculated to 2.9 Å resolution using the density modified molecular replacement phase information, was already interpretable and used to build a structural model comprising residues Met-1 to Asn-326. Molecular replacement was achieved using CCP4 program PHASER [96] by first placing the 7TM bundle of a rhodopsin monomer (rotation function Z-score (RFZ) = 3.7; translation function Z-score (TFZ) = 9.6 as defined in PHASER) followed by a second round (RFZ = 3.9; TFZ = 21.5). Crystallographic refinement of this model with the program CNS [97], employing simulated annealing in slow cooling mode starting at 2500 K, followed by conjugate gradient minimization refinement and refinement of individual B-factors resulted in R_{work} = 0.313 and R_{free} = 0.394. This step was followed by several rounds of model correction and model extension based on $2F_o$-F_c- and F_o-F_c-maps and refinement. The final opsin model, which contains two monomers in the asymmetric unit, comprises residues Met-1 to Asn-326, 10 water molecules, N-linked oligosaccharides attached to Asn-2 and Asn-15, a palmitoyl chain at Cys-322 of each opsin molecule, and six β-D-octylglucoside molecules (Figure 3.4). Additional electron density, which should belong to the twenty-two C-terminal amino acid residues (Pro-327 - Ala-348) that are missing in the structural model, showed only poor connectivity and was therefore not interpretable (Table 3.2). Coordinates were deposited in the Protein Data Bank with accession number 3CAP. Structure analysis of opsin was done together with my peer Patrick Scheerer (Charité – Universitätsmedizin Berlin, Institut für medizinische Physik und Biophysk) who did the majority of the analysis.

Table 3.2. Statistics of crystallographic refinement (opsin data see Table 3.1).

Resolution limits in refinement [Å]	50.0 - 2.91
No. of protein non-H atoms	5504
No. of atoms / residues (two monomers per asymmetric unit)	
Protein:	5184 / 652
Others:	320 / 30
Carbohydrate residues:	
N-Acetyl-D-Glucosamine	112 /8
β-D-Mannose	44/ 4
Palmitoylchains:	
Palmitic acid	34 /2
Detergent:	
β-D-octylglucoside	120 / 6
No. of solvent molecules (water)	10
No. of reflections used in Refinement	50,253
R_{work}[3]	22.9
R_{free}[4]	26.8
Average B-factor [Å^2]: all atoms	53.7
Ramachandran plot: residues in	
most favoured regions [%]	84.4
additional allowed regions [%]	15.1
generously allowed regions [%]	0.5
outliers [%]	0.0
R.m.s. deviations from parameters of Engh and Huber (1991; Ref. [110]):	
bond lengths [Å]	0.008
bond angles [°]	1.067

$$ ^3R_{work} = \sum_{hkl} \mid F_{hkl}(obs) - F_{hkl}(calc) \mid \ / \ \sum_{hkl} F_{hkl}(obs) $$

[4]R_{free} is the same as R-factor R_{work} but calculated with 5% of the reflections that were excluded from refinement.

3.4   Overall structure of opsin

Like the known structures of bovine [47] and squid rhodopsin [32], the β_1- and β_2-adrenergic receptors [33,36,55] and the A_{2A} adenosine receptor [56], the opsin structure shows seven TM helices followed by a cytoplasmic helix (H8) running along the lipid membrane (Figure 3.4). In native opsin, H8 is terminated by two palmitoylated Cys residues (Cys-322 and Cys-323). Interestingly, only one palmitoyl group at Cys-322 could be included into the opsin model. The lack of the second palmitoyl group may be explained as described by Jackson et al. [112] by preferred removal of palmitic acid from Cys-323 during treatment with hydroxylamine in the course of opsin preparation (see Methods 2.3.2). Whereas H8 is well ordered, the C-terminal tail following H8 is very flexible and could not be resolved. Also the cytoplasmic loops (C1 – C3) of opsin and rhodopsin have significantly higher temperature factors (B-factor) than the TM segments. On the other hand, the extracellular loops and the N-terminus form a compact extracellular domain, the so-called "retinal plug"[49,113]. The "retinal plug" consists of two antiparallel β-sheets in the N-terminus (strands $\beta1$ and $\beta2$) and in E2 (strands $\beta3$ and $\beta4$). Surprisingly, the compact conformation of the "retinal plug" in the opsin structure is similar to that of rhodopsin although there is no chromophore in the retinal binding pocket. The asymmetric unit shows a crystallographic opsin dimer in which TM1 and H8 form the dimer interface. Similar dimeric arrangements were found in previous structure determinations from two dimensional and three dimensional rhodopsin crystals [68,114] and rhodopsin models [115]. Based on atomic force microscopic studies [116], a model with TM4 and TM5 as interface of a physiological rhodopsin dimer was proposed [116,117,118].

As will be outlined below, opsin shows – relative to rhodopsin – prominent structural changes in the highly conserved E(D)RY and NPxxY(x)5,6F motifs, in TM5 and TM6, and in the retinal binding pocket which shows openings between TM5 and TM6 and TM1 and TM7, respectively.
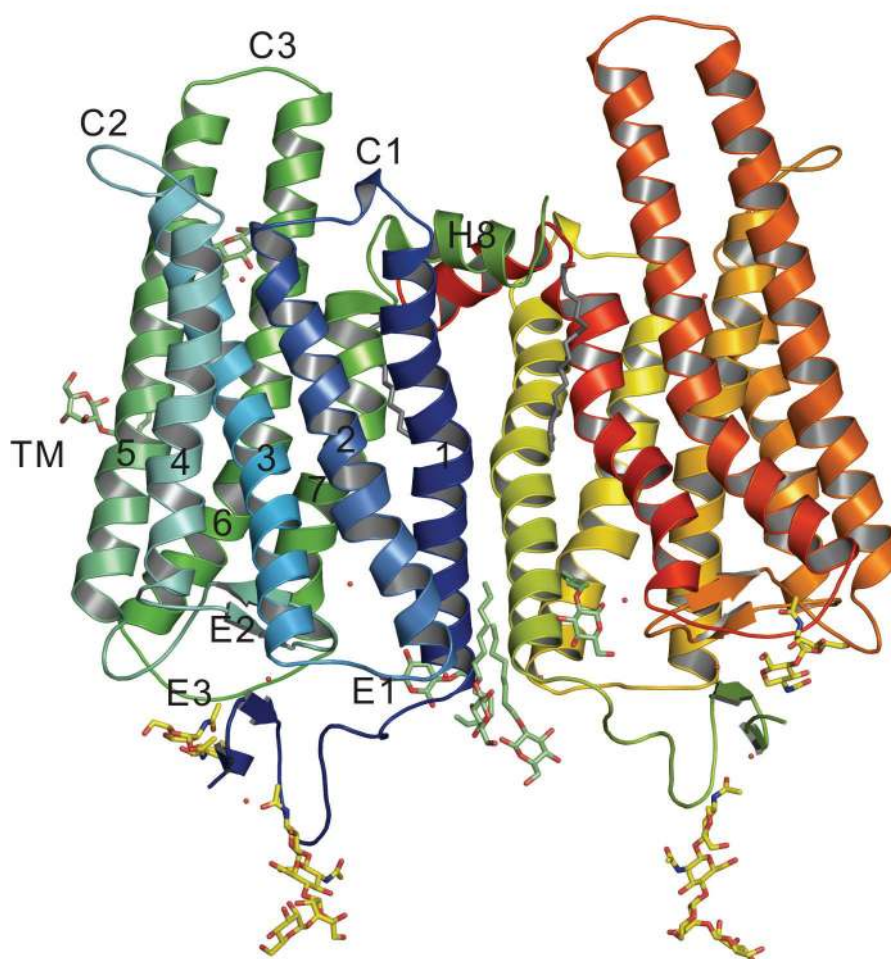
Figure 3.4. Crystal structure of opsin

Two monomers of opsin in the asymmetric unit are shown as cartoon model. Opsin is comprised of seven transmembrane helices (TM1 - TM7) connected by extracellular (E1 – E3) and cytoplasmic (C1 – C3) loops, a cytoplasmic helix (H8; following TM7), two oligosaccharides and a palmitoyl chain. Ligands are presented as stick models: four oligosaccharides consisting of N-acetyl-D-glucosamine and β-D-mannose are shown in yellow, six β-D-octylglucoside molecules in green and two palmitoyl chains in grey. Red dots indicate water molecules. 22 C-terminal amino acid residues (Pro-327 - Ala-348) are missing in the opsin model.

3.5   Helix movements in low pH opsin

The known GPCR structures are similar to the rhodopsin ground state structure and are thought to represent inactive GPCR conformations [31,32,33,36,47,48,66,67,68,109]. By engineering metal ion binding sites into rhodopsin linking TM3 and TM6 or by electron para-

magnetic resonance (EPR) and double electron-electron resonance (DEER) spectroscopy on spin-labeled rhodopsin, a 6 - 7 Å movement of TM6 relative to TM3 was found to accompany rhododopsin photoactivation [71,73,75,119].
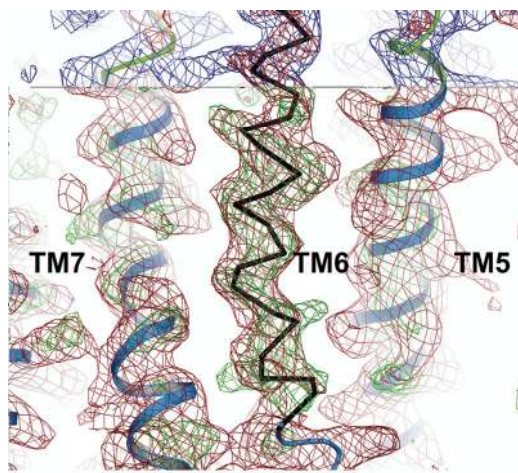
Figure 3.5. TM6 as observed in initial phase of refinement

$2F_o$-F_c and F_o-F_c electron density maps contoured at 1.0 σ (blue mesh) and 2.0 σ (red mesh), respectively. Red indicates positive different electron density. Electron density maps were calculated using data to 4.0 Å resolution and initial molecular phases, which were obtained using a truncated rhodopsin model (PBD accession 1U19) lacking both extracellular and cytoplasmic regions and the cytoplamic half of TM6. The truncated initial model is shown as a green cartoon and the first Cα trace of the cytoplasmic half of TM6 is shown as a black ribbon model.

 A similar large movement of the cytoplasmic half of TM6 is observed in the opsin structure. Figure 3.5 shows a positive difference electron density map, which was obtained using the CCP4 program PHASER [96] during initial refinement.

  Relative to the rhodopsin ground state, a movement of TM5 is observed, which occurs besides TM6 movement. A core structure composed of TM1 - TM4, on the other hand, remains almost unchanged (Figure 3.6). Figure 3.6 shows a superposition of the structures of opsin and different rhodopsin models.
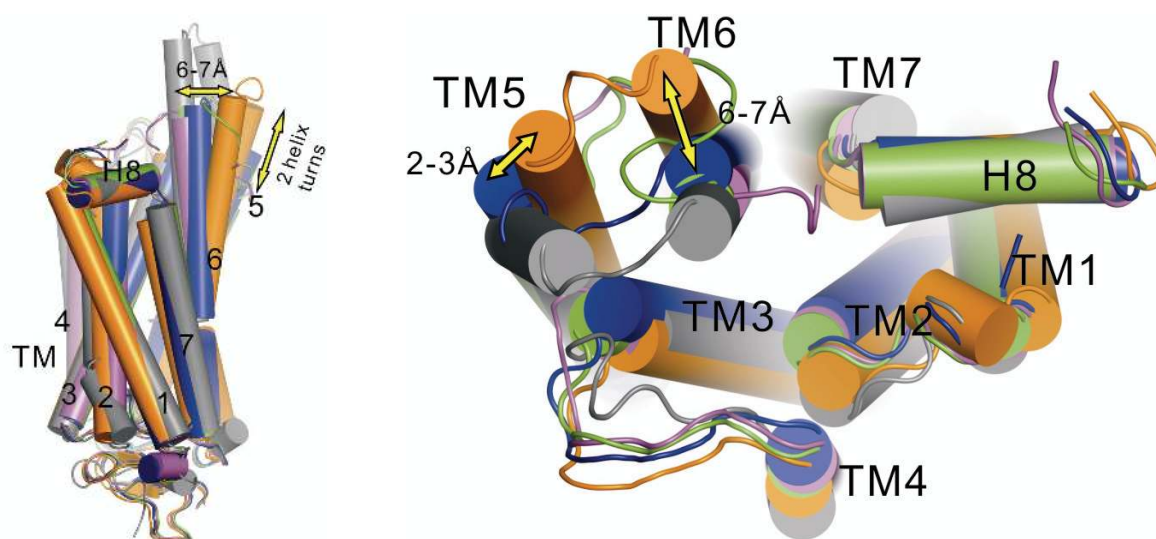
Figure 3.6. Structural comparison of opsin and different rhodopsin structures
Each structure is shown as cylindrical helix model. Bovine rhodopsin is shown in magenta (PDB accession: 1F88; [31]), green (PDB accession: 1U19; [47]), and blue (PDB accession: 1GZM; [48]), respectively. Squid rhodopsin is shown in grey (PDB accession: 2Z73; [32]). Opsin is shown in orange (PDB accession: 3CAP; [120]). Side-view and cytoplasmic view of superposed rhodopsin and opsin models are shown in left and right panels, respectively

TM5 of opsin is longer than that of rhodopsin ground state and is elongated by 1.5 to 2.5 helix turns depending on the reference model (Figure 3.6). As a result, loop C3 of opsin is shorter than that of rhodopsin. However, TM5 and TM6 in the squid rhodopsin structure adopt longer cytoplasmic helices than bovine opsin because of the larger C3 loop. At the cytoplasmic end, TM6 of opsin is tilted outward from the helix bundle by 6 - 7 Å with Trp-265 as a pivot point whereas the movement of helix TM5 toward TM6 is smaller (approx. 2 - 3 Å; Figure 3.6).

In addition, TM7 which is connected to H8 shows a slight helix movement (H8). The rigid body movements of TM5 and TM6 found in opsin are consistent with GPCR activation-dependent mobility changes of spin labels introduced into C3 of rhodopsin by site-directed spin labeling [121].

Large helix movements of TM6 relative to the rhodopsin ground state were observed directly in the crystal structure of opsin or upon light activation of rhodopsin by distance measurements using electron paramagnetic resonance (EPR) spectroscopy [71,73]. Together with the possibility to convert opsin into an active conformation by low pH as known from FTIR spec-

troscopy [91], the structure of opsin obtained under the conditions of crystallization at pH 5.6 - 6 may represent an active GPCR conformation. However, besides TM6 movement additional features involving the conserved E(D)RY and NPxxY(x)$_{5,6}$F regions, which act as switch regions, are known to indicate activating conformational changes of rhodopsin.

3.6 Changes in E(D)RY and NPxxY(x)$_{5,6}$F motifs

 The Glu(Asp)-Arg-Tyr triad or so-called E(D)RY motif is highly conserved in GPCRs [57]. In the crystal structure of rhodopsin residues Glu-134, Arg-135 and Tyr-136 are located near the cytoplasmic end of TM3. Arg-135 forms an intrahelical salt bridge with its neighbor Glu-134 and forms an interhelical salt bridge with Glu-247 on TM6 to stabilize the inactive conformation of rhodopsin (Figure 3.7A). These two salt bridges are part of a more extended hydrogen bonded network between Glu-134, Arg-135, Glu-247 and Thr-251, the so-called "ionic lock", which links the cytoplasmic segments of TM3 and TM6 (Figure 3.7B) [31,47]. In the course of rhodopsin activation and breakage of the "ionic lock", proton uptake occurs which is abolished when Glu-134 is replaced by glutamine [53,72,81,94].

 In contrast to rhodopsin, the "ionic lock" is also broken in opsin due to rearrangement of the cytoplasmic ends of TM5 and TM6. Both ends are close to each other in opsin and are locked by two new interactions, a new hydrogen bond between Arg-135 (on TM3) and Tyr-223 (on TM5) and a new interhelical salt bridge which is formed between Lys-231 (on TM5) and Glu-247 (on TM6; Figure 3.7C). To allow such a rearrangement, Arg-135 is released from Glu-134 and Glu-247, and Tyr-223 flipped over into the helix bundle due to movement of TM5. Moreover, the conserved Glu-134 rotates toward TM2 and TM4 where it does not interfere with Arg-135. The movement of TM5 towards TM6 enables stabilization of Arg-135 by Tyr-223 and stabilization of the outward tilted TM6 by the Glu-247/Lys-231 interaction, thus forming a cytoplasmic TM5/TM6 pair.

 In contrast to opsin, the crystal structure of a photoactivated form of rhodopsin shows relatively small helix movements (Figure 3.8) [68]. To obtain a structure of photoactivated rhodopsin, ground state rhodopsin was crystallized and the crystals were illuminated prior to diffraction data collection. Retinal isomerization in photoactivated rhodopsin was shown by

the absorption shift to 380 nm, the absorption maximum of Meta II. The small displacement of TM6 relative to TM3 in photoactivated rhodopsin has an effect on the "ionic lock", but does not disrupt the TM3 – TM6 interaction as in opsin (Figures 3.8 B and C).

In photoactivated rhodopsin, Arg-135 is still stabilized by Glu-134, but Arg-135 on TM3 forms a hydrogen bond with the carbonyl oxygen of Val-250 on TM6. Thus TM3 is still tethered to TM6, however in a weaker interaction as seen in the larger distances of Arg-135 and its interaction partners (Table 3.3 and Figure 3.8.).
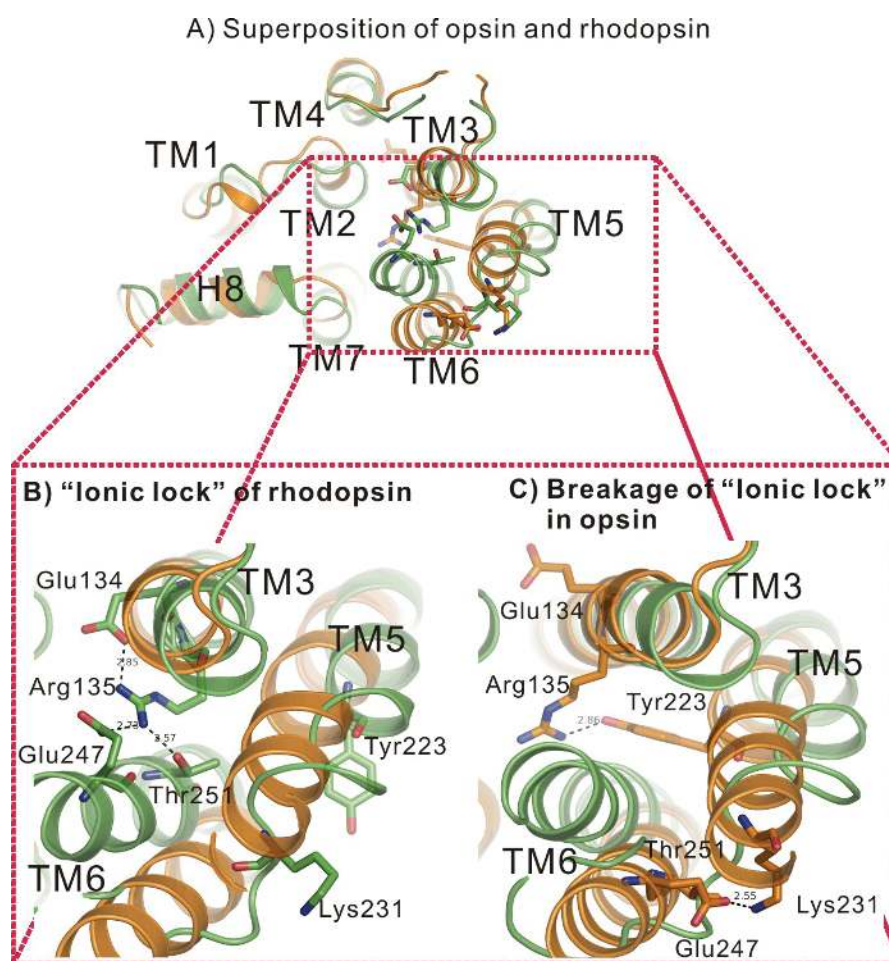
Figure 3.7. "Ionic lock" of opsin and rhodopsin

Rhodopsin is shown as green (PDB accession: 1U19; [47]) and opsin as orange (PDB accession: 3CAP; [120]) cartoon and stick model, respectively. A) Cytoplasmic view of the superimposed receptors. B) In rhodopsin (green), Glu-134 and Arg-135 on TM3 form together with Glu-247 and Thr-251 on TM6 an H-bonded network ("ionic lock") tethering TM3 to TM6. C) In opsin (orange), the "ionic lock" is broken. Instead, new hydrogen bonds are formed between Arg-135 (TM3) and Tyr-223 (TM5), and Glu-247 (TM6) and Lys-231 (TM5), respectively.
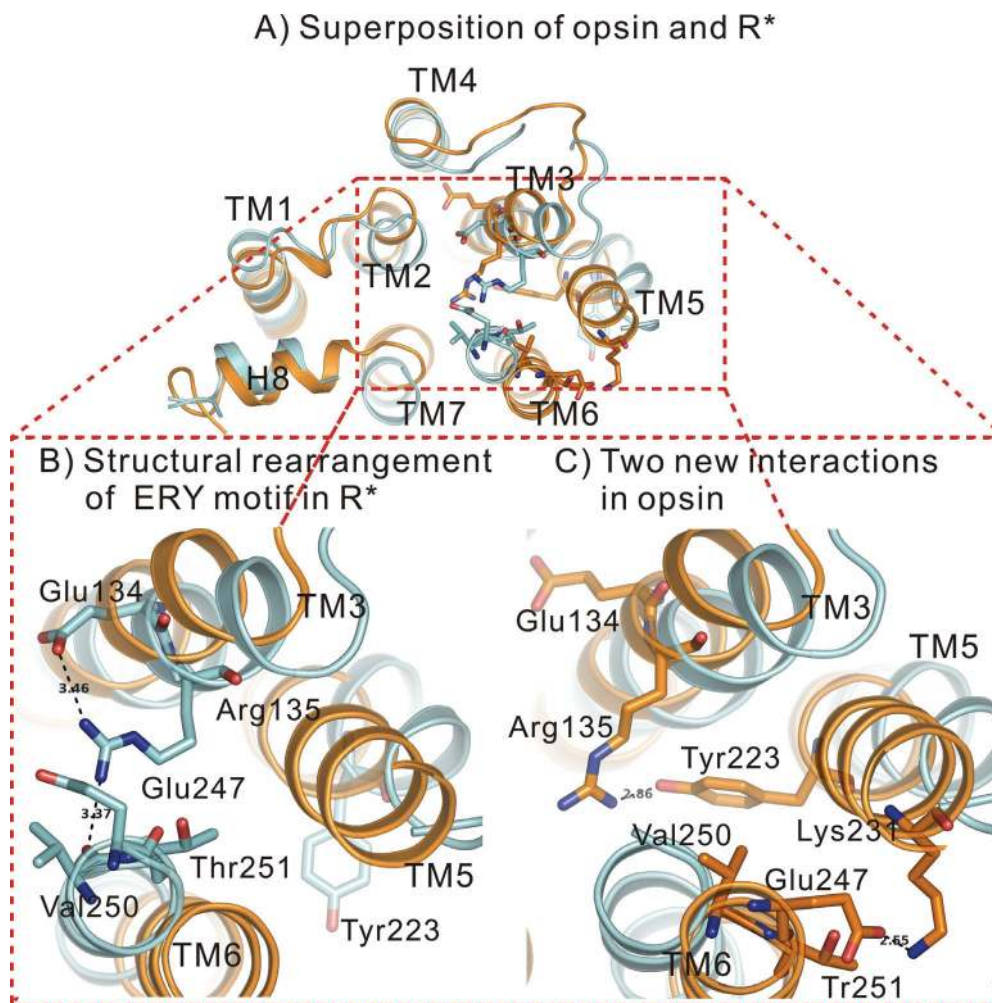
Figure 3.8. "Ionic lock" of opsin and photoactivated rhodopsin

*Photoactivated rhodopsin is shown as cyan (PDB accession: 2I37; [68]) and opsin as orange (PDB accession: 3CAP; [120]) cartoon and stick model, respectively. **A)** Cytoplasmic view of the superimposed receptors. **B)** In photoactivated rhodopsin, the "ionic lock" observed in dark state rhodopsin is replaced by a weak interaction of Arg-135 (on TM3) with carbonyl oxygen of Val-250 (on TM6). **C)** New side chain interactions in opsin (orange) enabled by the broken "ionic lock" are shown in comparison to photoactivated rhodopsin (cyan), which shows an arrangement of TM3, TM5 and TM6 similar to ground state rhodopsin.*

Besides bovine rhodopsin, the ground state of squid rhodopsin, which contains an Asp-Arg-Tyr sequence in its E(D)RY motif, shows an "ionic lock". The distances of the central Arg residues to its Asp and Glu interaction partners on TM3 and TM6, respectively, are similar to the distances in bovine rhodopsin (Table 3.3).

Table 3.3. "Ionic lock" in four different structures of rhodopsin and opsin

Inactive bovine rhodopsin (PDB accession: 1U19)				Photoactivated bovine rhodopsin (PDB accession: 2I37)			
Atoms			Distance (Å)	Atoms			Distance (Å)
Glu134	$O^{\epsilon 1}$	Arg135	NH2	2.85	Glu134	$O^{\epsilon 2}$	Arg135	NH2	3.46
Arg135	NH1	Glu247	$O^{\epsilon 1}$	2.73	Arg135	NH1	Glu247	$O^{\epsilon 1}$	4.12
Thr251	O^{γ}	Arg135	NH1	2.57	Arg135	NH1	Val250	O	3.37
					Thr251	O^{γ}	Arg135	NH1	4.02

Bovine opsin (PDB accession: 3CAP)				Squid rhodopsin (PDB accession: 2Z73)			
Atoms			Distance (Å)	Atoms			Distance (Å)
Glu134	$O^{\epsilon 1}$	Arg135	NH2	8.69	Asp132	$O^{\delta 1}$	Arg133	NH2	2.70
Arg135	NH1	Tyr223	O	2.86	Arg133	NH1	Glu256	$O^{\epsilon 2}$	2.80
Glu247	$O^{\epsilon 2}$	Lys231	N^{ζ}	2.55	Arg133	NH2	Glu256	$O^{\epsilon 2}$	3.10

TM movements in opsin relative to the rhodopsin ground state also lead to changes in the arrangement of cytoplasmic loops (especially of loop C3) as seen in a superposition of both structures in Figure 3.9A. When the models of rhodopsin (Figure 3.9B) and opsin (Figure 3.9C) in surface representation are compared, a large crevice in the cytoplasmic domain of opsin becomes obvious. This opening or "blossoming" of the receptor may be a prerequisite for binding of the G protein to the active receptor state. The crevice which contains Arg-135 at its floor could be the binding site for the C-terminus of the Gα subunit as previously proposed from binding assays [122,123,124]. Further, residues in loops C2 and C3 are important to enable coupling to the G protein [123,125,126]. By the significant rearrangement of loop C3 due to helix movement of TM5 and TM6, some residues in C3 are exposed, i.e. Leu-226, Phe-228 and Thr-229 on TM5, Ser-240 in C3, and Thr-242, Thr-243 and Met-253 on TM6 [127].

Figure 3.9. Arrangement of cytoplasmic loops in inactive rhodopsin and opsin
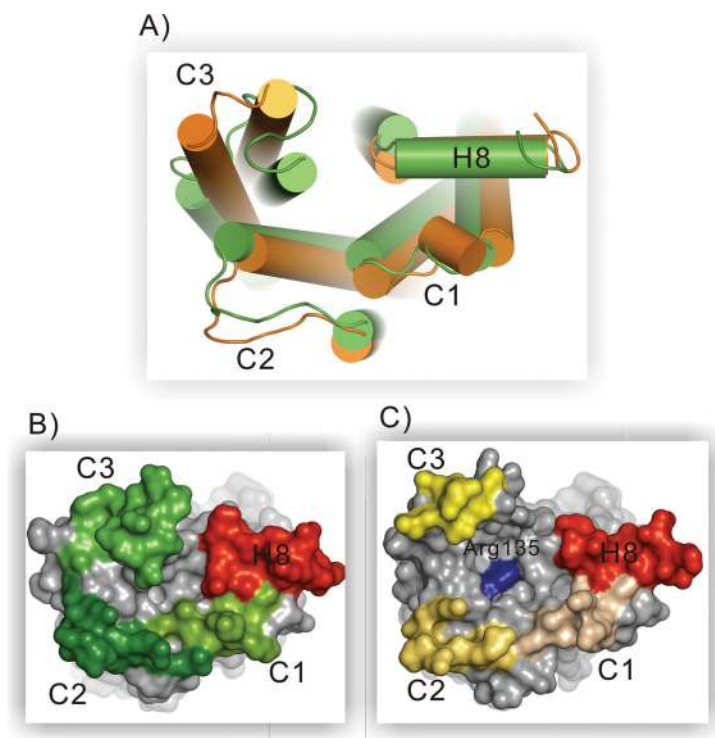**A)** *Rhodopsin (green; PDB accession: 1U19; [47]) and opsin (orange; PDB accession: 3CAP; [120]) are superimposed as cylindrical cartoon models, respectively, with view from the cytoplasm to illustrate the arrangement of loops C1 – C3.* **B)** *Cytoplasmic view of inactive rhodopsin shown in surface representation with loops C1 – C3 highlighted in different green colors.* **C)** *Cytoplasmic view of opsin shown in surface representation with loops C1 – C3 highlighted in different orange colors. Helix H8 is shown in red. The large groove observed only in opsin contains Arg-135 (shown in blue) at its floor.*

Besides the E(D)RY motif, most GPCRs contain the NPxxY motif in TM7 or an NPxxY(x)$_{5,6}$F motif, with the additional Phe residue in H8 (see Figure 1.2). The NPxxY(x)$_{5,6}$F motif was identified – like the E(D)RY motif – to be an important element for the interaction of activated GPCR and G protein [77,128]. Biochemical and biophysical studies indicated that a structural rearrangement of the NPxxY(x)$_{5,6}$F motif occurs upon receptor activation [77,129,130]. As seen in Figure 3.10, a large structural change of the NPxxY(x)$_{5,6}$F motif is also found in the opsin structure. In rhodopsin an interaction between the aromatic side chains of Tyr-306 and Phe-313 is observed. This interaction is broken in the opsin structure because of the TM6 tilt outward of the helix bundle, allowing the Tyr-306 side chain to rotate into the helix bundle. Tyr-306 thereby blocks TM6 from moving back toward TM3 to adopt an inactive conformation corresponding to the rhodopsin ground state (Figure 3.10B).
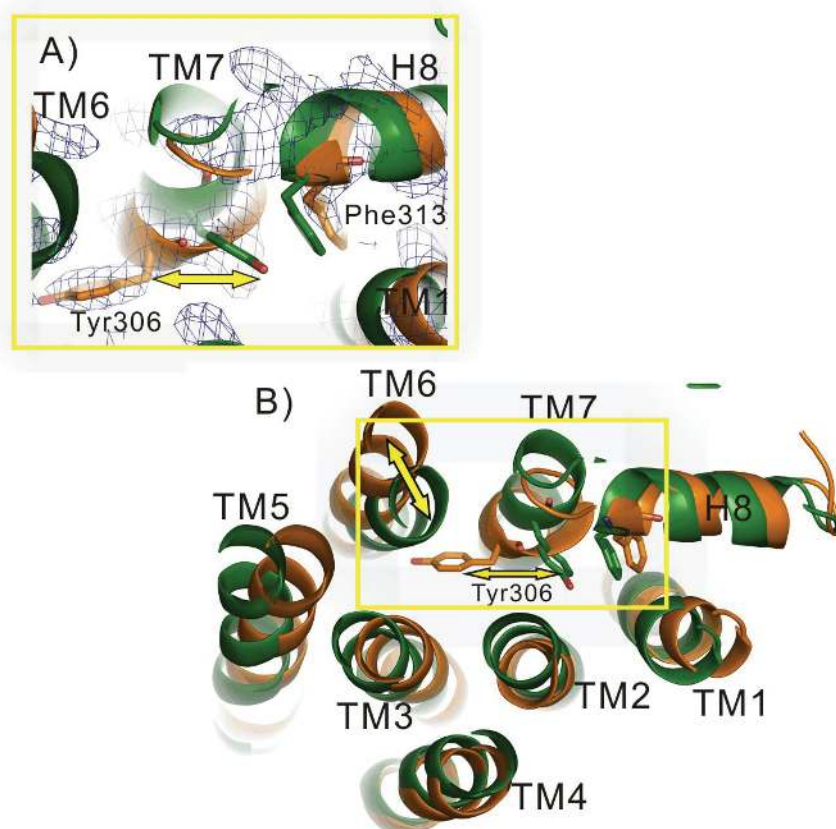
Figure 3.10. Structural changes in the NPxxY(x)$_{5,6}$F region of rhodopsin vs. opsin

A, B) *Cytoplasmic views of rhodopsin and opsin shown as green and orange cartoon models, respectively. The side chains of the NPxxY(x)$_{5,6}$F residues Tyr-306 and Phe-313 are shown as stick models. A) Close-up view of Tyr-306 and Phe-313 with electron density map. In opsin, the electrostatic interaction between Tyr-306 and Phe-313 is broken and Tyr-306 is rotated inside the helix bundle to stabilize TM6 in its outward position. Yellow arrows indicate structural changes of TM6 and the side chain of Tyr-306 in rhodopsin vs. opsin.*

3.7   Alterations in the retinal binding site

A comparison of the rhodopsin and opsin structures shows three main alterations in the retinal binding pocket around the Schiff base, the C19 methyl group of retinal and the β-ionone ring of retinal (Figure 3.11). A salt bridge between Glu-113 and the protonated Schiff base (Lys-296) is observed in rhodopsin. This salt bridge breaks in the course of rhodopsin activation [131]. Similarly, Glu-113 and Lys-296 are thought to form a salt bridge in opsin to constrain the inactive receptor conformation. Removal of either charge consequently causes constitutive activity of the receptor, i.e. enhanced activity in the absence of an activating ligand

[92,132,133]. Breakage of the salt bridge in such opsin mutants caused changes of the helix bundle at the cytoplasmic surface as observed by electron paramagnetic resonance spectroscopy [132]. The opsin crystal structure also shows a broken salt bridge in the retinal binding pocket. The side chain of Lys-296 appears to be very flexible and not stabilized by the counterion or possible water clusters. The distance between the counterion (Glu-113) and the ε-amino group of Lys-296 increased to ca. 6.5 Å in the opsin model. Interestingly, Glu-181 is moved toward Lys-296 by ca. 4.0 Å, whereas Glu-181 in rhodopsin is positioned 7.1 Å away from Lys-296 (see Table 3.4).

Table 3.4. Distances between Lys-296 and Glu-113 or Glu-181 in rhodopsin and opsin

	Lys-296 (rhodopsin ground state/ opsin)
Glu-113	3.45 / 6.50 Å
Glu-181	7.14 / 3.97 Å

 The bulky side chain of Phe-293 adjacent to the Schiff base is rotated away from the helix bundle, thereby giving access to the retinal binding pocket (see below). Further, Tyr-191, which is part of the "retinal plug" and in rhodopsin close to the C19 methyl group of retinal, shows a rotamer change in opsin and is shifted backward. In rhodopsin, the C20 methyl group, which is attached to C13, interacts with Trp-265 and contributes to the twist around the C11-C12 bond. The orientation of the β-ionone ring is locked in rhodopsin in a set of hydrophobic residues comprising Phe-212, Phe-261 and Trp-265 [47]. In opsin, the two bulky hydrophobic residues Phe-261 and Trp-265 (on TM6) are moved due to the outward tilt of TM6. The side chains are shifted towards the position which is occupied in rhodopsin by the β-ionone ring.

 The structures of Lumi and a late photoactivated rhodopsin state have been reported. Unfortunately the crystallographic model of photoactivated rhodopsin, which was obtained from illuminated rhodopsin crystals showing spectral characteristics of an active Meta II state, does not contain retinal due to the poor resolution of the structure. In Figure 3.12 superpositions of rhodopsin, opsin, photoactivated rhodopsin and Lumi structures are presented [47,67,68,120]. Both, the Lumi structure and the structure of photoactivated rhodopsin do not show gross

structural features indicative for an active conformation. However, small alterations in the position of side chains of hydrophobic Met-207 and Trp-265 residues adjacent to the β-ionone ring are observed in Lumi. Compared with rhodopsin, photoactivated rhodopsin shows small rotamer and backbone changes in the retinal binding site, i.e. for residues Glu-113, Glu-181, Tyr-191, Met-207, Phe-212, Trp-265 and Phe-261.
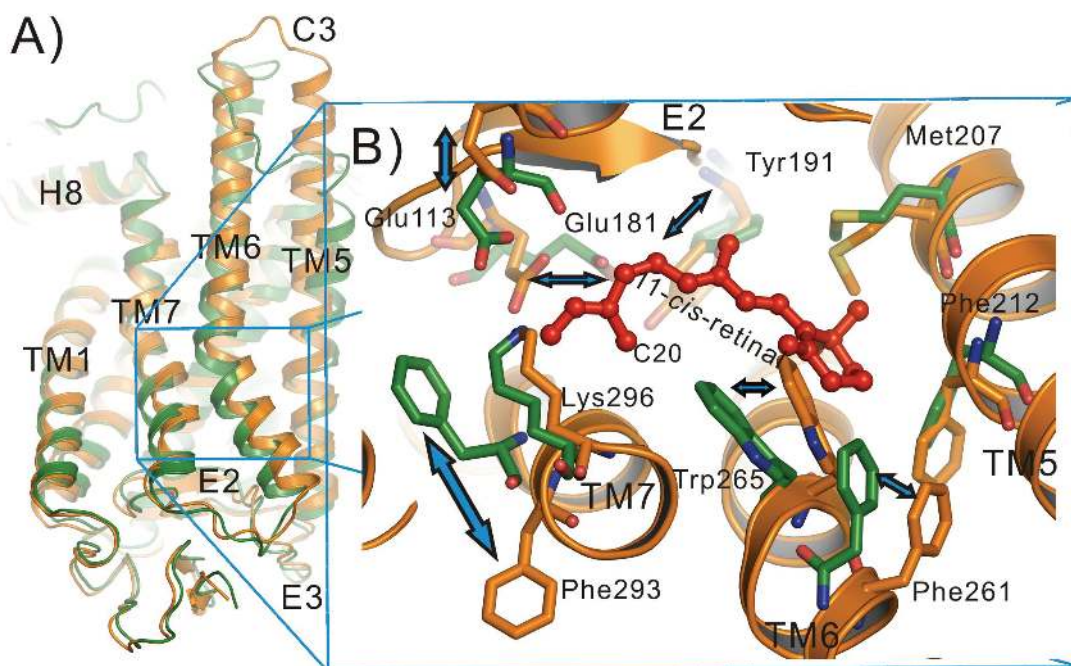
Figure 3.11. Retinal binding pocket in rhodopsin and opsin

A) Superposition of rhodopsin (green) and opsin (orange) structures, presented as cartoon models. B) Close-up view of retinal binding pocket. Amino acid residues are shown as stick model whereas retinal is shown as red ball and stick model. Blue arrows indicate change of position of residues in rhodopsin vs. opsin.
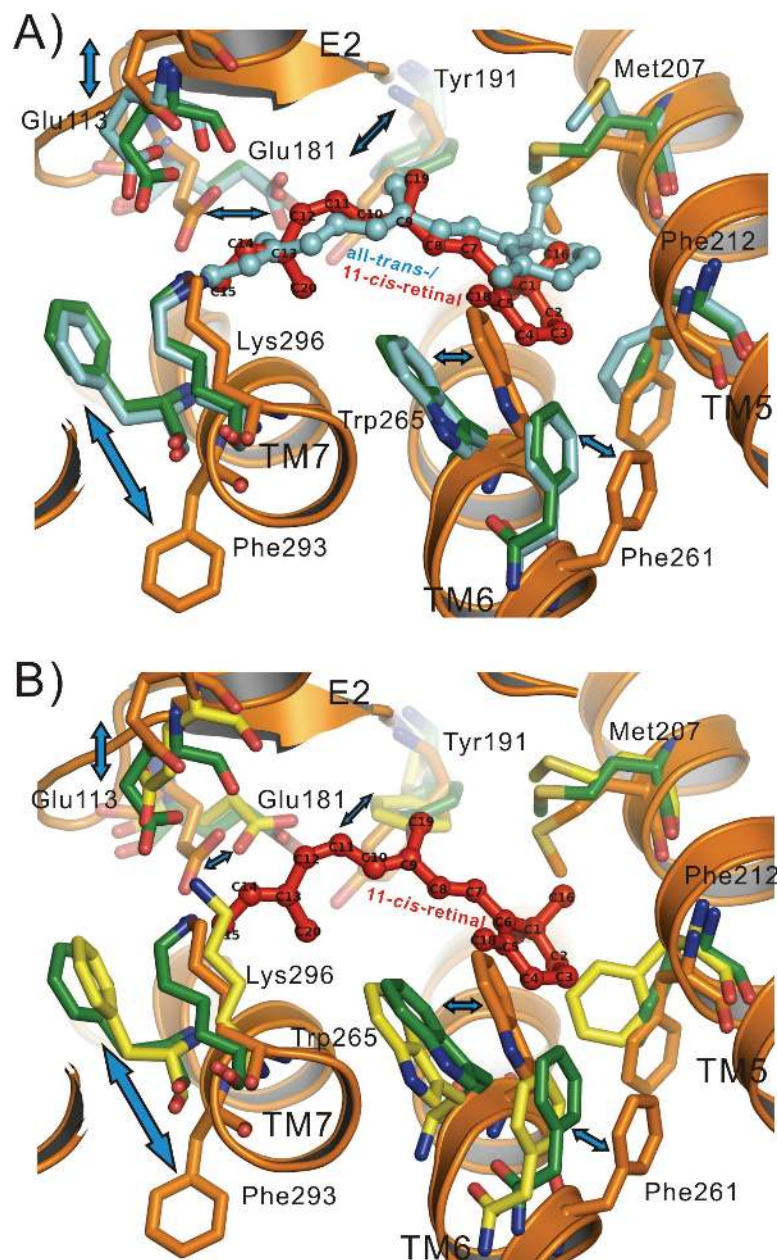
Figure 3.12. Retinal binding pocket in rhodopsin, lumirhodopsin and opsin

A) *Superposition of rhodopsin (green; [47]), lumirhodopsin (Lumi, cyan; [67]) and opsin (orange; [120]) crystal structures (shown as cartoon model); residues close to retinal are in stick representation.* **B)** *Superposition of rhodopsin (green; [47]), photoactivated rhodopsin (yellow; retinal not resolved; [68]) and opsin (orange; [120]). Retinal is shown as ball and stick model. Blue arrows indicate structural changes of amino acid side chains.*

3.8   Two openings of retinal binding pocket

In contrast to all other known rhodopsin crystal structures, the opsin structure reveals two openings of the retinal binding pocket (Figures 3.13 - 3.15). The openings are located in the extracellular half of TM1/TM7 and TM5/TM6, respectively. The opening is made possible by structural changes of membrane-facing hydrophobic residues. In addition, helix movements are observed at the cytoplasmic ends of TM5, TM6 and TM7 as shown in Figure 3.6. Four proline residues, Pro-215, Pro-267, Pro-291 and Pro-303, which are located in transmembrane helices, are highly conserved in class A GPCRs. Interestingly, three proline residues except Pro-303 are located in or adjacent to the two openings of the retinal binding site, indicating a role in the opening process.
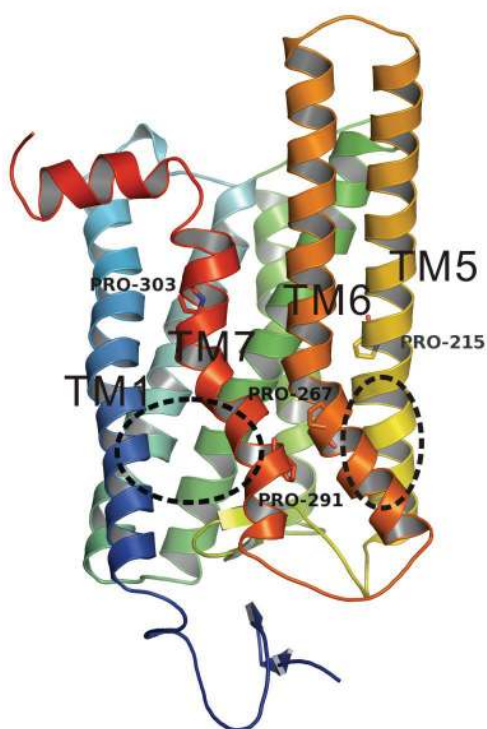
Figure 3.13. Proline residues in transmembrane helices of opsin

The opsin structure is presented as cartoon model. Highly conserved proline residues Pro-267 on TM6; Pro-291 on TM7 and Pro-303 on TM7 are shown as stick model. Black dotted circles indicate position of two openings of the retinal binding site.

Figure 3.14 shows a comparison of surface models of rhodopsin and opsin viewing TM1 (shown in cyan) and TM7 (shown in blue). In opsin an opening is seen, which is formed by rearrangement of Leu-40 and Tyr-43 on TM1, Met-183 in loop E2, Thr-289, Ile-290, Phe-293 and Phe-294 on TM7 (Figure 3.14C). Two residues, Phe-293 and Phe-294, show significant

rotamer changes and small backbone movements to induce the formation of the opening in opsin.
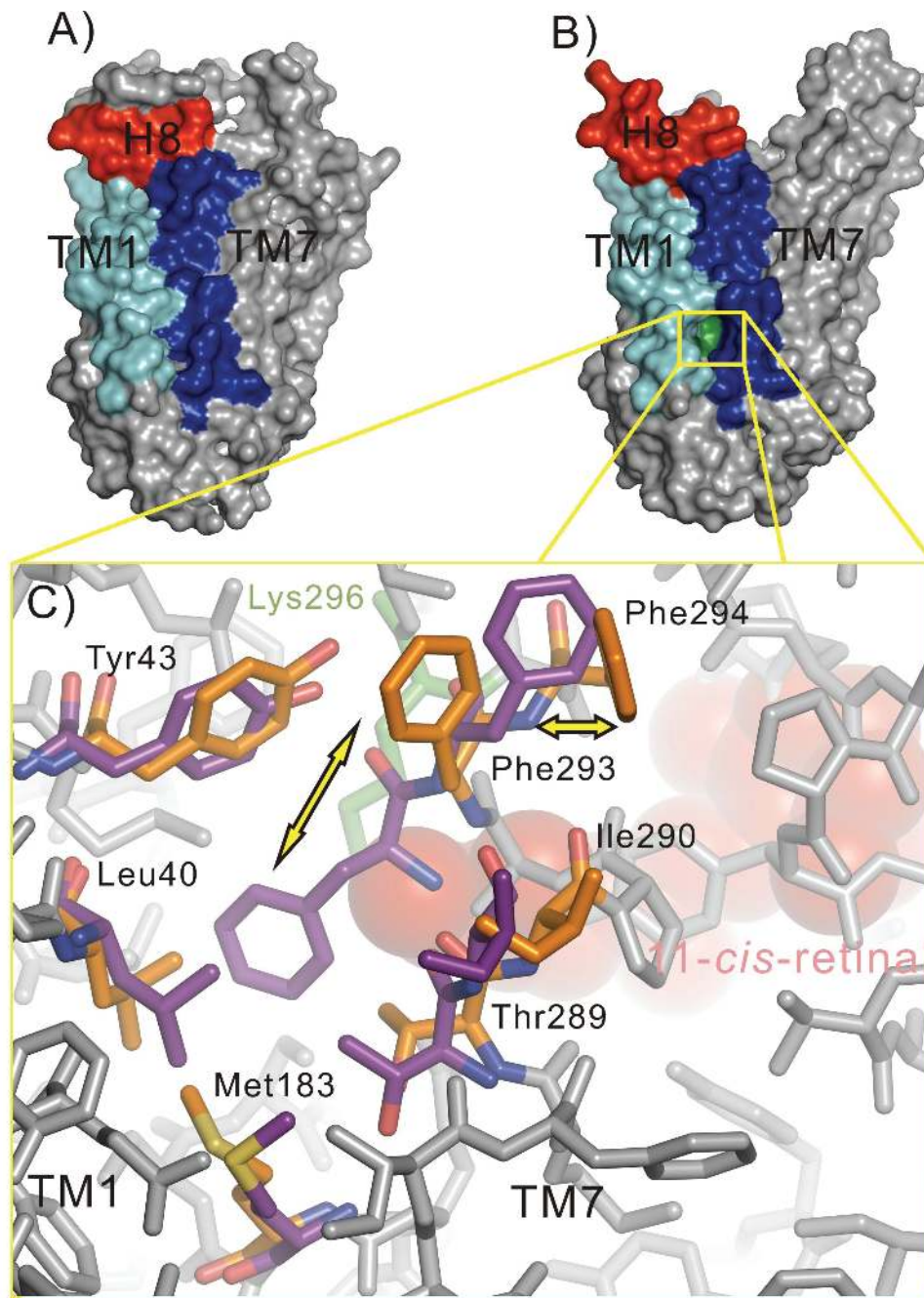
Figure 3.14. Opening of the retinal binding site between TM1 and TM7

Surface models of A) rhodopsin and B) opsin. In opsin an opening of the retinal binding site (presented as green surface) is observed between TM1 (cyan) and TM7 (blue); H8 is shown in red. C) Close-up view of opening; superposition of rhodopsin and opsin; side chains are shown as magenta (rhodopsin) and orange (opsin) stick models, respectively. 11-cis-retinal is shown as red sphere model. Yellow arrows indicate structural changes of amino acid residues.

A second opening of the retinal binding site in opsin is observed between TM5 and TM6, the two helices which show largest helix movements when opsin and rhodopsin structures are compared (Figure 3.15). Small backbone movements of Val-204, Ile-205 on TM5 and Phe-273 on TM6, different side chain orientations of Phe-208, Phe-212 on TM5 and Phe-276 on TM6 enable formation of the opening (Figure 3.14C). Interestingly, a weak hydrogen bond between Glu-201 on TM5 and Gln-279 in loop E3 observed in rhodopsin is broken in opsin. Breakage of the Glu-201 / Gln-279 hydrogen bond likely is concomitant with formation of the second opening.
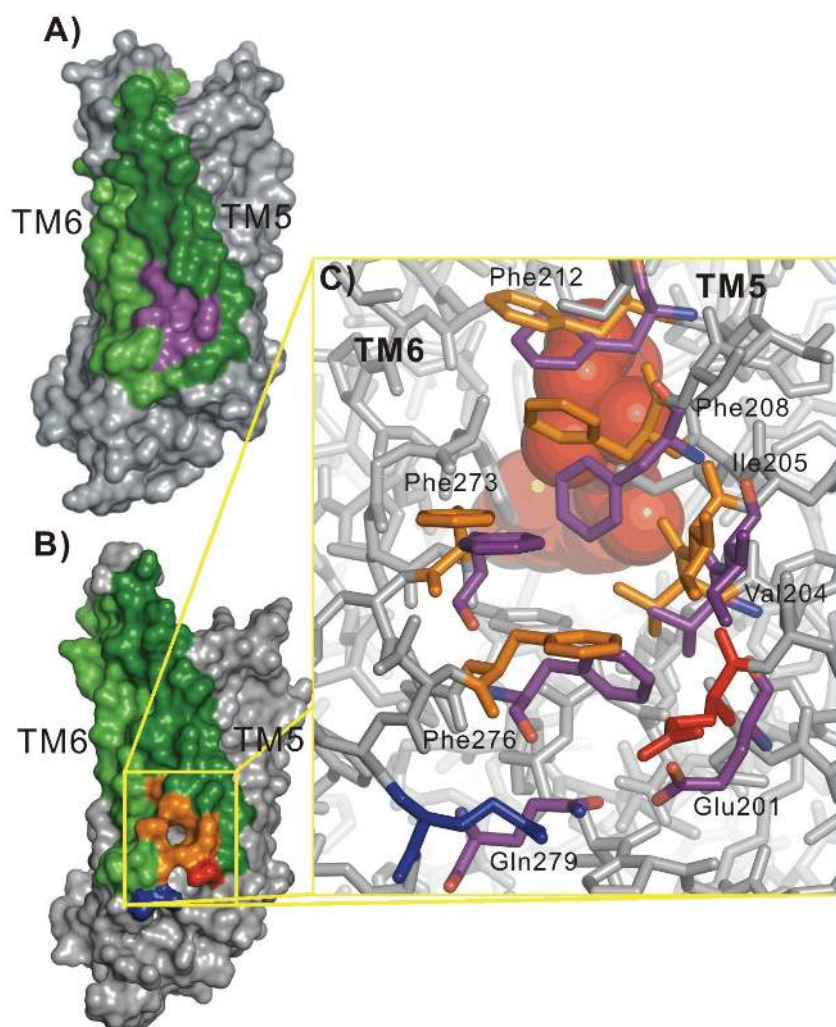
Figure 3.15. Opening of the retinal binding site between TM6 and TM5

*Surface models of **A)** rhodopsin [47] and **B)** opsin [120]. The second opening of the retinal binding site in opsin is observed between TM5 (forest green) and TM6 (green) and shown as orange surface representation. **C)** Close-up view of opening; superposition of rhodopsin and opsin; amino acid side chains are shown as magenta (rhodopsin) and orange (opsin) stick models, respectively. 11-cis-retinal is shown as red sphere model. Side chains of Glu-201 and Gln-279 in opsin are shown as red and blue stick model, respectively.*

4   DISCUSSION

The crystal structure of rhodopsin solved in the year 2000 by Palczewski and colleagues represents a hallmark in GPCR research. The last two years now revealed several new GPCR structures including that of the ligand-free GPCR opsin presented in this work. Among the known rhodopsin crystal structures are: i) dark state rhodopsin (PDB accessions: 1F88; [31], 1GZM; [48], 1U19; [47]), ii) bathorhodopsin (Batho, PDB accession: 2G87; [66]) lumirhodopsin (Lumi; PDB accession: 2HPY; [67]), a photoactivated rhodopsin state (PDB accession: 2I37; [68]) and opsin (PDB accessions: 3CAP; [120] and 3DQB; [134]). First insight into the Meta I state was provided by low resolution electron crystallography (EMD accession: EMD-1079; [70]). Further, the high resolution structures of squid rhodopsin (PDB accession: 2Z73; [32]), the β1-AR (PDB accession: 2VT4; [33]), the β2-AR (PDB accession: 2RH1; [36]) and the A_{2A} adenosine receptor (PDB accession: 3EML; [56]) have been solved.

All GPCR structures show the same overall fold with little differences in TM helix arrangement. Small variations are seen as receptor specific features. Among the different receptor conformations observed in these structures, the difference between rhodopsin and opsin is the largest. This is expressed in TM6/TM5 helix motion, breakage of the "ionic lock" between TM3 (E(D)RY motif) and TM6, breakage of the electrostatic interaction between Tyr-306 and Phe-313 (NPxxY$(x)_{5,6}$F motif), and reorganization of some amino acid side chains in the retinal binding pocket. An explanation might be that rhodopsin represents a maximally inactivated GPCR, whereas the opsin structure might be close to an active conformation as in Meta II. There are several lines of evidence which justify this view.

4.1   Evidence for an active opsin* conformation

1) The active conformation of metarhodopsin and opsin is dependent on pH and the lipid environment

Detergent and low pH are known to facilitate formation of the active Meta II conformation, whereas rhodopsin and opsin in the native membrane are inactive under physiological condi-

tions [81,87]. However, in the native membrane, low pH can force proton uptake by opsin and thus formation of a state which shows a FTIR spectroscopic signature that is comparable to active Meta II [91]. The spectroscopic results argue for a similar conformation of Meta II and ligand-free active opsin (opsin*), which is forming in disk membranes with a pK_a of ca. 4. In agreement with this observation, the E134Q opsin mutant showed increased activity towards the G protein, suggesting that removal of the negative charge at Glu-134, e.g. by protonation, facilitates formation of the active receptor conformation [91,92,135]. In rhodopsin, the energy which is provided by photon absorption and used for retinal *cis/trans* isomerization shifts the pK_a for proton uptake and formation of the Meta II conformation to higher values compared with formation of the opsin* conformation [136,137].

2) Meta II and opsin* show a movement of TM6 at the cytoplasmic surface

 Multiple lines of evidence show that TM6 motion relative to TM3 is decisive for forming the active receptor conformation. The restriction of the movement of TM6 relative to TM3 by engineered disulfide bridges [71] or Zn^{2+} binding sites and Zn^{2+} chelation [75] abolished transducin activation. The tilt movement of TM6 outward of the helix bundle upon light-induced rhodopsin activation was confirmed by EPR [71,73,119] and fluorescence spectroscopy [138]. Recent EPR spectroscopic data using the DEER method identified a movement of TM6 by 5-6 Å [73]. These changes of the 7TM bundle due to receptor activation – and initiated in the retinal binding site – indicate an opening or 'blossoming' of the GPCR [139]. Such a blossomed receptor is also seen in the structure of the 'blossomed' opsin* molecule (see Figure 3.9). The cytoplasmic part of opsin* and Meta II may thus be very similar.

3) Changes in microdomains containing the E(D)RY and NPxxY(x)₅,₆F motifs

 The role of the active cytoplasmic conformation of Meta II in catalyzing nucleotide exchange in the Gα subunit was investigated by peptide competition experiments [124], mutagenesis [94,126,135,140,141,142], and biochemical assays [143]. These studies showed that some key residues (e.g. Glu-134 and Arg-135 on TM3) in the cytoplasmic surface are important for G protein interaction. The disruption of the intrahelical salt bridge between Glu-134 and Arg-135 (the charge pair in the conserved E(D)RY motif in TM3) altered receptor-catalyzed GDP release from the G protein [86]. The residues of the E(D)RY motif are part of an extended

hydrogen bonding network known as "ionic lock", which stabilizes TM3 (Arg$^{3.50}$, Ballesteros-Weinstein numbering) and TM6 (Glu$^{6.30}$) in the inactive ground state of rhodopsin (Figure 4.1). Arg-135 does not only form an intrahelical salt bridge to Glu-134, it also forms interactions with Glu-247 and Thr-251 (in TM6) [31,32,47] (Figures 4.1A, B, D and E). These interactions are broken when TM3 and TM6 separate upon receptor activation.

In the β_2-AR, conformational changes of the "ionic lock" during activation of the receptor by agonists have been demonstrated by fluorescence spectroscopic studies [144]. The data are in agreement with a broken "ionic lock" as seen in the opsin structure. However, the structures of β-adrenergic receptors and adenosine receptor in their ligand-bound state (antagonist cyanopindolol, β_1-AR; partial inverse agonist carazolol, β_2-AR; antagonist ZM-241,385, A_{2A}-adenosine receptor) show – relative to inactive rhodopsin and active opsin* – only a partially broken "ionic lock". The distance between TM3 and TM6 and thus between Arg$^{3.50}$ and Glu$^{6.30}$ is increased. Glu$^{6.30}$ (the equivalent to Glu-247 of opsin) is completely released from Arg$^{3.50}$, but the intrahelical interaction between Glu$^{3.49}$ and Arg$^{3.50}$ of the E(D)RY motif is still intact (Figure 4.1). The partially broken "ionic lock" facilitates further TM6 motion and may explain why the antagonist-bound GPCRs (β_1-AR, β_2-AR and A_{2A}-adenosine receptor) display some basal activity but do not feature the completely active conformation of the receptors [55]. In contrast, rhodopsin ground state structures (bovine and squid) show the full "ionic lock" which firmly stabilizes the inactive receptor state (Figure 4.1, see table 3.3).

Previous mutagenesis, fluorescence and EPR studies [71,72,73,86,135,144] suggested that the disruption of the "ionic lock" as observed in the opsin* structure is induced by a rotational and translational movement of TM6. The opsin* crystal structure revealed that due to TM6 and TM5 movement the "ionic lock" residues can engage in new interactions, i.e. between Arg-135 in TM3 and Tyr-223 in TM5 (Arg135-Tyr223), and Lys-231 in TM5 and Glu-247 in TM6 (Lys-231 & Glu-247) (see Figures 3.7, 3.8 and 4.1A, B, D and E). The breakage of the "ionic lock" accompanied with helix movement leads to rearrangement of the cytoplasmic loops to form a large cytoplasmic crevice where the G protein can bind for catalytic nucleotide exchange. Importantly, the key residue Arg-135 (Arg$^{3.50}$) stabilized by Tyr-223 (Tyr$^{5.58}$) can now display a new role in interaction with the G protein (see below).

Rhodopsins

A) TM6, TM7, H8, Glu^6.30, Tyr^5.58, Arg^3.50, TM1, TM2, TM5, Tyr^3.51, Glu^3.49, TM3

B) TM6, TM7, H8, Glu^6.30, Tyr^5.58, Arg^3.50, TM1, Tyr^3.51, TM2, TM5, TM3, Glu^3.49

C) Phe^7.60, H8, TM6, Tyr^7.53, Asn^7.49, Pro^7.50, TM1, TM7

Bovine rhodopsin ground state (PDB: 1U19)
Bovine photoactivated rhodopsin (PDB: 2I37)
Bovine opsin (PDB: 3CAP)
Squid rhodopsin ground state (PDB: 2Z73)
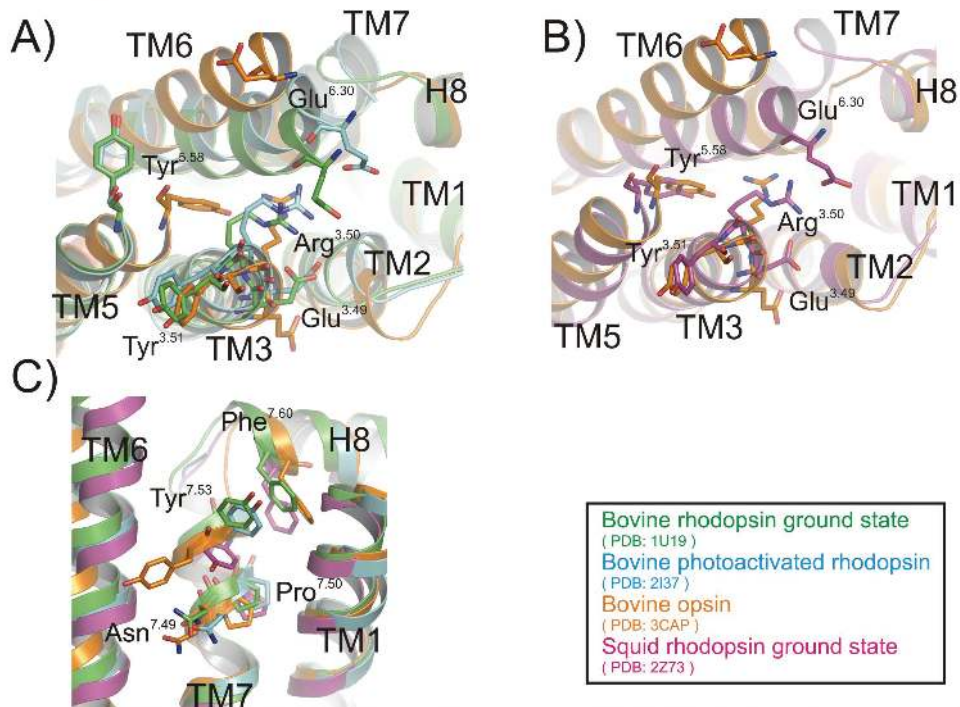
β-Adrenergic receptors & A$_{2A}$-Adenosin receptor

D) TM6, TM7, Glu^6.30, H8, Tyr^5.58, Arg^3.50, TM1, Tyr^3.51, TM2, TM5, Glu/Asp^3.49, TM3

E) TM6, TM7, Glu^6.30, H8, Tyr^5.58, Arg^3.50, Tyr^3.51, TM1, TM2, TM5, TM3, Glu/Asp^3.49

F) Phe^7.60, H8, TM6, Tyr^7.53, Pro^7.50, Asn^7.49, TM1, TM7

Bovine opsin (PDB: 3CAP)
Turkey β$_1$-adrenergic receptor (PDB: 2VT4)
Human β$_2$-adrenergic recptor (PDB: 2RH1)
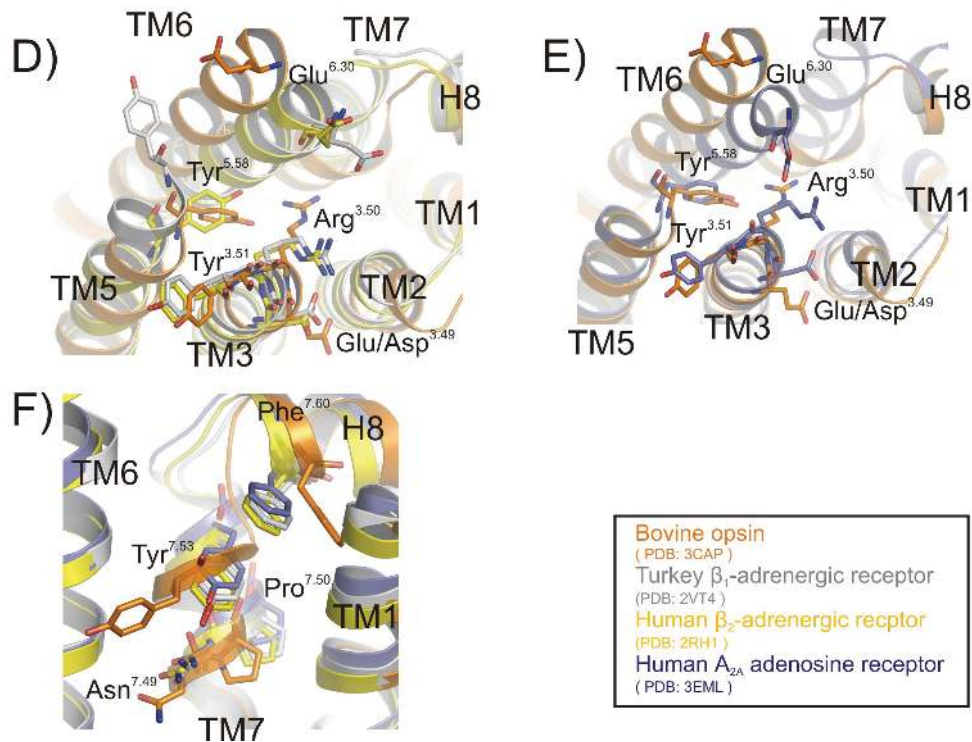Human A$_{2A}$ adenosine receptor (PDB: 3EML)

Figure 4.1.   Comparison of GPCR microdomains containing the E(D)RY and NPxxY(x)$_{5,6}$F motifs

The conserved E(D)RY and NPxxY(x)$_{5,6}$F motifs are part of two functional microdomains. Various rhodopsin states (top) and different GPCR structures (bottom) are compared. Structures are presented as cartoon and stick model, respectively. Superpositions based on C$_\alpha$ traces were performed using CCP4 program LSQKAB [101]. The superposition shows rhodopsin ground state (green), photoactivated rhodopsin (cyan), squid rhodopsin ground state (magenta), opsin (orange), β$_1$-AR (grey), β$_2$-AR (yellow) and A$_{2A}$-adenosine receptor (deep blue), respectively. A), B), D) and E) indicate superpositions of the "ionic lock" microdomain including the E(D)RY motif. C) and F) show a comparison of the NPxxY(x)$_{5,6}$F microdomain. Residues are numbered according to Ballesteros and Weinstein to facilitate the comparison of data obtained from different GPCRs [1]. In this system, two numbers (residue $^{x.y}$) denote the location of each residue. The first number (x) denotes the TM helix. The second number (y) gives the position of the residue relative to the most highly conserved residue in that TM helix. The most highly conserved residue is given the number 50, e.g. Asn$^{1.50}$, Asp$^{2.50}$, Arg$^{3.50}$, Trp$^{4.50}$, Pro$^{5.50}$, Pro$^{6.50}$ and Pro$^{7.50}$; y decreases towards the N terminus and increases towards the C terminus.

Like the E(D)RY motif, the NPxxY(x)$_{5,6}$F motif is part of a functional microdomain. In the rhodospin ground state, and analogously in other GPCR structures, Asn-302 (Asn$^{7.49}$ in TM7) forms a hydrogen bonding network with Asn-55 (Asn$^{1.50}$) and Asp-83 (Asp$^{2.50}$) in the protein interior whereas in the cytoplasmic domain Tyr-306 (Tyr$^{7.53}$) and Phe-313 (Phe$^{7.60}$; on cytoplasmic helix 8) are tethered by electrostatic interactions (Figures 4.1C and F). FTIR spectroscopic studies have suggested that Asp-83 (Asp$^{2.50}$) is protonated in Meta II and that with Meta II formation a change of the hydrogen bonding network between Asn-55, Asp-83 and Asn-302 occurs (Figure 4.2A) [31,47,142,145,146]. The network includes water molecules used to link the TMs. In the known GPCR structures, water clusters were identified which extend from the ligand binding pocket to the cytoplasmic surface of TMs [147]. Waters are often bound to highly conserved residues (Asn$^{1.50}$, Asp$^{2.50}$, Asn$^{7.49}$ and Tyr$^{7.53}$) and are part of functionally important microswitches/ microdomains (the "toggle switch" which enables to modulate the bend angle of TM6 around highly conserved proline [54,148,149] and the NPxxY(x)$_{5,6}$F motif; Figures 4.2A and B, see also Figure 4.6).

The NPxxY(x)$_{5,6}$F microdomain is an important element for the catalytic interaction between activated GPCR and G protein [77,130,150]. Fritze et al. have reported that disruption of the electrostatic interaction between Tyr$^{7.53}$ and Phe$^{7.60}$ by mutagenesis facilitated formation of active Meta II [77]. Consistent with biochemical and biophysical studies of the Meta II state [77,129,130], the Tyr$^{7.53}$ and Phe$^{7.60}$ interaction is broken in opsin* as shown in Figure 3.10. The side chain of Tyr-306 is rotated towards TM6 in opsin*, whereas all other GPCR structures (squid rhodopsin, inactive form; β$_1$-AR, β$_2$-AR and A$_{2A}$-adenosine receptor, all three

represent partially activated forms) maintain the electrostatic interaction between Tyr$^{7.53}$ and Phe$^{7.60}$ (Figures 4.1C and F).
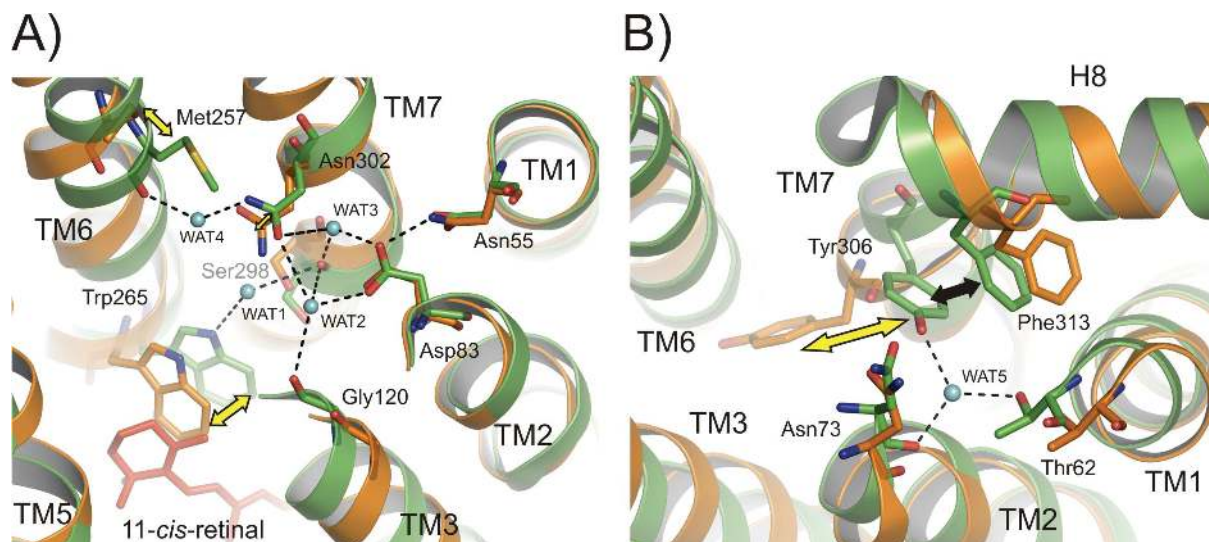

Figure 4.2. Interhelical interaction mediated by water molecules in rhodopsin and opsin
A) *Superposition of crystallographic models of rhodopsin (green) and opsin* (orange). Water molecules (WAT) of a water cluster found in the rhodopsin structure (PDB accession 1U19) are presented as cyan spheres [47]. Dotted lines indicate hydrogen bonding interaction between amino acid residues and water molecules. Yellow arrows indicate conformational changes of amino acid residues.* ***B)*** *Interhelical interactions between TM1, TM2 and TM7. Black arrow indicates electrostatic interaction between Tyr-306 and Phe-313.*

 The question arises why Tyr-306 shows a rotamer change toward TM6 in opsin*. According to the opsin* structure, the Tyr-306 side chain rotates in opsin* into a space opened by TM6 movement and stabilizes TM6 in the outward position. Changes in the TM6/TM7 interface upon rhodopsin activation was also suggested by a mutagenesis study [151]. A specific interhelical interaction between TM6 (Met-257) and TM7 was concluded from activity changes in opsin mutants where Met-257 was replaced by 18 different amino acids [151]. Most of the opsin mutants displayed constitutive activity, which was largest for the M257Y mutant. Han et al. suggested that Met-257 might act as an interaction partner for a residue in the NPxxY(x)$_{5,6}$F motif to stabilize the inactive rhodopsin conformation by preventing TM6 movement. The suggested interhelical interaction was not found in the high-resolution rhodopsin structure. However an interhelical interaction between the cytoplasmic end of TM1 (Thr-62), TM2 (Asn-73) and TM7 (Tyr-306) mediated by a water molecule was observed as a hydrogen bonding network (Figure 4.2B) [47]. The structural change of Tyr-306 (as part of

the NPxxY(x)$_{5,6}$F microdomain) between rhodopsin and opsin* not only causes breakage of the electrostatic interaction between TM7 and TM8, but also removes the cytoplasmic inter-helical interaction between TM1 (Thr-62) and TM2 (Asn-73). The opsin* structure therefore shows small helix motions of TM7 and H8. Recent precise double electron-electron resonance (DEER) distance measurements on light-activated rhodopsin in detergent solution has confirmed the TM6 helix motion paradigm and has also identified smaller relative motions of TM1, TM7 and the C-terminal domain [73].

The Tyr-306 side chain probably flips over in opsin* to interact with Met-257 in a hydrogen-bonded interaction, which may be mediated by a water molecule (Figures 4.3B and C). Evidence for such a water molecule comes from the structure of the complex between opsin* and a peptide derived from the G$_t$α C terminus (G$_t$αCT peptide) [120,134] (see also Appendix), showing a water molecule, which is coordinated to Asn-302 in the vicinity of Met-257 and Tyr-306 (Figure 4.3D). In inactive rhodopsin, a water molecule is coordinated with Met-257 in TM6 and Tyr-301 and Asn-302 in TM7 (Figures 4.2A and 4.6A) [47,134]. In the opsin*•G$_t$αCT peptide complex structure, the water molecule appears to be released from Tyr-301 and shifted slightly closer towards the cytoplasmic surface. In opsin*, this water molecule could – as part of the new TM6/TM7 network – contribute to stabilization of the blossomed cytoplasmic surface.

Based on several lines of evidence as outlined above, the rotational change of the Tyr-306 side chain in opsin* – and likely Meta II – may induce a stabilizing interaction between TM6 (Met-257) and TM7 (Tyr-306). This stabilization depends on the rearrangement of a water molecule needed for mediating the Met-257/Tyr-306 interaction. Thereby, Tyr-306 can act as a blocker to prevent TM6 from moving back toward TM3 to adopt the inactive conformation of rhodopsin.
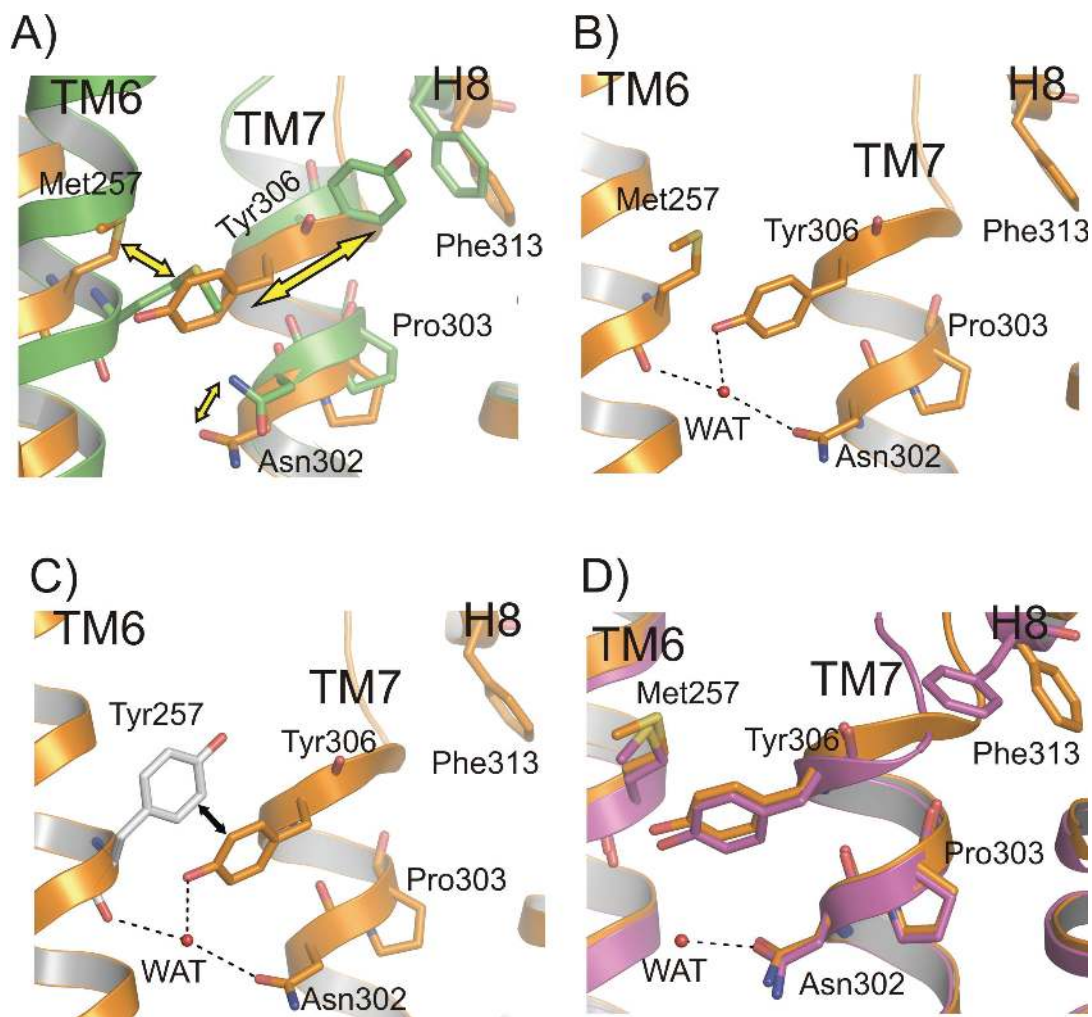
Figure 4.3. Role of Tyr-306 and constitutive activity due to Met-257 mutation

Role of Tyr-306 in opsin* derived from crystallographic models of rhodopsin and opsin*. A) Superposition of rhodopsin ground state (green) and opsin* (orange). Yellow arrows indicate structural changes between rhodopsin and opsin*. The side chain of Tyr-306, which is rotated toward TM6 in opsin* would overlap with Met-257 in rhodopsin. Therefore, the Met-257 side chain in opsin* is shifted away from Tyr-306 due to TM6 movement. B) Putative interhelical hydrogen bond interaction between TM6 (Met-257) and TM7 (Asn-302 and Tyr-306). The interaction may be mediated by a water molecule which is coordinated with Met-257, Asn-302 and Tyr-306, respectively. C) A possible structural interpretation of the large constitutive activity of the M257Y opsin mutant. In this mutant, Tyr-257 and Tyr-306 in opsin* may form a new electrostatic interaction, stabilizing Tyr-306 in addition to the putative hydrogen bonded network. Thereby the M257Y opsin mutant would stabilize TM6 in the outward position and block TM6 from moving back toward TM3 to adopt the inactive conformation corresponding to the rhodopsin ground state. D) A water molecule coordinated to Asn-302 is observed in the complex between opsin* and a C-terminal $G_t\alpha$-derived peptide (magenta; PDB: 3DQB). The crystal structure of opsin* (orange, PDB: 3CAP) is superimposed. This water molecule indicates a possible hydrogen bonding interaction between Met-257, Asn-302 and Tyr-306.

4) Conformational similarity between opsin* and opsin*•G$_t$αCT peptide complex

Previous protein-protein interaction studies identified Meta II as interaction partner for transducin and fragments thereof [72,86,123,134,152,153,154,155]. As key Meta II binding site on the G protein, the C-terminus of the G$_t$α subunit was found [153,154,156,157]. Biochemical, biophysical and mutagenesis studies [158] provided evidence that the G$_t$α C terminus might bind into the cytoplasmic crevice of the 'blossomed' opsin* (Figure 3.9). The precise type of binding was recently shown by a crystal structure obtained from co-crystallization of the G$_t$αCT peptide (a synthetic 11mer peptide derived from the C-terminus of G$_t$α) and opsin [134] (see also the Appendix). Importantly, the conformation of opsin in the opsin•G$_t$αCT peptide complex structure is similar to that of native opsin*, except for the peptide binding site (see Figure 7.2). Amino acid side chains of opsin, which are associated with the synthetic 11mer peptide, show some rearrangements relative to unliganded opsin*. The main binding modes between opsin* and the G$_t$αCT peptide (as part of the C-terminal α5 helix of G$_t$α) are hydrophobic contacts between side chains and hydrogen bonds from main chain carbonyl oxygens of the peptide. A hydrogen bonding network is formed between Arg-135 of opsin* (on TM3) and Cys-347 of G$_t$α (on helix α5), and between Gln-312 of opsin* (in the NPxxY(x)$_{5,6}$F motif) and Lys-345 of G$_t$α (on helix α5). The structure of the cytoplasmic domain of opsin* may thus be seen as active conformation similar to the active cytoplasmic conformation of Meta II. Interestingly, the active cytoplasmic domain experiences only small changes when the G$_t$αCT peptide binds.

4.2   Constitutively active mutants of rhodopsin

To date, many mutagenesis studies on rhodopsin have been performed to find out what residues are critical for G protein activation. The trials are very important for elucidating of activation process as well as finding out a cause of rhodopsin related disease. The first mutation in rhodopsin (K296E) causing constitutive activity, i.e. retinal-independent activity of opsin, has been suggested by Keen et al. in 1991 [159]. Since then many more mutations leading to the same phenotype have been reported (see Table 4.1). Mutations which cause high constitutive activity include mutations affecting inactivating constraints in the receptor like the salt bridge between Glu-113 and Lys-296 and interactions in the "ionic lock". Similarly, mutations

of Met-257 interfere as outlined above with TM6/TM7 packing of the inactive receptor conformation.

Constitutive activity by disruption of the salt bridge between Lys-296 and Glu-113

Cohen and co-workers reported that at pH 6.1 wild-type opsin displayed, when compared with Meta II, a small activity towards transducin [135]. Mutagenesis studies of two residues (Glu-113 and Lys-296) showed a strongly increased, pH-dependent constitutive activity of opsin when one interaction partner of the Lys-296/Glu-113 salt bridge was removed (Table 4.1) [92,93,135,159,160]. In contrast to the E113Q or K296G mutants, the K296R opsin mutant was inactive like wild-type opsin at pH 6.7 [92,93,135]. Therefore disruption of the salt bridge between Lys-296 (or Arg-296 in the K296R mutant) and the counterion Glu-113 appears to be decisive for forming the active conformation. In the (active) opsin* structure, corresponding alterations in the retinal binding pocket are seen, i.e. Glu-113 (on TM3) is shifted backward from Lys-296 (on TM7) to disrupt the salt bridge. Constitutive activity of opsin may thus be caused by a decrease of stabilization of TM3/TM7 interhelical interactions.

Similarly in rhodopsin, a salt bridge between Lys-296 and the counterion Glu-113 is present, however Lys-296 is linked by a protonated Schiff base to 11-*cis*-retinal. Light induced retinal *cis→trans* isomerization in rhodopsin causes rearrangements in the retinal binding site, leading to the disrupture of the Schiff base/ Glu-113 salt bridge by proton transfer to Glu-113 [161]. Glu-113 was suggested as Schiff base counterion and predicted to be the cause of energy increase and spectral red shift in the primary photon-induced event [58]. The role of Glu-113 as counterion was confirmed by the spectral shift observed in the E113D (λ_{max} = 505 nm) and E113Q (λ_{max} = 380 nm) mutants [50]. The structures of rhodopsin and opsin show how the compact "retinal plug" formed by extracellular loop E2 and the N-terminus shields the retinal binding site from the aqueous phase and thus enables the Lys-296/Glu-113 interaction [25,47].

The Glu-134/Arg-135 charge pair is important for transition of the inactive to the active receptor state

Meta II formation (indicated by Schiff base deprotonation) is enhanced at the expense of Meta I by the interaction with the G protein, which established Meta II as the active, G protein binding species [155]. It was early noticed as paradoxon that Meta II formation goes along with proton uptake from solution, although the Schiff base is deprotonated [64]. It is now understood that this occurs because two proton transfer reactions take place, which are linked to two independent, but thermodynamically coupled, functional domains in the protein. These are the region near the retinal Schiff base and the Glu(Asp)-Arg-Tyr triad (the E(D)RY motif). In the course of rhodopsin activation, proton transfer from the retinal Schiff base to its counterion, Glu-113, and proton uptake by Glu-134 as proton acceptor or mediator occur sequentially [53,72,81,94].

Several mutations of Glu-134 (Gln, Ile and Ser) had been tested whether they result in constitutive activity of rhodopsin or not [86,135]. The E134Q mutant showed pH dependent activity of opsin (pH range 5.0 - 7.0) and Meta II (pH 5 - 9.5). The two residues in the intrahelical interaction between Glu-134 and Arg-135 appear to have different roles as concluded from the fact that many substitutions of Glu-134 (Gln, Ile or Ser) did not reduce activity [86]. The importance of Arg-135 in nucleotide exchange catalysis was derived from the severe effect on transducin activation by the R135A, R135L, R135G and E134R/R135E mutations [86,125,162]. In conclusion, the Glu-134/Arg-135 charge-pair, which is located near the cytoplasmic surface, is an important element in regulating the active cytoplasmic conformation. Recently, the opsin*•$G_t\alpha CT$ peptide structure further confirmed that in the active receptor conformation Arg-135 plays a key role in the interaction with the C-terminus of $G_t\alpha$ (Figure 7.2) [134].

*Relationship between Met-257 and Tyr-306 in Meta II and opsin**

The opsin* structure provides an explanation why mutations of Met-257 frequently lead to constitutive activity [151]. Water-mediated hydrogen bonding interactions tether TM6 (Met-257) and TM7 (Tyr-301 and Asn-302). Also TM1 (Thr-62), TM2 (Asn-73) and TM7 (Tyr-306) are linked by a water molecule (Figure 4.2B) [47]. In biochemical studies, the opsin M257Y mutant displayed highest constitutive activity [151]. The reason for the high-level activity may be explained by stabilization of the Tyr-306 rotamer in its active conformation, which forces TM6 into the outward position, as suggested in figure 4.2C. The interaction is

probably also mediated by a water molecule which is present in a common interhelical cavity found in GPCRs (see Figure 4.6). A release of the above mentioned interhelical constraints upon receptor activation may cause the smaller relative motions of TM1, TM7, and the C-terminal domain in Meta II as seen by DEER EPR measurements [73].

Table 4.1. Constitutively active mutations of opsin

Mutation	Location	References
	(Ballesteros-Weinstein numbering)	
Lys → Glu	Lys-296$^{7.43}$	[159]
Lys → Gln	Lys-296$^{7.43}$	[93,135]
Lys → Met, Gly	Lys-296$^{7.43}$	[160]
Glu → Gln	Glu-113$^{3.28}$	[160]
Glu → Ile, Gln, Ser	Glu-134$^{3.49}$	[86,135]
Met → all natural amino acid residues except Arg	Met-257$^{6.40}$	[151]

4.3   Opening of the "ionic lock" in GPCR structures

 To date, several GPCR crystal structures from bovine rhodopsin structure to A$_{2A}$-adenosin receptor have been reported [31,32,33,36,47,48,55,56,68,120,134]. In structural aspect, they can be grouped into two groups, receptors with closed and receptors with "blossomed"/ open cytoplasmic conformation. Rhodopsin (bovine and squid) show most inactive conformations with constraints by the "ionic lock" and the NPxxY(x)$_{5,6}$F microdomain (Figure 4.1). The other extreme is the opsin* conformation with TM5/TM6 motion and rearrangement of the "ionic lock" and the NPxxY(x)$_{5,6}$F microdomain. The different structures of GPCRs containing water soluble diffusible ligands show only partial transition into the opsin* conformation. TM5 is moved largely like in opsin* and Tyr$^{5.58}$ is approaching the "ionic lock" to open it by eventual interaction with Arg$^{3.50}$ (Figure 4.1). In contrast the outward movement of TM6 is only small and not enough to fully open the cytoplasmic crevice for coupling with intracellular G protein, but sufficiently large to disrupt the salt bridge between Arg$^{3.50}$ and Glu$^{6.30}$. Partial TM movements are seen in the GPCR structures with bound partial inverse agonists and

antagonists and may thus explain the partial activity of these GPCR-ligand complexes to-wards the G protein. In this regard, a photoactivated form of rhodopsin with deprotonated Schiff base shows a similar low degree of TM6 motion [68]. In the sequence of rhodopsin activation, Schiff base deprotonation leads to formation of Meta II_a, which then converts into Meta II_b when TM6 fully moves outward [68]. The structure of photoactivated rhodopsin (Figure 3.8) likely represents Meta II_a and a partially activated GPCR conformation.

The GPCRs with bound antagonist (antagonist cyanopindolol, β_1-AR; partial inverse agonist carazolol, β_2-AR; antagonist ZM-241,385, A_{2A}-adenosine receptor) show a constraining inter-action between TM3 and cytoplasmic loop C2. The new interaction occurs between $Asp^{3.49}$ and $Tyr^{3.60}$ or $Ser^{3.62}$ of loop C2 where the sequence identity in GPCRs is low [56]. The low activity of GPCRs with bound antagonist may thus be related to the semi-opening (relative to opsin*) of the cytoplasmic surface. Further, because of the small TM6 movement, the struc-tural rearrangements in the NPxxY$(x)_{5,6}$F microdomain did not occur relative to opsin* and the opsin*•$G_t\alpha$CT peptide complex. In the structures of β_2-AR and the A_{2A}-adenosine recep-tor, loop C3 was replaced by T4-lysozyme, and in the β_2-AR a large part of loop C3 was de-leted. These modifications were necessary for crystallization of the recombinant GPCRs, however, it is not clear how much they influence movement of TM5 and TM6 or breakage of the ionic lock and thus formation of the active receptor conformation (Figures 4.1D and E).

4.4 Ligand channeling

Previous biochemical experiments and molecular dynamic simulations studies have suggested that uptake and release of retinal may proceed through different gates [163,164]. However, the rhodopsin structure does not show openings of the retinal binding site for retinal entry or re-lease. In contrast, opsin* contains two openings in the TM region between TM1/TM7 and TM5/TM6, respectively (Figures 3.15 and 3.16).
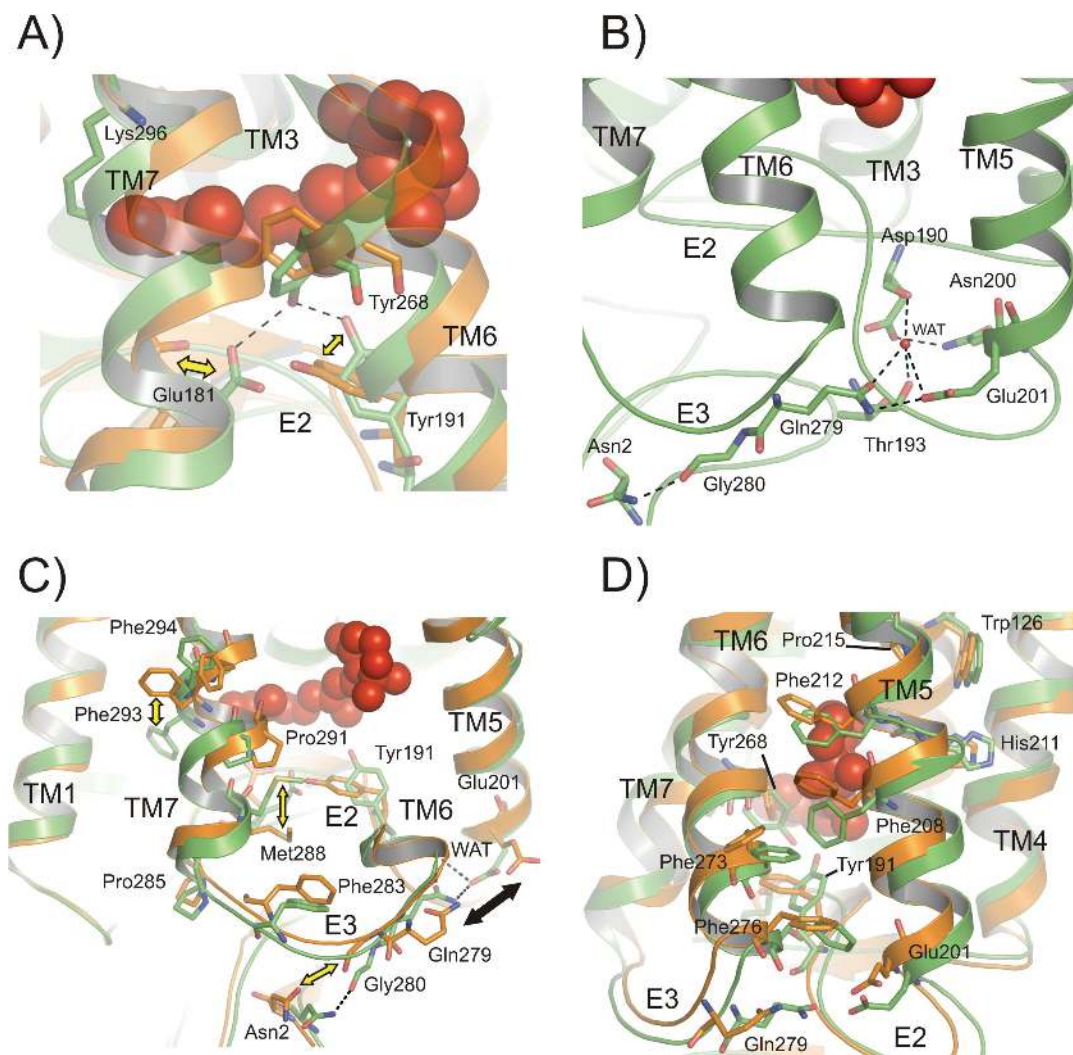
Figure 4.4. Rearrangement of loops E2 and E3 and formation of the two openings of the retinal binding site in opsin*

A) *A hydrogen bonding network between Glu-181 and Tyr-191 (both in E2) and Tyr-268 (on TM6) is present in rhodopsin (green), but not in opsin* (orange). 11-cis-retinal is presented as a red sphere model.* **B)** *A hydrogen bonding network mediated by a water molecule (WAT) at the extracellular surface of rhodopsin.* **C)** *and* **D)** *Superposition of rhodopsin (green) and opsin* (orange) structures, showing different orientations of membrane-facing hydrophobic residues involved in forming the openings of the retinal binding site. In rhodopsin, but not in opsin*, a hydrogen bonding network between TM5 (Glu-201), TM6 (Gln-279) and a water molecule is present (dotted line). Breakage of the network may consequently induce a breakage of hydrogen bonding between Gly-280 and Asn-2 and rearrangement of loop E3. Relative to rhodopsin, opsin* shows a rotamer change of Tyr-191 which leads to a steric hindrance between the side chain of Tyr-191 and Met-288. Relocation of Met-288 has an influence on Pro-291 which may free the restricted residues Phe-293 and Phe-294, allowing their rotational change to form one opening of the retinal binding site between TM1 and TM7.* **D)** *Opening of the retinal binding site between TM5 and TM6. Formation of the second opening is allowed due to conformational changes breaking the Glu-201/Gln-279 hydrogen bond, which enables rearrangement of Phe-273 and Phe-276. A hydrogen bonding network between Glu-122, Trp-126 and His-211 links TM3 and TM5; this network is likely weakened in opsin* to enable changes of Phe-208 and Phe-212. Pro-215 induces a kink in TM5 which likely facilitates conformational changes in the extracellular TM5 segment.*

The first opening between TM1 and TM7 is induced by a prominent rotation of Phe-293 and a rotamer change of Phe-294, the second opening between TM5 and TM6 is induced by reorientation of side chains of hydrophobic residues (Val-204, Ile-205, Phe-273, Phe-208, Phe-212 and Phe-276) due to movement of TM5 and TM6. A channel through the protein linking the two openings was suggested from the opsin* structure and the idea were extended by retinal docking experiments in the retinal binding site [120,165].

Formation of the two channel openings in the TM surface may be initiated by rearrangement of the extracellular loops E2 and E3 (Figure 4.4). A movement of loop E2 upon light-activation of rhodopsin was recently shown by solid state NMR experiments [166]. In rhodopsin a disulfide bond between Cys-110 on TM3 and Cys-187 in E2 tethers a compact extracellular domain, the so-called "retinal plug", to the 7TM domain. E2 folds back into the protein to contribute Ser-186 to Ile-189 of strand β4 to the retinal binding site. The retinal chromophore in its binding pocket is surrounded by hydrophobic residues (Cys-187, Ile-189, Met-207, Phe-212, Phe-261, Trp-265 and Ala-292) [25,31]. TM6 (Tyr-268) is tethered to Glu-181 and Tyr-191 in E2, i.e. linked to the "retinal plug" (Figure 4.4A). E2 is further tethered to the extracellular end of TM5 in rhodopsin ground state by an interaction between Asp-190 and Thr-193 (in E2) and Asn-200 (on TM5) (Figure 4.4B). In addition, rhodopsin contains a hydrogen bond between Glu-201 at the extracellular end of TM5 and Gln-279 on TM6.

In opsin*, where the two openings of the retinal binding site are present, the "retinal plug" domain is maintained but is not less tightly tethered to the 7TM domain. The interaction between Tyr-268 on TM6 and Glu-181 and Tyr-191 in E2 is lost, allowing rearrangement of E2 (Figure 4.4A) and breakage of the hydrogen bond at the extracellular ends of TM5 (Glu-201) and TM6 (Gln-279) (Figure 4.4C), thus facilitating formation of the opening between TM5 and TM6.

Concomitant with the breakage of the hydrogen bond between Glu-201 and Gln-279, a rearrangement of loop E3 occurs. In opsin*, Asn-282 (in E3) interacts with Asn-2 whereas in rhodopsin Gly-280 (in E3) interacts with Asn-2 (Figure 4.4C). The rearrangement of E3 induces structural alterations in the extracellular segments of TM6 and TM7 (Figures 4.4C and D). Accordingly, changes of bulky residues on TM7 (Phe-293 and Phe-294) enable formation of the opening between TM7 and TM1, whereas changes of bulky residues on TM6 (Phe-273 and Phe-276) enable formation of the opening between TM5 and TM6. Formation of the latter

opening also involves changes of bulky residues on TM5 (Phe-208 and Phe-212), likely facilitated by a weak hydrogen bonding network between TM3 (Glu-122 and Trp-126) and TM5 (His-211) in opsin* (Figure 4.4D).
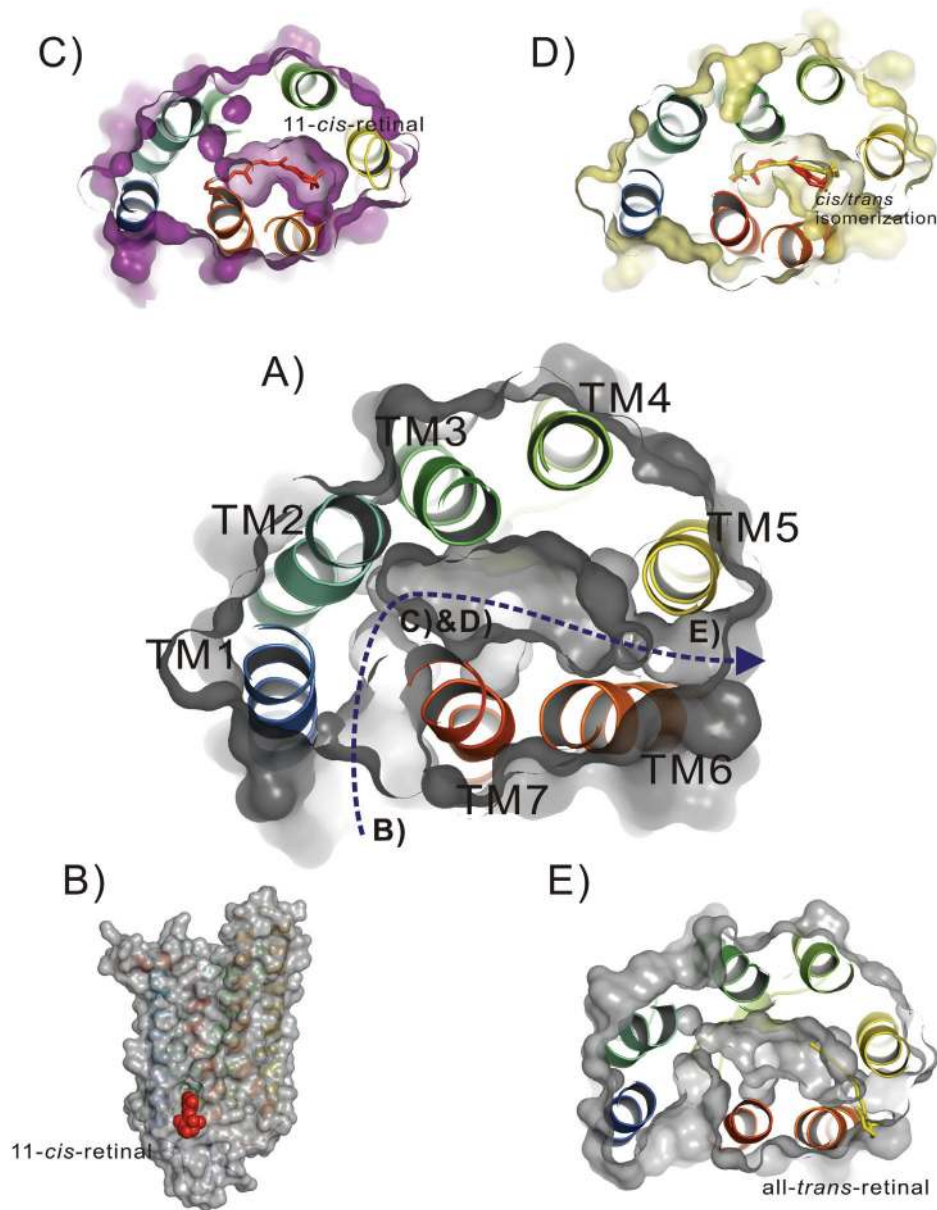

Figure 4.5. Proposal for retinal channeling

A) *Cytoplasmic view of coplanar cut through opsin* monomer revealing the channel for retinal. All 7TM helices in the surface and cartoon model are labelled and shown in blue (TM1) to red (TM7). The blue dotted line indicates a possible route for retinal uptake and release. Presumptive retinal entry and exit sites are shown in **B)** and **E)**, respectively. 11-cis retinal is shown as red ball and stick, all-trans-retinal close to a putative exit site is shown as yellow stick model. **C)** After retinal entry, the Schiff base with the ε-amino group of Lys-296 is formed. **D)** Light-induced retinal cis/trans isomerization in rhodopsin.*

In summary, rearrangement of loops E2 and E3 and concomitant formation of the two openings of the retinal binding site in opsin* yielded a ligand channel which traverses opsin over a distance of ca. 70 Å and is between 11.6 and 3.2 Å wide [165]. Although there are two possible routes for uptake and release of retinal, the current proposal favours a unidirectional passage of retinal as shown in Figure 4.5. The channel form a sharp bent around Lys-296, which suggests that only the bent 11-*cis*-retinal can pass this restriction site.

Interestingly, the regeneration of visual pigments starts with an initial non-covalent binding of 11-*cis*-retinal, which increases receptor activity transiently until rhodopsin is regenerated [167]. Such non-covalent retinal binding is modelled in Figure 4.5B. It eventually results in formation of the retinal Schiff base and of the rhodopsin ground state conformation (Figure 4.5C). The release of all-*trans*-retinal is favoured with the pH dependence of active Meta II [168], arguing for the necessity of the opsin* conformation and thus the openings of the retinal binding site for the release step. Possibilities for the release route of all-*trans*-retinal after light-induced retinal isomerization and retinal Schiff base hydrolysis are illustrated in figures 4.5D and E.

4.5   A water cluster in GPCR structures and the activation process of rhodopsin

Another common feature of the reported high-resolution crystallographic models of class A GPCRs are similar water clusters in interhelical cavities. These cavities might be able to form a long hydrogen bonding network between TM1-TM3 and TM6-TM7 extending from the transmembrane helical bundle to the cytoplasmic surface [32,36,47,56] (Figure 4.6). The interhelical cavity is filled with five (bovine rhodopsin), six (β2-AR receptor and A_{2A}-adenosine receptor) or nine (squid rhodopsin) water molecules, and the hydrogen bonding network is usually extended from the toggle switch residue (Trp-265 in rhodopsin, Trp-274 in squid rhodopsin and Trp-286 in β2-AR, except His-278 in A_{2A}-adenosine receptor) to the NPxxY$(x)_{5,6}$F motif as shown in figure 4.6. A water molecule is coordinated to the indole nitrogen atom of the toggle switch Trp$^{6.48}$ residue, likely to maximize the proline-induced kink (Pro$^{6.50}$) in TM6 and to facilitate helix movements [147] (Figure 4.6). TM5/TM6 movement upon receptor activation may rearrange water molecules in the hydrogen bonding network. It

is likely that this network, which interacts with a number of highly conserved amino acids, may be important in transmitting structural changes from the ligand-binding pocket to distal sites.
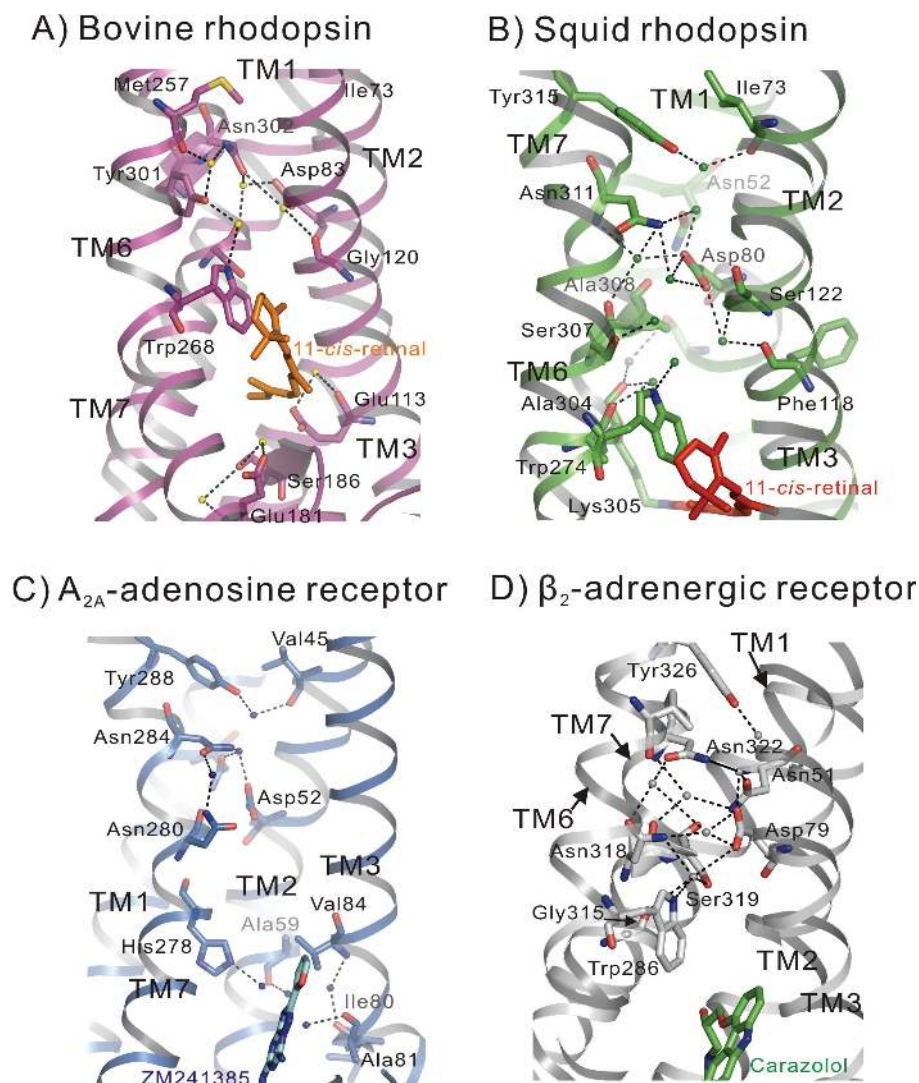

Figure 4.6. Comparison of interhelical water clusters in GPCRs structures

*Overall structures of GPCRs and water clusters in interhelical cavities are presented as cartoon models: **A)** Bovine rhodopsin (magenta, PDB accession: 1U19), **B)** Squid rhodopsin (green, PDB accession: 2Z73), **C)** A_{2A}-adenosine receptor (blue, PDB accession: 3EML) and **D)** β2-AR (grey, PDB accession: 2RH1). Residues coordinated with water molecules are shown as stick model. Water molecules are presented as yellow (bovine rhodopsin), forest (squid rhodopsin), dark blue (A_{2A}-adenosine receptor) and grey (β2-AR) sphere models, respectively. Ligands in the different GPCR models are presented as stick model. Dotted lines indicate hydrogen bonds between coordination partners.*

Interestingly, in the GPCR structures, some water molecules that are located in the termini of the water cluster interact with $Asn^{7.49}$ and $Tyr^{7.53}$ in the NPxxY motif. More than two water molecules are always shared by the $Asn^{7.49}$ residue, whereas one water molecule is coordinated by the $Tyr^{7.53}$ residue. To elucidate the role of water in the opsin* conformation, it may take different crystallization methods like the cubic phase method to get a high-resolution structure with refined water molecules [32,36,56].

4.6   Sequential activation process of rhodopsin

To date, the crystal structures of GPCRs in the inactive or partially photoactivated state could not be used to derive the complete activation process because these structures are lacking the known prominent features of the active receptor conformation. However, the opsin* structure shows the prominent features in agreement with previous biochemical and biophysical data. Therefore an attempt was made to summarize the activation process of rhodopsin based on the available rhodopsin and opsin* structures. In the ground state, the crystallographic model of rhodopsin contains three prominent constraints, in the retinal binding pocket and in two functional regions (regions containing the E(D)RY and $NPxxY(x)_{5,6}F$ motifs) [25,31,47]. The structural features in the retinal binding pocket of rhodopsin comprise the Schiff base and its stabilizing counterion, the constraint on the β-ionone ring by a set of hydrophobic residues ($Phe^{5.47}$ on TM5, $Phe^{6.44}$ and $Trp^{6.48}$ on TM6), and an interaction between C19 of retinal and Tyr-191 of the "retinal plug". These features contribute to stabilization of the extracellular part of the rhodopsin molecule. The two functional E(D)RY and $NPxxY(x)_{5,6}F$ regions are located at the cytoplasmic surface. They are strongly constrained by the "ionic lock" between the cytoplasmic segments of TM3 and TM6, and an electrostatic interaction between $Tyr^{7.53}$ and $Phe^{7.60}$, respectively. Protein structural alterations and release of the constraints are induced by *cis*/*trans* isomerization of the chromophore following light absorption [51,52,53,54,77,129,130]. Due to retinal isomerization, the stabilizing salt bridge present in the inactive rhodopsin ground state between the protonated 11-*cis*-retinal Schiff base and the Glu-113 (on TM3) counterion is broken [25,31,58]. As a consequence, conformational rearrangements of the opsin moiety occur, giving raise to a succession of several different photoproducts in the activation process, i.e. Batho, Lumi, Meta I and Meta II. These photoproducts show several small structural changes in each state as shown by X-ray crystallographic studies

and electron crystallography [66,67,68,70]. Up to Lumi no large conformational changes in the retinal binding pocket and large rigid-body movements of TMs are not observed, but specific changes for each state, i.e. a distorted polyene chain of retinal in Batho, a nearly undistorted all-*trans* chromophor in Lumi and a rearrangement of side chains close to the kink in TM6. Interestingly, from the Meta I structure, a rearrangement of residues Trp-265 (adjacent to Pro-267 at the bend of TM6) was suggested to occur relative to the rhodopsin dark state. Based on the electron crystallographic data, the rotamer change of the Trp-265 side chain "toggle switch" as consequence of the photoactivation event may have occurred in Meta I [70]. It was also suggested that a proton relay via proton wires from the retinal binding pocket to the cytoplasmic surface (as shown in figure 4.6) may occur upon receptor activation [147]. The deprotonation of the Schiff base is a prerequisite characteristic for the Meta II state and precedes structural changes known from FTIR and EPR spectroscopic data [53,71,72,73,77,80,81,92,93,133,135]. The transition to the active state of rhodopsin is then accompanied by multiple structural alterations, comprising the breakage of the "ionic lock", rearrangement of the NPxxY(x)$_{5,6}$F microdomain, changes in protonation switches, i.e. protonation of Glu-113 due to deprotonation of the Schiff base, and protonation of Glu-134 at the cytoplasmic surface as a consequence of TM5/TM6 movements [72].

Based on the available structures of rhodopsin, photointermediates and opsin, the proposed activation process of rhodopsin is summarized as follows [31,47,48,66,67,68,70,120,134] and presented in figure 4.7.

In step one, the protonation process of Glu-113 may be induced by rotamer changes of aromatic residues Tyr-191 and Tyr-192 of the "retinal plug".

As described in 4.2 and figures 3.11 and 3.12, a broken salt bridge between counterion Glu-113 and the ε-amino group of Lys-296 is observed in the retinal binding pocket of opsin, whereas in rhodopsin dark state, stabilization of the protonated Schiff base is provided by its salt bridge to the counterion [92,93,120,133]. The breakage of the salt bridge may be facilitated by rotamer changes of aromatic side chains of residues Tyr-191 and Tyr-192 and backbone movements (Figures 3.11 and 3.12). Both aromatic residues belong to the "retinal plug" which limits accessibility to the retinal binding site. The change of Tyr-191 due to the altered chromophore geometry caused by *cis/trans* isomerization may break van der Waals contacts between the carboxyl group of Tyr-191 and C19 of the chromophore. As a result of disruption

of the contact, Glu-181 may shift toward the counterion Glu-113. The charge-charge repulsion force between the Glu-113 and Glu-181 carboxyl groups may facilitate breakage of the salt bridge between Glu-113 and the retinal Schiff base, supported by rearrangement of water molecules in the retinal binding pocket due to a change of the hydrogen bonding network around the Schiff base. Protonation of Glu-113 may be linked to the arrangement of the water cluster in the retinal binding pocket depending on the retinylidene geometry (11-*cis*- or all-*trans*).

In step two, Trp-265 shifts towards the position previously occupied by the β-ionone ring and induces movement of helix TM6.

In the opsin and opsin* structure, Trp-265 on TM6 is shifted toward the position previously occupied by the retinal β-ionone ring, which in the rhodopsin structure is tethered by a set of hydrophobic residues (Phe-212, Phe-261 and Trp-265) [47,120,134]. As shown in figure 3.11 and 4.6, the highly conserved Trp-265 [148,149] plays an important role in GPCRs as a "toggle switch" to facilitate helix movement and rearrangement of water molecules. The change of the toggle switch, depending on *cis/trans* isomerisation, may produce a domino effect, i.e. a maximization of the proline-induced kink in TM6 to facilitate helices movements, a breakage of the "ionic lock", a rearrangement of cytoplasmic loops and helices, leading to an "open" cytoplasmic surface [71,72,73,169,170]. Moreover, the residue (Trp-265) may also act as a gatekeeper which is able to mediate the signal transfer from the extracellular region to the cytoplasmic surface for coupling to the G protein.

In the third step, the helix movement of TM6 facilitates breakage of the "ionic lock" and formation of the extended hydrogen bonded network including Arg-135 of the E(D)RY motif.
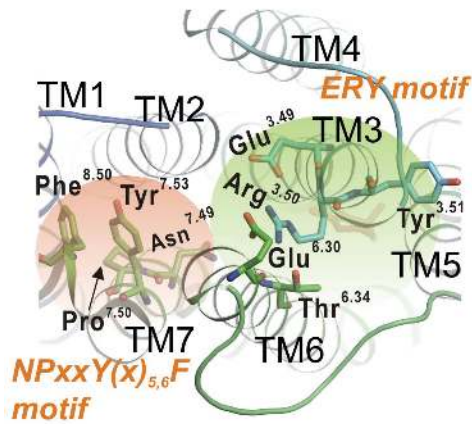
As described above, the change of the toggle switch residue (Trp-265), which in opsin and the opsin*•G$_t$αCT complex structure (see Appendix) is shifted towards the space occupied by the β-ionone ring of retinal, may also induce a helix rotation and a maximization of the helix kink caused by the conserved Pro-267 residue (Figure 3.13).

Consequently, the "ionic lock" is broken and as shown in figure 3.7C, a new hydrogen bond between Arg-135 and Tyr-223, and a new interhelical salt bridge between Lys-231 and Glu-247 is formed. However, the TM6 movement is not enough for keeping the active conformation because the protonation of Glu-134 appears to be a prerequisite for coupling to the G protein [53,76,86,94,131,135,171,172,173,174].

Finally, protonation of Glu-134 in the E(D)RY motif may be induced by rearrangement of the NPxxY(x)$_{5,6}$F region.
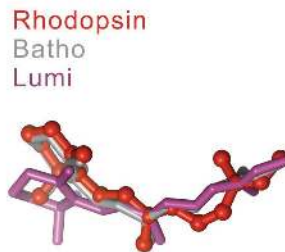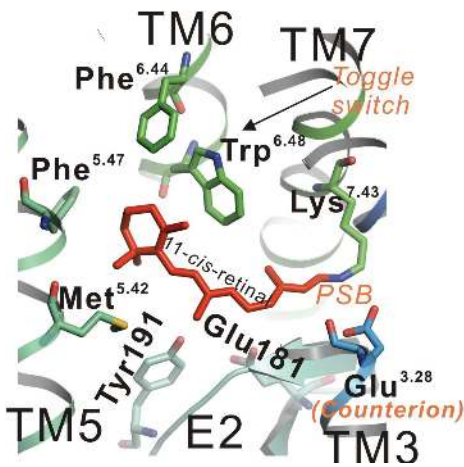
Rhodopsin activation usually progresses as a protonation-dependent process, i.e. by protonation of the Schiff base counterion Glu-113 and of Glu-134 involved in proton uptake from the solvent [131,175,176]. The latter, protonation of Glu-134 in the Meta II$_b$ photoproduct facilitates coupling to the G protein [94]. In the bovine rhodopsin model, a water cluster is distributed from the toggle switch (Trp-265) to the cytoplasmic surface. The water cluster, which consists of five water molecules close to TM1-TM3, TM6, and TM7, extends from Trp-265 to Tyr-306 of bovine rhodopsin. As shown in figures 4.2 and 4.6, a similar rearrangement of the NPxxY(x)$_{5,6}$F microdomain of opsin relative to rhodopsin may occur in the Meta II$_b$ state and may be accompanied by rearranged water molecules in the water cluster to facilitate proton uptake by the E(D)RY region (Glu-134).

Two conserved motifs

TM4

ERY motif

TM1   TM2

Glu 3.49   TM3

Phe 8.50   Tyr 7.53

Arg 3.50

Asn 7.49

Tyr 3.51

Glu 6.30   TM5

Pro 7.50

Thr 6.34

TM7   TM6

NPxxY(x)_{5,6}F
motif

Rhodopsin $\xrightarrow{h\nu}$ Batho & Lumi $\longrightarrow$ Meta I $\rightleftarrows$ Schiff depro

Retinal binding pocket

TM6   TM7

Phe 6.44   Toggle switch

Phe 5.47   Trp 6.48

Lys 7.43

Met 5.42   11-cis-retinal   PSB

Tyr191   Glu181   Glu 3.28 (Counterion)

TM5   E2   TM3

Changes of Chromophore geometry
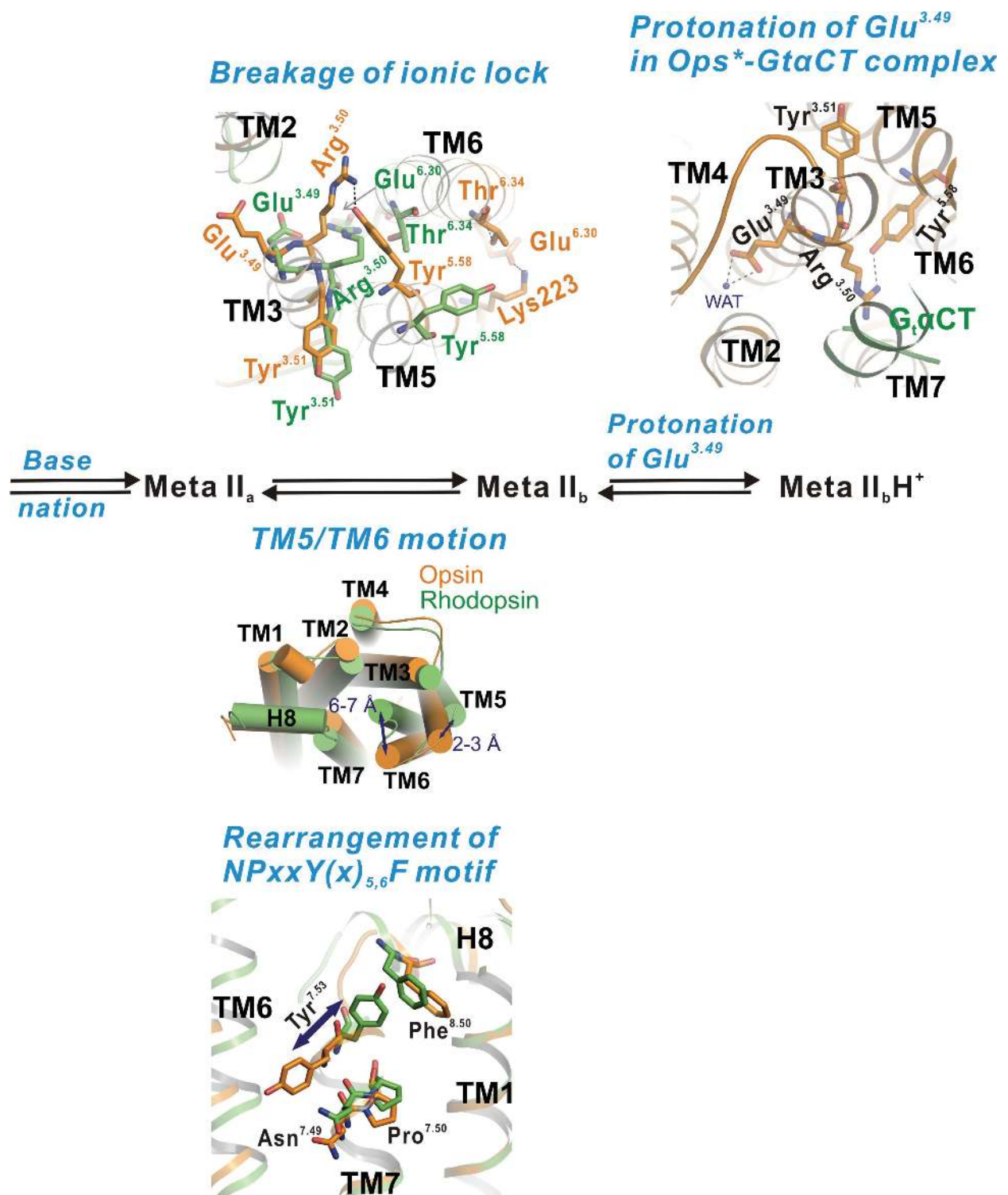
Rhodopsin
Batho
Lumi

Figure 4.7. Hypothetical rhodopsin activation process

 Based on the available structural information on different rhodopsin states a model for the rhodopsin activation process is proposed (see text). For illustration, known structures of rhodopsin and rhodopsin photoproducts are presented as cartoon, ball and stick, and/or cylinder models, respectively. In the Meta intermediates, inactive and active conformations are shown in green (inactive) and orange (active), respectively.

4.7 Open questions

 Although the opsin* structure allowed elucidation of many features of the active receptor conformation [120,134], questions still remain:

1. What are the structural differences between inactive and active opsin conformations occurring in a pH-dependent manner?

2. Under what conditions and how can the two putative entry and exit sites for retinal be formed?

3. Is there a unidirectional passage for retinal in the retinal channel?

4. What is the structural difference between opsin* and the non-covalent all-*trans*-retinal•opsin* complex to explain a difference of binding affinity for G protein?

5. How does the active Meta II structure look like relative to opsin*? What are the differences in the retinal binding site of Meta II and opsin*? What is the effect of transducin binding on the Meta II conformation?

5   CONCLUSION

The following conclusions can be made from the X-ray crystallographic analysis of opsin:

1.   The movement of the cytoplasmic segment of TM6 with Trp-265 as pivot point is a prominent feature of the active receptor conformation as present in opsin*. The TM6 movement observed by crystallography is in good agreement with measurements by EPR spectroscopy. Moreover, smaller movements of TM5 and TM7 at the cytoplasmic surface are accompanied with TM6 movement.

2.   In opsin*, the microdomains containing the highly conserved E(D)RY and $NPxxY(x)_{5,6}F$ motifs are rearranged due to movement of TM5, TM6 and TM7. The structural rearrangements in both microdomains are important for transition from Meta II_a to Meta II_b and subsequent protonation of Glu-134.

3.   Two other structural rearrangements between rhodopsin and opsin are two openings of the retinal binding site located in the TM domain. The openings may act as entry and exit sites for retinal.

4.   The crystal structures of ligand-free opsin and the opsin*•$G_t\alpha CT$ peptide complex are very similar, except for the $G_t\alpha CT$ peptide binding site. The opsin crystal structure therefore likely represents the active opsin* conformation.

5.   The successful crystallization of opsin alone and in complex with G protein fragments (see Appendix) provides a basis for further structural approaches to reveal the interaction of GPCRs with ligands and interacting proteins.

6 BIBLIOGRAPHY

1. Ballesteros JA, Weinstein H (1995) Integrated methods for the construction of three-dimensional models and computational probing of structure-function relations in G-protein coupled receptors. Methods Neurosci 25: 366-428.

2. Rosenbaum DM, Rasmussen SG, Kobilka BK (2009) The structure and function of G-protein-coupled receptors. Nature 459: 356-363.

3. Christopoulos A, Kenakin T (2002) G protein-coupled receptor allosterism and complexing. Pharmacol Rev 54: 323-374.

4. Bissantz C (2003) Conformational changes of G protein-coupled receptors during their activation by agonist binding. J Recept Signal Transduct Res 23: 123-153.

5. Davies MN, Gloriam DE, Secker A, Freitas AA, Mendao M, et al. (2007) Proteomic applications of automated GPCR classification. Proteomics 7: 2800-2814.

6. Hanson MA, Stevens RC (2009) Discovery of new GPCR biology: one receptor structure at a time. Structure 17: 8-14.

7. Fredriksson R, Lagerstrom MC, Lundin LG, Schioth HB (2003) The G-protein-coupled receptors in the human genome form five main families. Phylogenetic analysis, paralogon groups, and fingerprints. Mol Pharmacol 63: 1256-1272.

8. Lagerstrom MC, Schioth HB (2008) Structural diversity of G protein-coupled receptors and significance for drug discovery. Nat Rev Drug Discov 7: 339-357.

9. Horn F, Bettler E, Oliveira L, Campagne F, Cohen FE, et al. (2003) GPCRDB information system for G protein-coupled receptors. Nucleic Acids Res 31: 294-297.

10. Fredriksson R, Hoglund PJ, Gloriam DE, Lagerstrom MC, Schioth HB (2003) Seven evolutionarily conserved human rhodopsin G protein-coupled receptors lacking close relatives. FEBS Lett 554: 381-388.

11. Klabunde T, Hessler G (2002) Drug design strategies for targeting G-protein-coupled receptors. Chembiochem 3: 928-944.

12. Heximer SP, Knutsen RH, Sun X, Kaltenbronn KM, Rhee MH, et al. (2003) Hypertension and prolonged vasoconstrictor signaling in RGS2-deficient mice. J Clin Invest 111: 445-452.

13. Asico LD, Ladines C, Fuchs S, Accili D, Carey RM, et al. (1998) Disruption of the dopamine D3 receptor gene produces renin-dependent hypertension. J Clin Invest 102: 493-498.

14. Spiegel AM, Weinstein LS (2004) Inherited diseases involving g proteins and g protein-coupled receptors. Annu Rev Med 55: 27-39.

15. Lania AG, Mantovani G, Spada A (2006) Mechanisms of disease: Mutations of G proteins and G-protein-coupled receptors in endocrine diseases. Nat Clin Pract Endocrinol Metab 2: 681-693.

16. Corvilain B, Van Sande J, Dumont JE, Vassart G (2001) Somatic and germline mutations of the TSH receptor and thyroid diseases. Clin Endocrinol (Oxf) 55: 143-158.

17. Schulz A, Sangkuhl K, Lennert T, Wigger M, Price DA, et al. (2002) Aminoglycoside pretreatment partially restores the function of truncated V(2) vasopressin receptors found in patients with nephrogenic diabetes insipidus. J Clin Endocrinol Metab 87: 5247-5257.

18. Dorsam RT, Gutkind JS (2007) G-protein-coupled receptors and cancer. Nat Rev Cancer 7: 79-94.

19. Ripps H (1982) Night blindness revisited: from man to molecules. Proctor lecture. Invest Ophthalmol Vis Sci 23: 588-609.

20. Ripps H, Carr RE, Siegel IM, Greenstein VC (1984) Functional abnormalities in vincristine-induced night blindness. Invest Ophthalmol Vis Sci 25: 787-794.

21. Lander ES, Linton LM, Birren B, Nusbaum C, Zody MC, et al. (2001) Initial sequencing and analysis of the human genome. Nature 409: 860-921.

22. Venter JC, Adams MD, Myers EW, Li PW, Mural RJ, et al. (2001) The sequence of the human genome. Science 291: 1304-1351.

23. Vassilatis DK, Hohmann JG, Zeng H, Li F, Ranchalis JE, et al. (2003) The G protein-coupled receptor repertoires of human and mouse. Proc Natl Acad Sci U S A 100: 4903-4908.

24. Kuhne W (1977) Chemical processes in the retina. Vision Res 17: 1269-1316.

25. Okada T, Ernst OP, Palczewski K, Hofmann KP (2001) Activation of rhodopsin: new insights from structural and biochemical studies. Trends Biochem Sci 26: 318-324.

26. Palczewski K, Saari JC (1997) Activation and inactivation steps in the visual transduction pathway. Curr Opin Neurobiol 7: 500-504.

27. Fukuda MN, Papermaster DS, Hargrave PA (1979) Rhodopsin carbohydrate. Structure of small oligosaccharides attached at two sites near the NH2 terminus. J Biol Chem 254: 8201-8207.

28. Ovchinnikov Yu A, Abdulaev NG, Bogachuk AS (1988) Two adjacent cysteine residues in the C-terminal cytoplasmic fragment of bovine rhodopsin are palmitylated. FEBS Lett 230: 1-5.

29. Brown NG, Fowles C, Sharma R, Akhtar M (1992) Mechanistic studies on rhodopsin kinase. Light-dependent phosphorylation of C-terminal peptides of rhodopsin. Eur J Biochem 208: 659-667.

30. Doan T, Mendez A, Detwiler PB, Chen J, Rieke F (2006) Multiple phosphorylation sites confer reproducibility of the rod's single-photon responses. Science 313: 530-533.

31. Palczewski K, Kumasaka T, Hori T, Behnke CA, Motoshima H, et al. (2000) Crystal structure of rhodopsin: A G protein-coupled receptor. Science 289: 739-745.

32. Murakami M, Kouyama T (2008) Crystal structure of squid rhodopsin. Nature 453: 363-367.

33. Warne T, Serrano-Vega MJ, Baker JG, Moukhametzianov R, Edwards PC, et al. (2008) Structure of a beta1-adrenergic G-protein-coupled receptor. Nature 454: 486-491.

34. Moffett S, Rousseau G, Lagace M, Bouvier M (2001) The palmitoylation state of the beta(2)-adrenergic receptor regulates the synergistic action of cyclic AMP-dependent protein kinase and beta-adrenergic receptor kinase involved in its phosphorylation and desensitization. J Neurochem 76: 269-279.

35. O'Dowd BF, Hnatowich M, Caron MG, Lefkowitz RJ, Bouvier M (1989) Palmitoylation of the human beta 2-adrenergic receptor. Mutation of Cys341 in the carboxyl tail leads to an uncoupled nonpalmitoylated form of the receptor. J Biol Chem 264: 7564-7569.

36. Cherezov V, Rosenbaum DM, Hanson MA, Rasmussen SG, Thian FS, et al. (2007) High-resolution crystal structure of an engineered human beta2-adrenergic G protein-coupled receptor. Science 318: 1258-1265.

37. Dereeper A, Guignon V, Blanc G, Audic S, Buffet S, et al. (2008) Phylogeny.fr: robust phylogenetic analysis for the non-specialist. Nucleic Acids Res 36: W465-469.

38. Baylor DA, Hodgkin AL (1973) Detection and resolution of visual stimuli by turtle photoreceptors. J Physiol 234: 163-198.

39. Dowling JE, editor (1987) In "The retina: An approachable part of brain".

40. Muller F, Kaupp UB (1998) [Signal transduction in photoreceptor cells]. Naturwissenschaften 85: 49-61.

41. Wolfrum U, Salisbury JL (1998) Expression of centrin isoforms in the mammalian retina. Exp Cell Res 242: 10-17.

42. Lamb TD, Pugh EN, Jr. (2004) Dark adaptation and the retinoid cycle of vision. Prog Retin Eye Res 23: 307-380.

43. McBee JK, Kuksa V, Alvarez R, de Lera AR, Prezhdo O, et al. (2000) Isomerization of all-trans-retinol to cis-retinols in bovine retinal pigment epithelial cells: dependence on the specificity of retinoid-binding proteins. Biochemistry 39: 11370-11380.

44. Hofmann KP, Pulvermuller A, Buczylko J, Van Hooser P, Palczewski K (1992) The role of arrestin and retinoids in the regeneration pathway of rhodopsin. J Biol Chem 267: 15701-15706.

45. Wald G, Brown PK (1958) Human rhodopsin. Science 127: 222-226.

46. Hecht (1920) J Gen Physiol 2: 499-517.

47. Okada T, Sugihara M, Bondar AN, Elstner M, Entel P, et al. (2004) The retinal conformation and its environment in rhodopsin in light of a new 2.2 A crystal structure. J Mol Biol 342: 571-583.

48. Li J, Edwards PC, Burghammer M, Villa C, Schertler GF (2004) Structure of bovine rhodopsin in a trigonal crystal form. J Mol Biol 343: 1409-1438.

49. Filipek S, Stenkamp RE, Teller DC, Palczewski K (2003) G protein-coupled receptor rhodopsin: a prospectus. Annu Rev Physiol 65: 851-879.

50. Sakmar TP, Franke RR, Khorana HG (1989) Glutamic acid-113 serves as the retinylidene Schiff base counterion in bovine rhodopsin. Proc Natl Acad Sci U S A 86: 8309-8313.

51. Ballesteros JA, Jensen AD, Liapakis G, Rasmussen SG, Shi L, et al. (2001) Activation of the beta 2-adrenergic receptor involves disruption of an ionic lock between the cytoplasmic ends of transmembrane segments 3 and 6. J Biol Chem 276: 29171-29177.

52. Huang P, Visiers I, Weinstein H, Liu-Chen LY (2002) The local environment at the cytoplasmic end of TM6 of the mu opioid receptor differs from those of rhodopsin and monoamine receptors: introduction of an ionic lock between the cytoplasmic ends of helices 3 and 6 by a L6.30(275)E mutation inactivates the mu opioid receptor and reduces the constitutive activity of its T6.34(279)K mutant. Biochemistry 41: 11972-11980.

53. Vogel R, Mahalingam M, Ludeke S, Huber T, Siebert F, et al. (2008) Functional role of the "ionic lock"--an interhelical hydrogen-bond network in family A heptahelical receptors. J Mol Biol 380: 648-655.

54. Bhattacharya S, Hall SE, Vaidehi N (2008) Agonist-Induced Conformational Changes in Bovine Rhodopsin: Insight into Activation of G-Protein-Coupled Receptors. J Mol Biol.

55. Rasmussen SG, Choi HJ, Rosenbaum DM, Kobilka TS, Thian FS, et al. (2007) Crystal structure of the human beta2 adrenergic G-protein-coupled receptor. Nature 450: 383-387.

56. Jaakola VP, Griffith MT, Hanson MA, Cherezov V, Chien EY, et al. (2008) The 2.6 angstrom crystal structure of a human A2A adenosine receptor bound to an antagonist. Science 322: 1211-1217.

57. Mirzadegan T, Benko G, Filipek S, Palczewski K (2003) Sequence analyses of G-protein-coupled receptors: similarities to rhodopsin. Biochemistry 42: 2759-2767.

58. Honig B, Ebrey T, Callender RH, Dinur U, Ottolenghi M (1979) Photoisomerization, energy storage, and charge separation: a model for light energy transduction in visual pigments and bacteriorhodopsin. Proc Natl Acad Sci U S A 76: 2503-2507.

59. Vogel R, Ludeke S, Radu I, Siebert F, Sheves M (2004) Photoreactions of metarhodopsin III. Biochemistry 43: 10255-10264.

60. Ritter E, Zimmermann K, Heck M, Hofmann KP, Bartl FJ (2004) Transition of rhodopsin into the active metarhodopsin II state opens a new light-induced pathway linked to Schiff base isomerization. J Biol Chem 279: 48102-48111.

61. Soubias O, Teague WE, Gawrisch K (2006) Evidence for specificity in lipid-rhodopsin interactions. J Biol Chem 281: 33233-33241.

62. Ernst OP, Bartl FJ (2002) Active states of rhodopsin. Chembiochem 3: 968-974.

63. Bartl FJ, Vogel R (2007) Structural and functional properties of metarhodopsin III: recent spectroscopic studies on deactivation pathways of rhodopsin. Phys Chem Chem Phys 9: 1648-1658.

64. Matthews RG, Hubbard R, Brown PK, Wald G (1963) Tautomeric Forms of Metarhodopsin. J Gen Physiol 47: 215-240.

65. Parkes JH, Liebman PA (1984) Temperature and pH dependence of the metarhodopsin I-metarhodopsin II kinetics and equilibria in bovine rod disk membrane suspensions. Biochemistry 23: 5054-5061.

66. Nakamichi H, Okada T (2006) Crystallographic analysis of primary visual photochemistry. Angew Chem Int Ed Engl 45: 4270-4273.

67. Nakamichi H, Okada T (2006) Local peptide movement in the photoreaction intermediate of rhodopsin. Proc Natl Acad Sci U S A 103: 12729-12734.

68. Salom D, Lodowski DT, Stenkamp RE, Le Trong I, Golczak M, et al. (2006) Crystal structure of a photoactivated deprotonated intermediate of rhodopsin. Proc Natl Acad Sci U S A 103: 16123-16128.

69. Borhan B, Souto ML, Imai H, Shichida Y, Nakanishi K (2000) Movement of retinal along the visual transduction path. Science 288: 2209-2212.

70. Ruprecht JJ, Mielke T, Vogel R, Villa C, Schertler GF (2004) Electron crystallography reveals the structure of metarhodopsin I. EMBO J 23: 3609-3620.

71. Farrens DL, Altenbach C, Yang K, Hubbell WL, Khorana HG (1996) Requirement of rigid-body motion of transmembrane helices for light activation of rhodopsin. Science 274: 768-770.

72. Knierim B, Hofmann KP, Ernst OP, Hubbell WL (2007) Sequence of late molecular events in the activation of rhodopsin. Proc Natl Acad Sci U S A 104: 20290-20295.

73. Altenbach C, Kusnetzow AK, Ernst OP, Hofmann KP, Hubbell WL (2008) High-resolution distance mapping in rhodopsin reveals the pattern of helix movement due to activation. Proc Natl Acad Sci U S A 105: 7439-7444.

74. Menon ST, Han M, Sakmar TP (2001) Rhodopsin: structural basis of molecular physiology. Physiol Rev 81: 1659-1688.

75. Sheikh SP, Zvyaga TA, Lichtarge O, Sakmar TP, Bourne HR (1996) Rhodopsin activation blocked by metal-ion-binding sites linking transmembrane helices C and F. Nature 383: 347-350.

76. Kim JM, Altenbach C, Thurmond RL, Khorana HG, Hubbell WL (1997) Structure and function in rhodopsin: rhodopsin mutants with a neutral amino acid at E134 have a partially activated conformation in the dark state. Proc Natl Acad Sci U S A 94: 14273-14278.

77. Fritze O, Filipek S, Kuksa V, Palczewski K, Hofmann KP, et al. (2003) Role of the conserved NPxxY(x)5,6F motif in the rhodopsin ground state and during activation. Proc Natl Acad Sci U S A 100: 2290-2295.

78. Janz JM, Farrens DL (2004) Role of the retinal hydrogen bond network in rhodopsin Schiff base stability and hydrolysis. J Biol Chem 279: 55886-55894.

79. Meyer CK, Bohme M, Ockenfels A, Gartner W, Hofmann KP, et al. (2000) Signaling states of rhodopsin. Retinal provides a scaffold for activating proton transfer switches. J Biol Chem 275: 19713-19718.

80. Mahalingam M, Martinez-Mayorga K, Brown MF, Vogel R (2008) Two protonation switches control rhodopsin activation in membranes. Proc Natl Acad Sci U S A 105: 17795-17800.

81. Arnis S, Hofmann KP (1993) Two different forms of metarhodopsin II: Schiff base deprotonation precedes proton uptake and signaling state. Proc Natl Acad Sci U S A 90: 7849-7853.

82. Vogel R, Ruprecht J, Villa C, Mielke T, Schertler GF, et al. (2004) Rhodopsin photoproducts in 2D crystals. J Mol Biol 338: 597-609.

83. Ritter E, Elgeti M, Bartl FJ (2008) Activity Switches of Rhodopsin. Photochem Photobiol.

84. Surya A, Foster KW, Knox BE (1995) Transducin activation by the bovine opsin apoprotein. J Biol Chem 270: 5024-5031.

85. Hofmann KP, Emeis D, Schnetkamp PP (1983) Interplay between hydroxylamine, metarhodopsin II and GTP-binding protein in bovine photoreceptor membranes. Biochim Biophys Acta 725: 60-70.

86. Acharya S, Karnik SS (1996) Modulation of GDP release from transducin by the conserved Glu134-Arg135 sequence in rhodopsin. J Biol Chem 271: 25406-25411.

87. Melia TJ, Jr., Cowan CW, Angleson JK, Wensel TG (1997) A comparison of the efficiency of G protein activation by ligand-free and light-activated forms of rhodopsin. Biophys J 73: 3182-3191.

88. Sachs K, Maretzki D, Meyer CK, Hofmann KP (2000) Diffusible ligand all-trans-retinal activates opsin via a palmitoylation-dependent mechanism. J Biol Chem 275: 6189-6194.

89. Surya A, Knox BE (1998) Enhancement of opsin activity by all-trans-retinal. Exp Eye Res 66: 599-603.

90. Jager S, Palczewski K, Hofmann KP (1996) Opsin/all-trans-retinal complex activates transducin by different mechanisms than photolyzed rhodopsin. Biochemistry 35: 2901-2908.

91. Vogel R, Siebert F (2001) Conformations of the active and inactive states of opsin. J Biol Chem 276: 38487-38493.

92. Cohen GB, Oprian DD, Robinson PR (1992) Mechanism of activation and inactivation of opsin: role of Glu113 and Lys296. Biochemistry 31: 12592-12601.

93. Robinson PR, Cohen GB, Zhukovsky EA, Oprian DD (1992) Constitutively active mutants of rhodopsin. Neuron 9: 719-725.

94. Arnis S, Fahmy K, Hofmann KP, Sakmar TP (1994) A conserved carboxylic acid group mediates light-dependent proton uptake and signaling by rhodopsin. J Biol Chem 269: 23879-23881.

95. Otwinowski ZM, W. (1997) Processing of X-ray diffraction data collected in oscillation mode. Methods Enzymol 276: 307.

96. Collaborative Computational Project N (1994) The CCP4 suite: programs for protein crystallography. Acta Crystallogr D Biol Crystallogr 50: 760-763.

97. Brunger AT, Adams PD, Clore GM, DeLano WL, Gros P, et al. (1998) Crystallography & NMR system: A new software suite for macromolecular structure determination. Acta Crystallogr D Biol Crystallogr 54: 905-921.

98. Emsley P, Cowtan K (2004) Coot: model-building tools for molecular graphics. Acta Crystallogr D Biol Crystallogr 60: 2126-2132.

99. Laskowski RA, MacArthur, M. W., Moss, D. S. & Thornton, J. M (1993) PROCHECK: a program to check the stereochemical quality of protein structures. J Appl Crystallogr 26: 283-291.

100. Hooft RW, Vriend G, Sander C, Abola EE (1996) Errors in protein structures. Nature 381: 272.

101. CCP4 (1994) Collaborative Computational Project. Number 4. The CCP4 suite: programs for protein crystallography. Acta Crystallogr D Biol Crystallogr 50: 760-763.

102. DeLano WL (2002) The PyMOL Molecular Graphics System.

103. Papermaster DS (1982) Preparation of retinal rod outer segments. Methods Enzymol 81: 48-52.

104. Smith HG, Jr., Stubbs GW, Litman BJ (1975) The isolation and purification of osmotically intact discs from retinal rod outer segments. Exp Eye Res 20: 211-217.

105. McPherson A, DeLucas L (1999) Crystal-growing in space. Science 283: 1459.

106. McPherson A, editor (1989) In "Preparation and analysis of protein crystals" Krieger publishing company.

107. Zeppezauer M, Eklund H, Zeppezauer ES (1968) Micro diffusion cells for the growth of single protein crystals by means of equilibrium dialysis. Arch Biochem Biophys 126: 564-573.

108. Jancarik J KS (1991) Sparse matrix sampling. A screening method for crystallization of proteins. Journal of Applied Crystallography 24: 409.

109. Teller DC, Okada T, Behnke CA, Palczewski K, Stenkamp RE (2001) Advances in determination of a high-resolution three-dimensional structure of rhodopsin, a model of G-protein-coupled receptors (GPCRs). Biochemistry 40: 7761-7772.

110. Engh R, & Huber, R (1991) Accurate Bond and Angle Parameters for X-ray Protein-Structure Refinement. Acta Cryst A 47: 392-400.

111. Matthews BW (1968) Solvent content of protein crystals. J Mol Biol 33: 491-497.

112. Jackson W, Ablonczy Z, Crouch RK (2008) Quantitation of the Effect of Hydroxylamine on Rhodopsin Palmitylation. Photochem Photobiol.

113. Janz JM, Fay JF, Farrens DL (2003) Stability of dark state rhodopsin is mediated by a conserved ion pair in intradiscal loop E-2. J Biol Chem 278: 16982-16991.

114. Krebs A, Edwards PC, Villa C, Li J, Schertler GF (2003) The three-dimensional structure of bovine rhodopsin determined by electron cryomicroscopy. J Biol Chem 278: 50217-50225.

115. Liu W, Eilers M, Patel AB, Smith SO (2004) Helix packing moments reveal diversity and conservation in membrane protein structure. J Mol Biol 337: 713-729.

116. Liang Y, Fotiadis D, Filipek S, Saperstein DA, Palczewski K, et al. (2003) Organization of the G Protein-coupled Receptors Rhodopsin and Opsin in Native Membranes. J Biol Chem.

117. Filipek S, Krzysko KA, Fotiadis D, Liang Y, Saperstein DA, et al. (2004) A concept for G protein activation by G protein-coupled receptor dimers: the transducin/rhodopsin interface. Photochem Photobiol Sci 3: 628-638.

118. Fotiadis D, Liang Y, Filipek S, Saperstein DA, Engel A, et al. (2004) The G protein-coupled receptor rhodopsin in the native membrane. FEBS Lett 564: 281-288.

119. Hubbell WL, Altenbach C, Hubbell CM, Khorana HG (2003) Rhodopsin structure, dynamics, and activation: a perspective from crystallography, site-directed spin labeling, sulfhydryl reactivity, and disulfide cross-linking. Adv Protein Chem 63: 243-290.

120. Park JH, Scheerer P, Hofmann KP, Choe HW, Ernst OP (2008) Crystal structure of the ligand-free G-protein-coupled receptor opsin. Nature.

121. Altenbach C, Yang K, Farrens DL, Farahbakhsh ZT, Khorana HG, et al. (1996) Structural features and light-dependent changes in the cytoplasmic interhelical E-F loop region of rhodopsin: a site-directed spin-labeling study. Biochemistry 35: 12470-12478.

122. Terakita A, Yamashita T, Nimbari N, Kojima D, Shichida Y (2002) Functional interaction between bovine rhodopsin and G protein transducin. J Biol Chem 277: 40-46.

123. Acharya S, Saad Y, Karnik SS (1997) Transducin-alpha C-terminal peptide binding site consists of C-D and E-F loops of rhodopsin. J Biol Chem 272: 6519-6524.

124. Konig B, Arendt A, McDowell JH, Kahlert M, Hargrave PA, et al. (1989) Three cytoplasmic loops of rhodopsin interact with transducin. Proc Natl Acad Sci U S A 86: 6878-6882.

125. Franke RR, Konig B, Sakmar TP, Khorana HG, Hofmann KP (1990) Rhodopsin mutants that bind but fail to activate transducin. Science 250: 123-125.

126. Ernst OP, Hofmann KP, Sakmar TP (1995) Characterization of rhodopsin mutants that bind transducin but fail to induce GTP nucleotide uptake. Classification of mutant pigments by fluorescence, nucleotide release, and flash-induced light-scattering assays. J Biol Chem 270: 10580-10586.

127. Janz JM, Farrens DL (2004) Rhodopsin activation exposes a key hydrophobic binding site for the transducin alpha-subunit C terminus. J Biol Chem 279: 29767-29773.

128. Prioleau C, Visiers I, Ebersole BJ, Weinstein H, Sealfon SC (2002) Conserved helix 7 tyrosine acts as a multistate conformational switch in the 5HT2C receptor: Identification of a novel "locked-on" phenotype and double revertant mutations. J Biol Chem 277: 36577-36584.

129. Barak LS, Menard L, Ferguson SS, Colapietro AM, Caron MG (1995) The conserved seven-transmembrane sequence NP(X)2,3Y of the G-protein-coupled receptor superfamily regulates multiple properties of the beta 2-adrenergic receptor. Biochemistry 34: 15407-15414.

130. Prioleau C, Visiers I, Ebersole BJ, Weinstein H, Sealfon SC (2002) Conserved helix 7 tyrosine acts as a multistate conformational switch in the 5HT2C receptor. Identification of a novel "locked-on" phenotype and double revertant mutations. J Biol Chem 277: 36577-36584.

131. Vogel R, Sakmar TP, Sheves M, Siebert F (2007) Coupling of protonation switches during rhodopsin activation. Photochem Photobiol 83: 286-292.

132. Kim JM, Altenbach C, Kono M, Oprian DD, Hubbell WL, et al. (2004) Structural origins of constitutive activation in rhodopsin: Role of the K296/E113 salt bridge. Proc Natl Acad Sci U S A 101: 12508-12513.

133. Standfuss J, Zaitseva E, Mahalingam M, Vogel R (2008) Structural impact of the E113Q counterion mutation on the activation and deactivation pathways of the G protein-coupled receptor rhodopsin. J Mol Biol 380: 145-157.

134. Scheerer P, Park JH, Hildebrand PW, Kim YJ, Krauss N, et al. (2008) Crystal structure of opsin in its G-protein-interacting conformation. Nature 455: 497-502.

135. Cohen GB, Yang T, Robinson PR, Oprian DD (1993) Constitutive activation of opsin: influence of charge at position 134 and size at position 296. Biochemistry 32: 6111-6115.

136. Hofmann KP (2000) Late photoproducts and signaling states of bovine rhodopsin. In: Stavenga DG, DeGrip WJ, Pugh ENJ, editors. Molecular Mechanism in visual transduction. Amsterdam: Elsevier Science Publishers B.V. pp. 91-142.

137. Hofmann KP (1999) Signalling states of photoactivated rhodopsin. Novartis Found Symp 224: 158-175; discussion 175-180.

138. Dunham TD, Farrens DL (1999) Conformational changes in rhodopsin. Movement of helix f detected by site-specific chemical labeling and fluorescence spectroscopy. J Biol Chem 274: 1683-1690.

139. Meng EC, Bourne HR (2001) Receptor activation: what does the rhodopsin structure tell us? Trends Pharmacol Sci 22: 587-593.

140. Franke RR, König B, Sakmar TP, Khorana HG, Hofmann KP (1990) Rhodopsin mutants that bind but fail to activate transducin. Science 250: 123-125.

141. Franke RR, Sakmar TP, Graham RM, Khorana HG (1992) Structure and function in rhodopsin. Studies of the interaction between the rhodopsin cytoplasmic domain and transducin. J Biol Chem 267: 14767-14774.

142. Fahmy K, Jager F, Beck M, Zvyaga TA, Sakmar TP, et al. (1993) Protonation states of membrane-embedded carboxylic acid groups in rhodopsin and metarhodopsin II: a Fourier-transform infrared spectroscopy study of site-directed mutants. Proc Natl Acad Sci U S A 90: 10206-10210.

143. Kuhn H, Hargrave PA (1981) Light-induced binding of guanosinetriphosphatase to bovine photoreceptor membranes: effect of limited proteolysis of the membranes. Biochemistry 20: 2410-2417.

144. Yao X, Parnot C, Deupi X, Ratnala VR, Swaminath G, et al. (2006) Coupling ligand structure to specific conformational switches in the beta2-adrenoceptor. Nat Chem Biol 2: 417-422.

145. Rath P, DeGrip WJ, Rothschild KJ (1998) Photoactivation of rhodopsin causes an increased hydrogen-deuterium exchange of buried peptide groups. Biophys J 74: 192-198.

146. Nagata T, Terakita A, Kandori H, Shichida Y, Maeda A (1998) The hydrogen-bonding network of water molecules and the peptide backbone in the region connecting Asp83, Gly120, and Glu113 in bovine rhodopsin. Biochemistry 37: 17216-17222.

147. Angel TE, Chance MR, Palczewski K (2009) Conserved waters mediate structural and functional activation of family A (rhodopsin-like) G protein-coupled receptors. Proc Natl Acad Sci U S A.

148. Schwartz TW, Frimurer TM, Holst B, Rosenkilde MM, Elling CE (2006) Molecular mechanism of 7TM receptor activation--a global toggle switch model. Annu Rev Pharmacol Toxicol 46: 481-519.

149. Crocker E, Eilers M, Ahuja S, Hornak V, Hirshfeld A, et al. (2006) Location of Trp265 in metarhodopsin II: implications for the activation mechanism of the visual receptor rhodopsin. J Mol Biol 357: 163-172.

150. Ernst OP, Meyer CK, Marin EP, Henklein P, Fu WY, et al. (2000) Mutation of the fourth cytoplasmic loop of rhodopsin affects binding of transducin and peptides derived from the carboxyl-terminal sequences of transducin alpha and gamma subunits. J Biol Chem 275: 1937-1943.

151. Han M, Smith SO, Sakmar TP (1998) Constitutive activation of opsin by mutation of methionine 257 on transmembrane helix 6. Biochemistry 37: 8253-8261.

152. Koenig BW, Mitchell DC, Konig S, Grzesiek S, Litman BJ, et al. (2000) Measurement of dipolar couplings in a transducin peptide fragment weakly bound to oriented photo-activated rhodopsin. J Biomol NMR 16: 121-125.

153. Herrmann R, Heck M, Henklein P, Kleuss C, Hofmann KP, et al. (2004) Sequence of interactions in receptor-G protein coupling. J Biol Chem 279: 24283-24290.

154. Hamm HE, Deretic D, Arendt A, Hargrave PA, Koenig B, et al. (1988) Site of G protein binding to rhodopsin mapped with synthetic peptides from the alpha subunit. Science 241: 832-835.

155. Emeis D, Kuhn H, Reichert J, Hofmann KP (1982) Complex formation between metarhodopsin II and GTP-binding protein in bovine photoreceptor membranes leads to a shift of the photoproduct equilibrium. FEBS Lett 143: 29-34.

156. Kisselev OG, Meyer CK, Heck M, Ernst OP, Hofmann KP (1999) Signal transfer from rhodopsin to the G-protein: evidence for a two-site sequential fit mechanism. Proc Natl Acad Sci U S A 96: 4898-4903.

157. Herrmann R, Heck M, Henklein P, Hofmann KP, Ernst OP (2006) Signal transfer from GPCRs to G proteins: role of the G alpha N-terminal region in rhodopsin-transducin coupling. J Biol Chem 281: 30234-30241.

158. Oldham WM, Hamm HE (2008) Heterotrimeric G protein activation by G-protein-coupled receptors. Nat Rev Mol Cell Biol 9: 60-71.

159. Keen TJ, Inglehearn CF, Lester DH, Bashir R, Jay M, et al. (1991) Autosomal dominant retinitis pigmentosa: four new mutations in rhodopsin, one of them in the retinal attachment site. Genomics 11: 199-205.

160. Rim J, Oprian DD (1995) Constitutive activation of opsin: interaction of mutants with rhodopsin kinase and arrestin. Biochemistry 34: 11938-11945.

161. Jäger F, Fahmy K, Sakmar TP, Siebert F (1994) Identification of glutamic acid 113 as the Schiff base proton acceptor in the metarhodopsin II photointermediate of rhodopsin. Biochemistry 33: 10878-10882.

162. Shi W, Sports CD, Raman D, Shirakawa S, Osawa S, et al. (1998) Rhodopsin arginine-135 mutants are phosphorylated by rhodopsin kinase and bind arrestin in the absence of 11-cis-retinal. Biochemistry 37: 4869-4874.

163. Wang T, Duan Y (2007) Chromophore channeling in the G-protein coupled receptor rhodopsin. J Am Chem Soc 129: 6970-6971.

164. Schadel SA, Heck M, Maretzki D, Filipek S, Teller DC, et al. (2003) Ligand channeling within a G-protein-coupled receptor. The entry and exit of retinals in native opsin. J Biol Chem 278: 24896-24903.

165. Hildebrand PW, Scheerer P, Park JH, Choe HW, Piechnick R, et al. (2009) A ligand channel through the G protein coupled receptor opsin. PLoS ONE 4: e4382.

166. Ahuja S, Hornak V, Yan EC, Syrett N, Goncalves JA, et al. (2009) Helix movement is coupled to displacement of the second extracellular loop in rhodopsin activation. Nat Struct Mol Biol 16: 168-175.

167. Kefalov VJ, Crouch RK, Cornwall MC (2001) Role of noncovalent binding of 11-cis-retinal to opsin in dark adaptation of rod and cone photoreceptors. Neuron 29: 749-755.

168. Heck M, Schadel SA, Maretzki D, Hofmann KP (2003) Secondary binding sites of retinoids in opsin: characterization and role in regeneration. Vision Res 43: 3003-3010.

169. Shi L, Liapakis G, Xu R, Guarnieri F, Ballesteros JA, et al. (2002) Beta2 adrenergic receptor activation. Modulation of the proline kink in transmembrane 6 by a rotamer toggle switch. J Biol Chem 277: 40989-40996.

170. Elling CE, Frimurer TM, Gerlach LO, Jorgensen R, Holst B, et al. (2006) Metal ion site engineering indicates a global toggle switch model for seven-transmembrane receptor activation. J Biol Chem 281: 17337-17346.

171. Fahmy K, Sakmar TP, Siebert F (2000) Transducin-dependent protonation of glutamic acid 134 in rhodopsin. Biochemistry 39: 10607-10612.

172. Buczylko J, Saari JC, Crouch RK, Palczewski K (1996) Mechanisms of opsin activation. J Biol Chem 271: 20621-20630.

173. Periole X, Ceruso MA, Mehler EL (2004) Acid-base equilibria in rhodopsin: dependence of the protonation state of glu134 on its environment. Biochemistry 43: 6858-6864.

174. Ritter E, Elgeti M, Hofmann KP, Bartl FJ (2007) Deactivation and proton transfer in light-induced metarhodopsin II/metarhodopsin III conversion: a time-resolved fourier transform infrared spectroscopic study. J Biol Chem 282: 10720-10730.

175. Martinez-Mayorga K, Pitman MC, Grossfield A, Feller SE, Brown MF (2006) Retinal counterion switch mechanism in vision evaluated by molecular simulations. J Am Chem Soc 128: 16502-16503.

176. Vogel R, Siebert F, Yan EC, Sakmar TP, Hirshfeld A, et al. (2006) Modulating rhodopsin receptor activation by altering the pKa of the retinal Schiff base. J Am Chem Soc 128: 10503-10512.

177. Kisselev OG, Kao J, Ponder JW, Fann YC, Gautam N, et al. (1998) Light-activated rhodopsin induces structural binding motif in G protein alpha subunit. Proc Natl Acad Sci U S A 95: 4270-4275.

178. Koenig BW, Kontaxis G, Mitchell DC, Louis JM, Litman BJ, et al. (2002) Structure and orientation of a G protein fragment in the receptor bound state from residual dipolar couplings. J Mol Biol 322: 441-461.

179. Scheerer P, Heck M, Goede A, Park JH, Choe HW, et al. (2009) Structural and kinetic modeling of an activating helix switch in the rhodopsin-transducin interface. Proc Natl Acad Sci U S A 106: 10660-10665.

180. Hofmann K, Scheerer, P, Hildebrand, PW, Choe, HW, Park, JH, Heck, M & Ernst, OP (2009) A G protein-coupled receptor at work: the rhodopsin model. Trends Biochem Sci: in press.

7 APPENDIX

The structure of opsin at low pH is considered to represent an active receptor conformation. To elucidate the active opsin conformation in complex with a G protein fragment, several trials of co-crystallization of opsin with a fragment of G_t have been performed. The G_t fragments were prepared as synthetic peptides derived from the C-terminus of the $G_t\alpha$- or $G_t\gamma$-subunit, respectively. Both C-termini are key binding sites for Meta II (150). Opsin was co-crystallized either with an eleven amino acid synthetic peptide derived from the C-terminus of the $G_t\alpha$-subunit or a twelve amino acid synthetic peptide derived from the farnesylated $G_t\gamma$ C-terminus, respectively (Table 7.1).

Table 7.1. G_t-derived peptides used for co-crystallization with opsin

Peptide	Abbreviation	Sequence (derived from G_t)
$G_t\alpha(340\text{-}350)$	$G_t\alpha CT(wt)$	NH_2- ^{340}IKENLKDCGLF^{350} -COOH
$G_t\alpha(340\text{-}350)$ (K341L)	$G_t\alpha CT$	NH_2- ^{340}ILENLKDCGLF^{350} -COOH
$G_t\gamma(60\text{-}71)$far	$G_t\gamma CT$	NH_2- ^{60}DKNPFKELKGGC^{71}(farnesyl) -CONH$_2$

Opsin* and the G_t-derived peptides have been co-crystallized (Figure 7.1) by modifying the crystallization conditions of opsin, i.e. change of pH (pH 5.6-6.0), precipitant concentration (2.9-3.2 M ammonium sulphate) and crystallization buffers (sodium acetate, sodium citrate, sodium cacodylate or 2-(N-Morpholino)ethanesulfonic acid).
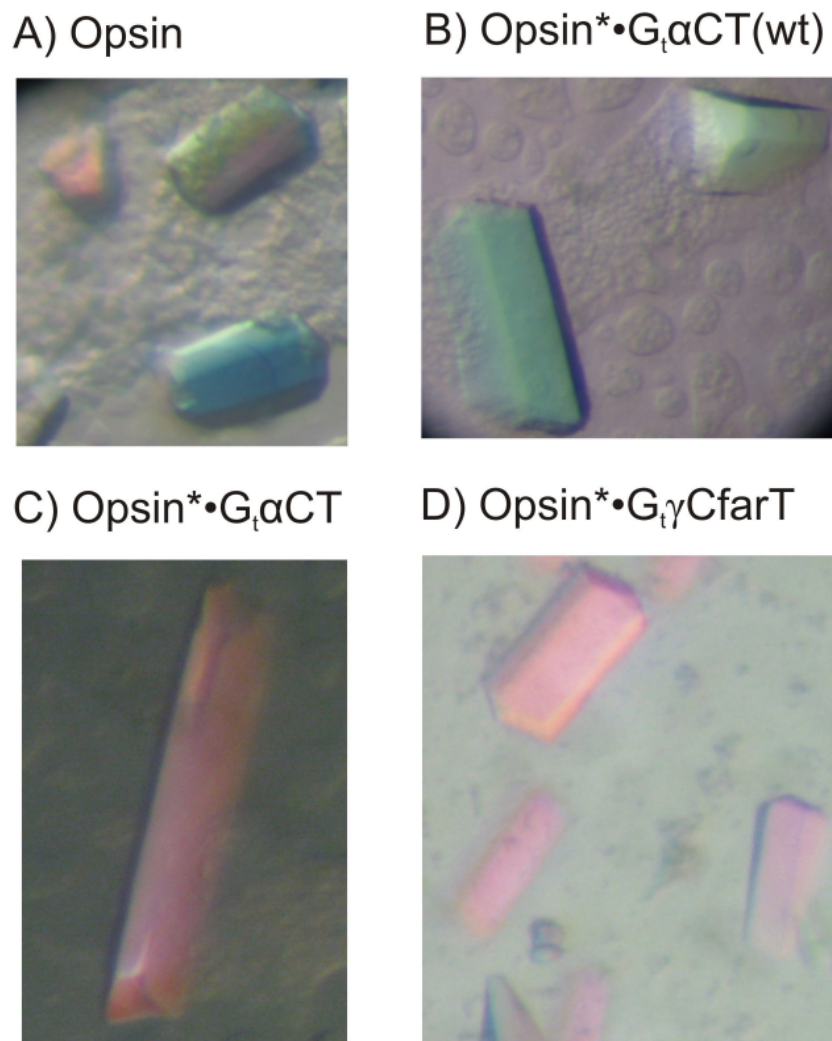
Figure 7.1. Images of crystals of opsin and opsin*•G$_t$CT complexes
*A) Opsin crystals grown in 3.2 M ammonium sulphate in 0.1 M MES or sodium acetate, pH 5.6. **B)** Crystals of opsin*•G$_t$αCT(wt, wild type) complex grown in 2.9-3.1 M ammonium sulphate in 0.1 M MES or sodium acetate, pH 5.6 **C)** Crystals of opsin*•G$_t$αCT complex obtained with 3.2 M ammonium sulphate in 0.1 M MES or sodium citrate, pH 6.0. **D)** Crystals obtained by co-crystallization of opsin with the farnesylated G$_t$γCT peptide, using 3.0 M ammonium sulphate in sodium cacodylate, pH 6.0.*

The crystal structures of the opsin*•G$_t$αCT complex [134] and opsin*•G$_t$αCT(wt) complex (unpublished) could be solved. Details of the structures will be reported in the thesis of Patrick Scheerer. The overall structure of opsin* in complex with the G$_t$αCT peptide is very similar to that of ligand-free opsin (Figure 7.2). Based on the helix movements of TM5 - TM7, breakage of the "ionic lock" between TM6 and TM3 (E(D)RY motif) and rearrangement of residues of the NPxxY(x)$_{5,6}$F motif, the crystal structure of ligand-free opsin represents an active receptor conformation.
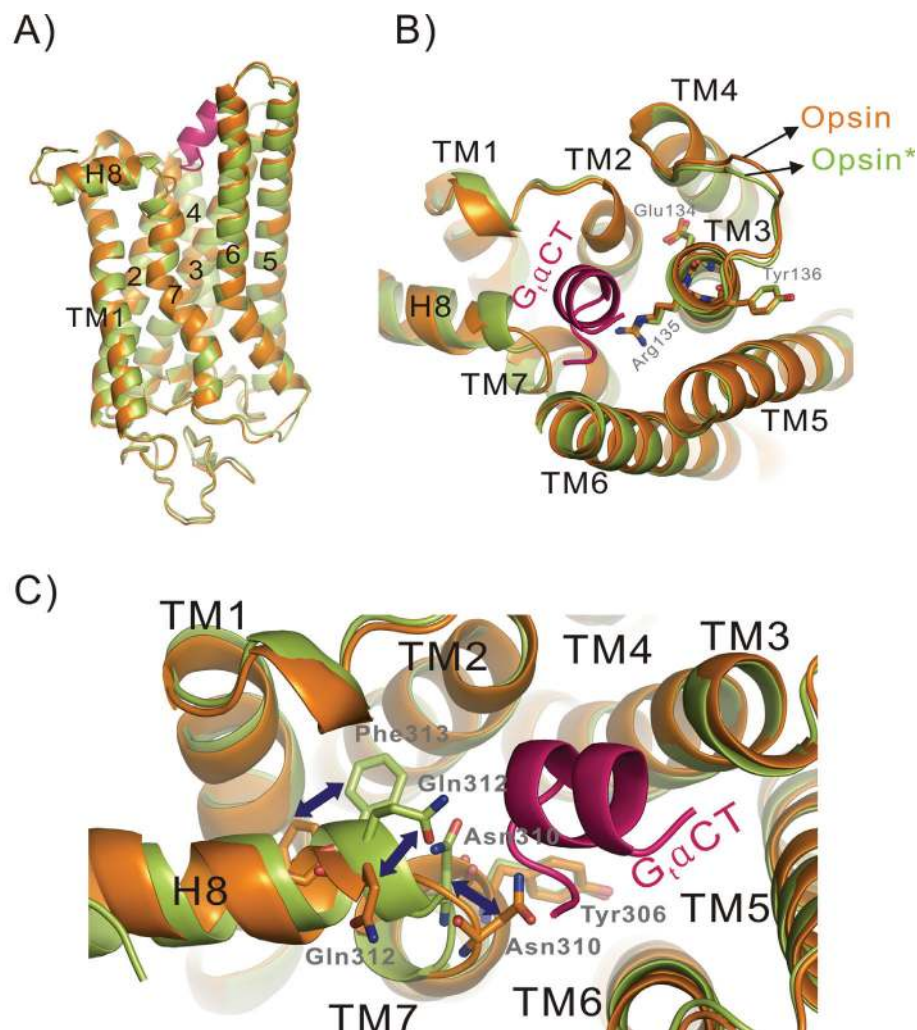
Figure 7.2. Comparison of ligand-free opsin and opsin*•G_tαCT structures
***A)** The overall topology of opsin* in the opsin*•G_tαCT complex (PDB accession 3DQB) is very simi-
lar to that of ligand-free opsin (PDB accession 3CAP) [120,134]. Each opsin structure is labelled and
shown as orange (ligand-free opsin) or green (opsin*) cartoon model, respectively. The interacting 11
amino acid C-terminal peptide G_tαCT derived from G_tα is presented as magenta cartoon. **B)** Compari-
son of the E(D)RY region in ligand-free opsin and opsin*•G_tαCT complex (cytoplasmic view). Residues
of the E(D)RY motif are presented as orange and green stick models, respectively. **C)** Comparison of
NPxxY(x)_{5,6}F regions in ligand-free opsin (orange) and opsin*•G_tαCT complex (green); cytoplasmic
view; blue arrows indicate rotamer changes of side chains.*

From NMR spectroscopy experiments it is known that the G_tαCT peptide in the op-
sin*•G_tαCT crystal adopts the same conformation as analogous G_tαCT peptides (containing
one or two amino acid substitutions) when bound to Meta II in native disc membranes
[177,178]. Thus, the cytoplasmic domain of opsin* in the ligand-free opsin and opsin*•G_tαCT
crystals, and the cytoplasmic domain of Meta II present in disc membranes are similar.
Knowledge of the opsin* conformation and the exact binding mode of the G_tαCT peptide fur-

ther allowed to propose mechanisms for rhodopsin activation and receptor-catalyzed nucleo-
tide exchange in the G protein [179,180].

ACKNOWLEDGEMENT

Hiermit erkläre ich gemäß §6 Abs. (3) der Promotionsordnung, dass ich die von mir vorgelegte Dissertation selbstständig und ohne unerlaubte Hilfe angefertigt, die benutzten Quellen und Hilfsmittel vollständig angegeben und die Stellen der Arbeit, die anderen Werken im Wortlaut oder dem Sinn nach entnommen sind, als solche kenntlich gemacht habe.
Ich habe mich weder anderwärts um einen Doktorgrad beworben noch besitze ich bisher einen Doktorgrad.

Jung Hee Park

Berlin, den 28. Aug. 2009